



Ministério da
**Ciência, Tecnologia
e Inovação**



sid.inpe.br/mtc-m19/2013/02.13.21.09-TDI

**ANALYSIS OF TOTAL ELECTRON CONTENT (TEC)
VARIATIONS OBTAINED FROM GPS DATA OVER
SOUTH AMERICA**

Olusegun Folarin Jonah

Dissertation Master at Graduation
Course in Space Geophysics, ad-
vised by Drs. Eurico Rodrigues
de Paula, and Severino Luiz
Guimarães Dutra, approved in
February 27, 2013.

URL of the original document:

<<http://urlib.net/8JMKD3MGP7W/3DHJF42>>

INPE
São José dos Campos
2013

PUBLISHED BY:

Instituto Nacional de Pesquisas Espaciais - INPE

Gabinete do Diretor (GB)

Serviço de Informação e Documentação (SID)

Caixa Postal 515 - CEP 12.245-970

São José dos Campos - SP - Brasil

Tel.:(012) 3208-6923/6921

Fax: (012) 3208-6919

E-mail: pubtc@sid.inpe.br

BOARD OF PUBLISHING AND PRESERVATION OF INPE INTELLECTUAL PRODUCTION (RE/DIR-204):**Chairperson:**

Marciana Leite Ribeiro - Serviço de Informação e Documentação (SID)

Members:

Dr. Antonio Fernando Bertachini de Almeida Prado - Coordenação Engenharia e Tecnologia Espacial (ETE)

Dr^a Inez Staciarini Batista - Coordenação Ciências Espaciais e Atmosféricas (CEA)

Dr. Gerald Jean Francis Banon - Coordenação Observação da Terra (OBT)

Dr. Germano de Souza Kienbaum - Centro de Tecnologias Especiais (CTE)

Dr. Manoel Alonso Gan - Centro de Previsão de Tempo e Estudos Climáticos (CPT)

Dr^a Maria do Carmo de Andrade Nono - Conselho de Pós-Graduação

Dr. Plínio Carlos Alvalá - Centro de Ciência do Sistema Terrestre (CST)

DIGITAL LIBRARY:

Dr. Gerald Jean Francis Banon - Coordenação de Observação da Terra (OBT)

DOCUMENT REVIEW:

Marciana Leite Ribeiro - Serviço de Informação e Documentação (SID)

Yolanda Ribeiro da Silva Souza - Serviço de Informação e Documentação (SID)

ELECTRONIC EDITING:

Maria Tereza Smith de Brito - Serviço de Informação e Documentação (SID)

Luciana Manacero - Serviço de Informação e Documentação (SID)



Ministério da
**Ciência, Tecnologia
e Inovação**



sid.inpe.br/mtc-m19/2013/02.13.21.09-TDI

**ANALYSIS OF TOTAL ELECTRON CONTENT (TEC)
VARIATIONS OBTAINED FROM GPS DATA OVER
SOUTH AMERICA**

Olusegun Folarin Jonah

Dissertation Master at Graduation
Course in Space Geophysics, ad-
vised by Drs. Eurico Rodrigues
de Paula, and Severino Luiz
Guimarães Dutra, approved in
February 27, 2013.

URL of the original document:

<<http://urlib.net/8JMKD3MGP7W/3DHJF42>>

INPE
São José dos Campos
2013

Cataloging in Publication Data

Jonah, Olusegun Folarin.
J597a Analysis of Total Electron Content (TEC) variations obtained
 from GPS data over South America / Olusegun Folarin Jonah. –
 São José dos Campos : INPE, 2013.
 xxii + 123 p. ; (sid.inpe.br/mtc-m19/2013/02.13.21.09-TDI)

Dissertation (Master in Space Geophysics) – Instituto Nacional
de Pesquisas Espaciais, São José dos Campos, 2013.

Advisers : Drs. Eurico Rodrigues de Paula, and Severino Luiz
Guimarães Dutra.

1. solar flux 2. perturbation 3. Sudden Stratospheric Warming
(SSW) 4. Total Electron Content (TEC) 5. Equatorial Ionization
Anomaly (EIA). I.Título.

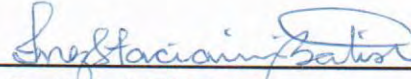
CDU 551.510.535

Copyright © 2013 do MCT/INPE. Nenhuma parte desta publicação pode ser reproduzida, armazenada em um sistema de recuperação, ou transmitida sob qualquer forma ou por qualquer meio, eletrônico, mecânico, fotográfico, reprográfico, de microfilmagem ou outros, sem a permissão escrita do INPE, com exceção de qualquer material fornecido especificamente com o propósito de ser entrado e executado num sistema computacional, para o uso exclusivo do leitor da obra.

Copyright © 2013 by MCT/INPE. No part of this publication may be reproduced, stored in a retrieval system, or transmitted in any form or by any means, electronic, mechanical, photocopying, recording, microfilming, or otherwise, without written permission from INPE, with the exception of any material supplied specifically for the purpose of being entered and executed on a computer system, for exclusive use of the reader of the work.

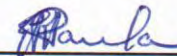
Aprovado (a) pela Banca Examinadora
em cumprimento ao requisito exigido para
obtenção do Título de **Mestre** em
Geofísica Espacial

Dra. Inez Staciariini Batista




Presidente / INPE / SJC Campos - SP

Dr. Eurico Rodrigues de Paula




Orientador(a) / INPE / SJC Campos - SP

Dr. Severino Luiz Guimarães Dutra



Orientador(a) / INPE / SJC Campos - SP

Dr. Ivan Jelinek Kantor



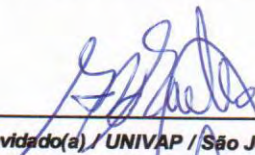
Membro da Banca / INPE / SJC Campos - SP

Dr. Jonas Rodrigues de Souza



Membro da Banca / INPE / SJC Campos - SP

Dr. Marcio Tadeu Assis Honorato Muella



Convidado(a) / UNIVAP / São José dos Campos - SP

Dr. Claudinei Rodrigues de Aguiar



Convidado(a) / UTFPR / Curitiba - PR

Este trabalho foi aprovado por:

() maioria simples

unanimidade

Aluno (a): **Olusegun Folarin Jonah**

São José dos Campos, 27 de Fevereiro de 2013

“We know that all things work together for good to them that love God, to them who have being called according to his purpose (Rom. 8:28)”.

I dedicate this dissertation work to my wife, Dra. Ifelaju Folarin-Jonah.

ACKNOWLEDGEMENT

I give all the glory, honour and majesty to the Almighty God who made ways where there seemed to be no way. Thank you Jesus!

I deeply appreciate to my supervisor Dr. Eurico R. de Paula for the strong academic supervision, guidance and intelligent suggestions he provided throughout the research period. He has not only been like a father but also a mentor and an inspiration to me. I am equally indebted to my co-supervisor Dr. Dutra S. L.G. for the positive criticism and his numerous contributions which are instrumental to the timely completion of the research. I am grateful to both of you for investing your time in me. Thank you so much.

Special appreciation goes to Dr Otsuka of the Nagoya University for making the Nagoya TEC model available in Brazil which was useful for the research. Also to every member of the examining board for their suggestions which contribute immensely to the improvement of this dissertation.

I must express my profound gratitude to all my lecturers who gave me basic foundation in Space Physics. I remain grateful to you all. My profound gratitude also goes to Dr. Bela G. Fejer of the Utah state University, Dr. M.A. Adbu, Dr. Alam Kherani, and Dra Patricia M. de Siqueira. I am grateful for those immense and important suggestions.

I wish to acknowledge Paul Pernomian and Anderson Dutra for their constant support in programming and computations without them this dissertation would have been delayed. I also appreciate the friendship of Ricardo Y.D.C. Cueva, Rodrigo Azambuja and Paulo Nogueira.

I am fortunate to have kind and generous colleagues people whose emotional support and enthusiasm have contributed to the success of my work. I thank all of them for their generosity, especially, Binod Adhikiri, Jonas Souza, Régia Pereira, Ricardo da Rosa Paes, Rhon Niw, Tardelli Stekel, Manuel Bravo, Barbara, Andre Iniesta, Carolina and Jeferson Alves. You are all wonderful people and I will never forget you.

I appreciate Dr. Alisson Dal Lago , Dr. Polinaya Muralikrishna for their encouragement and advises particularly during those times of great challenges that I faced as a foreigner during my course work. In the same vein, I like to appreciate the morally and motherly role of Dona

Yolanda I am immensely grateful and specially thank you for your ever warm hospitalities and concerns.

I thank the Brazilian government through the Conselho Nacional de Desenvolvimento Científico e Tecnológico (CNPq) for the Masters fellowship awarded me and for the sponsorship of my education. I also acknowledge "Instituto Nacional de Pesquisas Espaciais" for the quality education I received and for all the material and infrastructural resources that were made available during the course of my work. I wish to equally use this opportunity to thank the good people of Brazil whose hard earned resources were used to give me an opportunity of quality education.

Special acknowledgement also goes to Prof. and Mrs. Laseinde for their prayers, constant love and concern for me and my family. May the Almighty God reward you greatly. I thank Prof. Babatunde Rabiú and his family, and Dr. Fayose for all their support and trust.

This acknowledgement will be incomplete if I fail to mention my wife, Dra. Ifelaju Folarin-Jonah. Without her, I would not have started this programme in the first place. I thank you very much for your courage, understating, support and encouragement. I owe you a lot.

Finally, I am deeply grateful to my parents Mr. Olukayode Jonah and Olanike Jonah for their good moral, and spiritual supports, without which I would not have been able to attain this height. Also to all my siblings for every word of your prayers. I also appreciate my wife's parent and siblings. Thank you for your love. Thank you all.

Olusegun Folarin Jonah

ABSTRACT

Using dual frequency GPS receivers in the South American sector, the measurement of absolute ionospheric Total Electron Content (TEC) has been estimated applying the Nagoya ionospheric model for both 2009 and 2001, which represent low and high solar activities respectively. The diurnal, day-to-day, monthly, seasonal, latitudinal and longitudinal variations of TEC was studied for equatorial and low latitude region of South America. The strength and characteristics of the EIA were equally analyzed. We also investigated the TEC differences between the March and September equinoxes of both solar minimum and solar maximum and the effect of Sudden Stratospheric Warming on the ionosphere during the period of 2007/2008 and 2008/2009. The Physics based SAMI2 model was also used to provide possible TEC variations mechanisms. The equinoctial asymmetry in the ionosphere shows that TEC is larger in March month than in September month and that this phenomenon occurs at both equatorial and low latitude regions of both solar phases. The analyses also reveal the well know diurnal, seasonal and semidiurnal variation as well as the nighttime variability during the low and high solar activities. Wavelet power spectra analysis was employed to check the periodicities of the TEC data, F10.7 and zonal and meridional wind velocities measured by Meteor radar at an 100 km altitude. Many periods were found to be dominant in the zonal and meridional wind velocity corresponding with that of TEC periodicities. We believe this could be an evidence of planetary waves which could result in the modulation of the E region electric field during the day and consequently cause some enhancement in the ionosphere ionization. Finally, we present, evidence of the ionospheric response to Sudden Stratospheric Warming (SSW) of 2008 and 2009 events during solar minimum conditions. The response is characterized by semidiurnal, large amplitude and persistence perturbation for about 3 weeks after the peak of the stratospheric temperatures. Evidences from our study show that the EIA was enhanced during the morning hours, suppressed during afternoon hours and a secondary enhancement was also noticed after sunset. The progressive shift of EIA occurs at a different rate for different SSW events. In all, a total of five SSW events have been analyzed.

ANÁLISE DE CONTEÚDO ELETRÔNICO TOTAL (CET) OBTIDOS A PARTIR DO SISTEMA DE POSICIONAMENTO GLOBAL (GPS) DADOS SOBRE O SUL DA AMÉRICA

RESUMO

Usando receptores GPS de dupla frequência do sector da América do Sul, a medição do Conteúdo Eletrônico Total (TEC) absoluto foi estimada aplicando o modelo ionosférico Nagoya para 2009 e 2001, representando baixas e altas atividades solares respectivamente. As variações diurnas, dia-a-dia, mensal, sazonal, e de latitude e longitude do TEC foi estudado para regiões equatoriais e de baixas latitudes da América do Sul. A intensidade e as características da Anomalia da Ionização Equatorial (EIA) foram igualmente analisadas. Também foram investigadas as diferenças do TEC entre equinócios de março e setembro, tanto para o mínimo solar quanto para o máximo solar. O efeito do aquecimento estratosférico súbito na ionosfera polar durante os períodos de 2007/2008 e 2008/2009 são igualmente analisados. A Física baseada O modelo SAMI2 baseado em princípios físicos foi também usado para fornecer os possíveis mecanismos responsáveis pelas variações no TEC. A assimetria equinocial na ionosfera mostra que o TEC é maior nos meses de março do que nos meses de setembro e que este fenômeno ocorre em regiões de latitudes baixas e equatoriais, em ambas as fases do ciclo solar. As análises revelam também a bem conhecida variação diurna, sazonal e semi-diurna, bem como a variabilidade noturna, durante baixa e alta atividades solares. Wavelet análise dos espectros de potência foi empregada para verificar as periodicidades dos dados do TEC, F10.7 e velocidades do vento zonal e meridional medidos pelo rada meteorológico, a uma altitude de 100 km. Muitos períodos considerados dominantes na velocidade do vento zonal e meridional correspondente com os das periodicidades do TEC foram observados. Acreditamos que esta poderia ser uma evidência de ondas planetárias que poderiam causar modulação do campo elétrico E região durante o dia e, conseqüentemente, causar algum aumento na ionização da ionosfera. Por fim, apresentamos a evidência da resposta ionosférica aos eventos de Aquecimento Estratosférico Súbito (SSW) de 2008 e 2009 durante condições de mínima atividade solar. A resposta é caracterizada pela perturbação semidiurna de grande amplitude e persistência, por cerca de 3 semanas após o pico de temperatura da estratosfera. Evidências de nosso estudo mostram que o EIA foi mais intenso durante a manhã, suprimido durante as horas da tarde e um aumento secundário também foi notado após o pôr do sol. A mudança temporal progressiva do EIA ocorre em uma taxa diferente para os diferentes eventos SSW. Ao todo, um total de cinco eventos SSW foram analisados.

LIST OF FIGURES

Figure 1.1 - Time evolution of the polar vortex for the Antarctica region on the dates shown during September 2002.	6
Figure 2.1 - Illustration of the layers of the neutral atmosphere with temperature and the layers depending on the ionospheric electron density profile.	7
Figure 2.2 - Typical vertical profile of the ion and neutral densities in the mid-latitude	9
Figure 2.3 - Vertical profile of the ionosphere	10
Figure 2.4 - Asymmetry of the Equatorial Ionization Anomaly. E denotes an eastward electric field and B is the northward geomagnetic field	13
Figure 2.5 - Vertical plasma drifts due to the meridional neutral wind (W_M). $W_{ }$ is the meridional wind along the geomagnetic field line.	14
Figure 2.6 - E region electrodynamic.	16
Figure 2.7 - F region electrodynamic.	17
Figure 2.8 - Vertical profile of the Parallel, Pederson and Hall conductivities.	19
Figure 3.1 - The three segments that make up the GPS	22
Figure 3.2 - Location of the four unmanned stations (circles) and one Master Station (triangle) of the GPS Control Segment.	23
Figure 3.3 - IGS network of permanent GPS tracking stations	24
Figure 3.4 - Location and identification of the receiving stations of the IBGE network	25
Figure 3.5: Modulation of the code on the carrier wave.	27
Figure 4.1 - F10.7 cm flux and sum of Kp index indicating the data analyzed.	38
Figure 4.2 - Locations of RBMC and IGS stations that were used.	39
Figure 5.1 - Monthly diurnal TEC variation during 2009	47
Figure 5.2 - Monthly diurnal variation during 2001	51
Figure 5.3 - Monthly average and standard deviation for each month in 2009	55
Figure 5.4 - Monthly average and standard deviation for each month in 2001	61
Figure 5.5 - Seasonal variability during 2009	67
Figure 5.6 - Seasonal variability during 2001	68
Figure 5.7 - The monthly TEC average contour plots for low (left) and high (right) solar activity.	70
Figure 5.8 - TEC for March and September Equinoxes for 2009 (top panel), and 2001 (bottom panel)	72
Figure 5.9 - Correlation of TEC with solar flux for March and September Equinoxes	73
Figure 5.10 - Local time and longitudinal variations of vertical drift (m/s) in	

two equinoxes.	75
Figure 5.11- Diurnal TEC variation from typical SAMI2 physics-based model.	77
Figure 5.12 - Latitudinal distribution of March and September Equinoxes at 1400LT for 2009.	78
Figure 5.13 - Latitudinal TEC variation and the temperature and O/N ₂ ratio for 2009 from typical SAMI2 model	80
Figure 5.14 - Latitudinal TEC variation for 2001 from typical SAMI2 model.	81
Figure 5.15 - The latitudinal variation of mean TEC during all seasons of 2009 at 1400LT.	84
Figure 5.16 - Distribution of TEC variation as function of season and location.	86
Figure 5.17 - The Power spectra analysis distribution of 2009 hourly average TEC contour plots for Cachoeira, Porto Alegre, Arequipa and São Luís from top to bottom respectively. The vertical axis represent the daily period and the horizontal axis represent the day of the year.	88
Figure 5.18 - The Power spectra analysis distribution of 2009 solar minimum daily average TEC contour plots of Cachoeira, Porto Alegre, Arequipa and São Luís from top to bottom respectively. The vertical axis represent the daily period and the horizontal axis represent the day of the year.	90
Figure 5.19 - Power spectra analysis distribution of 2009 solar minimum daily average zonal wind, meridional winds and solar flux from top to bottom respectively. The vertical axis represent the daily period and the horizontal axis represent the day of the year.	91
Figure 5.20 - The Power spectra analysis distribution of 2001 solar maximum daily average TEC contour plots of Cachoeira, Porto Alegre, Arequipa and São Luís from top to bottom respectively. The vertical axis represent the daily period and the horizontal axis represent the day of the year.	93
Figure 5.21 - Power spectra analysis distribution of 2001 solar maximum daily average zonal wind, meridional winds and Solar flux from top to bottom respectively. The vertical axis represent the daily period and the horizontal axis represent the day of the year.	94
Figure 5.22 - Summary of stratospheric and geomagnetic conditions for the winter solstice of 2008–2009 SSW events.	97
Figure 5.23 - Vertical drift observations by Jicamarca radar (12°S, 75°W) at 200-500 Km above the ground.	98
Figure 5.24 - Latitudinal TEC variation as a function of local time during the January 2009 SSW event	99

Figure 5.25 - Summary of stratospheric and geomagnetic conditions for the winter solstice of 2007–2008 SSW events.	101
Figure 5.26 - Latitudinal TEC variation as a function of local time during the January 2009 SSW.	103
Figure 5.27 - The TEC variation as a function of local time during for the geomagnetic latitude of 60°W February 2008 SSW events.	106
Figure 5.28 - TEC mapping for days 10, 21, 24, 26, 28 and 30 of January 2008.	108
Figure 5.29 - TEC mapping for days 10, 21, 24, 26, 28 and 30 of January 2009.	109

LIST OF TABLES

Table 4.1 - List of RBMC and IGS stations used.	40
Table 4.2- Monthly mean solar indices	42
Table 4.3 : RINEX observation format	43

TABLE OF CONTENTS

1.0	INTRODUCTION	1
1.1	Aims and objectives	2
1.2	Motivation	2
1.2.1	Review on TEC	3
1.2.2	Review on SSW	4
1.3	Final Remarks	6
2.	EARTH'S ATMOSPHERE AND THE IONOSPHERE	7
2.1	Earth's atmosphere	7
2.2	Layers of the atmosphere	8
2.3	The earth ionosphere and its variability	9
2.4	Ionospheric layers	10
2.4.1	Low and equatorial latitudes	12
2.4.2	Middle latitude ionosphere.	13
2.5	E and F dynamo	15
2.5.1	E dynamo	15
2.5.2	F dynamo	17
2.6	Altitude variation of conductivity	18
3.	TEC MEASUREMENTS AND INSTRUMENTATION	21
3.1	Global Navigation Satellite System (GNSS)	21
3.2	Description of GPS	22
3.3	GPS signals structure	26
3.3.1	Pseudo random code	28
3.3.2	Ephemeris data	28
3.3.3	Almanac data	28
3.4	Sources of GPS signal errors	29
3.5	The effects of the ionosphere on the GPS signals	29
4.	METHODOLOGY AND STATISTIC USED	31
4.1	Nagoya model approach	31
4.1.1	Calculation of TEC from Pseudorange observation	31
4.1.2	Calculation of TEC from Carrier phase measurement	32

4.1.3	Leveling of the Carrier phase with the Pseudorange	33
4.2	Absolute TEC	33
4.3	The estimation of TEC map	34
4.4	Statistical method	36
4.5	Data used	37
4.6	RINEX Format	42
5.	RESULTS AND DISCUSSION	45
5.1	Diurnal variability	45
5.1.1	Diurnal variation in TEC for Solar Minimum of 2009	46
5.1.2	Diurnal variation in TEC for Solar Maximum of 2001	50
5.1.3	TEC Monthly Variability for 2009	54
5.1.4	TEC Monthly Variability for 2001	59
5.1.5	Seasonal variability in TEC	65
5.1.6	Monthly and seasonal TEC variation.	69
5.2	TEC equinoctial asymmetry	71
5.2.1	TEC diurnal variation using the Sami2 Ionospheric Model	76
5.2.2	Latitudinal TEC variation asymmetry between March and September	77
5.2.3	Latitudinal variation and seasonal evolution of TEC	82
5.2.4	Analysis of general TEC distribution	85
5.3	Wavelet analysis	87
5.4	Study of 2007-2008 and 2008-2009 Sudden Stratospheric Warmings effects over TEC	95
5.4.1	2008 - 2009 SSW observations	96
5.4.2	2007 - 2008 SSW observations	100
6.	CONCLUSIONS	111
6.2	FUTURE WORKS	115
	REFERENCES	117

1. INTRODUCTION

Exploring the ionosphere is of utmost interest due to the numerous complexities associated with the region. Although, over the last century humanity has learned to use the properties of the ionosphere in a tremendous ways, there are more to understand about the chemical and physical changes of this region of the Earth's atmosphere. One of the parameters that can be used to study the ionosphere is the Total Electron Content (TEC). It is an important descriptive quantity for the ionosphere. TEC is the integral of electron number density along the line of sight path from the satellite to the receiver and can vary dramatically (e.g. RASTOGI; KLOBUCHAR, 1990). In this study the plasmaspheric electron content was not considered.

Study of TEC variability over the South American continent is useful to investigate the processes responsible for the ionospheric behavior over this region. TEC is significant in helping us to understand the short and long term changes of our upper atmosphere during major phenomena caused by factors like solar activities, geomagnetic storms and meteorological influences. (e.g. FORBES et al; 2000, KANE, 2003, RISHBETH AND MENDILLO, 2001). Among the various phenomena in the ionosphere, TEC is responsible for time delay which produces range errors in the GPS radio signal of a satellite to ground radio communication. At the same time, the perturbations in the GPS signals can be used as scientific information to investigate the ionospheric variability.

These changes in the ionosphere affect navigation systems, surveillance systems and modern technologies such as communication systems since the signal from the satellite to the receiver must pass through the ionized layer (BAGIYA et al., 2009). As a consequence, a good description of the ionosphere is needed in order to improve the performance of the ionospheric models (BILITZA, 2000). Hence it is necessary to study the properties of the ionosphere such as its variability with respect to time of the day, season of the year, solar cycle, lunar tide effect, sudden stratospheric warming effect and magnetic storms effects. In this study however, the magnetic storm effects on TEC will not be analyzed

A lot of ionospheric studies have been observed mainly during disturbed time globally (e.g. DE PAULA et al., 2006, FEDRIZZI et al. 2001, TSURUTANI et al. 2008, DE SIQUEIRA et al. 2011, etc.), and only a few studies have been made for quiet time period. Yet the motions in the upper atmosphere are of two kinds, those whose immediate sources of energy are confined in the

upper atmosphere itself and those whose energy are transmitted from the lower atmosphere (CHARNEY AND DRAZIN; 1961).

Therefore, this study aims at general understanding of quiet time TEC variations in the South America regional sector and how the Sudden Stratospheric Warming (SSW), and Lunar tide effects could as well be a contributor to the ionospheric TEC variations over this region.

Data used in this study were obtained from International GNSS Service (IGS) and Rede Brasileira de Monitoramento Contínuo (RBMC). The absolute TEC values were obtained using the Nagoya ionospheric model (OTSUKA et al., 2002). Only quiet time data were analyzed and the geomagnetic Kp index ≤ 3.0 was used to specify such condition.

1.1 Aims and Objectives

This study will investigate the following variations of TEC:

1. The day-to-day variability
2. The monthly and seasonal variability
3. The variation with solar activity
4. The effect of SSW
5. Latitudinal and longitudinal effect including EIA
6. The TEC periodicities

The mechanisms responsible for the TEC variations are also investigated in this work.

1.2 Motivation

The South American sector is associated with highly variable electrodynamic processes which are particularly prominent at the equatorial and low-latitude regions. The declination of the magnetic field lines is the highest at the Brazilian region. The gradient between the trough and the crest is very sharp at this region, which results in large temporal and spatial variation of the ionospheric electron content (DASGUPTA et al., 2007). The ionized particles in the ionosphere are produced mainly during the daytime through absorption of solar extreme ultraviolet (EUV) and X-ray radiation by the atmospheric neutral species. Largest fraction of the solar radiant energy is centered mainly at the equatorial and low latitude regions, hence many interesting phenomena are presented at these regions.

The electron density of the ionosphere in the low latitudes exhibits a trough at the magnetic equator with two crests on both sides of the equator from ± 15 up to ± 20 magnetic latitudes. This

is referred to as the Equatorial Ionization Anomaly (EIA). The eastward electric field during daytime as a result of photoionization due to EUV radiation, followed by ionization diffusion along the magnetic field lines, contributes mainly to the development of this anomaly.

During geomagnetic quiet periods, the low-latitude electric field result from complex interactions of E and F region dynamos. According to Abdu (2005), the dynamo zonal electric fields cause major formation and structure of the ionosphere and the integral phenomenology of the equatorial and low latitude ionosphere during quiet conditions.

1.2.1 Review on TEC

Many researchers have studied the morphological features of TEC at low and equatorial latitudes (RAMA RAO et al., 2006 AND BHUYAN, 1992). Abdu et. al., (2007) studied the solar flux effects on equatorial ionization anomaly and total electron content over Brazil using maximum frequency of F2 layer (foF2) data set between 1996 - 2003 and TEC data set between 2002 - 2003. They found similar solar flux dependence of seasonal variation in both foF2 and TEC which shows maximum during equinox and minimum during June solstice. Solar activity dependence of TEC has also been studied by a large number of researchers (BALAN et al., 1993 and reference there in). Kane (2003) studied day-to-day variability of quiet-time ionosphere using foF2 data. He observed oscillations of day-to-day variation with peak spacing of ~7 days at several locations and he indicated that in the absence of solar or geomagnetic effects, planetary waves dominate the day-to-day variability. Batista and Abdu (2004) studied the ionospheric variability using the foF2 parameter over the Brazilian low and equatorial latitudes and comparing their results with IRI model. The climatology derived from TOPEX/POSEIDON measurements has also been investigated by many authors (e.g. CODRESCU et al., 1999 and 2001, JEE et al., 2004 and SCHERLISS et al. 2008). They established many interesting facts about longitudinal, seasonal, wave number four, and geomagnetic variation. Dabas et al.(1993) studied the variations in TEC with different solar indices, i.e. EUV, F10.7 solar flux and smoothed sunspot number (SSN) for summer, winter and equinoxes. They concluded that TEC exhibited nonlinear relationship with SSN in general and linear variations with EUV and F10.7 solar flux. Rama Rao et al. (2006) presented the temporal and spatial variations in TEC derived from the simultaneous and continuous measurements for the first time using the Indian GPS network of 18 receivers located from the equator to the northern crest of the equatorial ionization anomaly (EIA) region and beyond, covering a geomagnetic latitude range 10 - 24⁰N. In the analysis, they used 16 month data for the low sunspot activity period of

March 2004 - June 2005. In their findings, along with the diurnal and seasonal variations in TEC, the day-to-day variability was also significant at all the stations, particularly during the daytime, with maximum variations at the EIA crest regions. Bagiya et al. (2009) investigated diurnal and seasonal variations of TEC during low solar activity period (2005-2007) at Rajkot, a station near the equatorial ionization anomaly crest in India. It was found that TEC was maximum during equinoctial months (March, April, September and October) and minimum during winter months (November, December, January and February), with intermediate values during summer months (May, June, July and August).

1.2.2 Review on SSW

Large scale electrodynamics and plasma density variation of the ionized layer have been recently associated with SSW event which has been a subject of intensive study (FEJER et al., 2011).

SSW is a phenomenon characterized by a sudden temperature increase in the winter polar stratosphere. The interaction between the zonal mean flow and the growth of vertically propagating planetary waves is known to be the major driver of winter stratospheric dynamics (MATSUNO, 1971). The SSW was first observed in 1950s (SCHERHAG, 1952, 1960 and BROWN and WILLIAMS, 1971) and since then many literatures have reveal the coupling between stratosphere and ionosphere (e.g. CHAU et al., 2010, FEJER et al., 2010, LIU et al., 2011 and FULLER-ROWELL et al., 2011). Although the physics behind atmospheric tides and planetary waves influences over the ionosphere are generally well understood, it is not still certain about the processes responsible for generating ionospheric variability in connection with SSWs. Evidence from Goncharenko and Zhang (2008) shows a primarily semidiurnal modulation of the ionosphere during the 2008 SSW and they suggested that enhanced planetary wave activity associated with SSWs play an important role in producing the ionospheric perturbations. It is clear from the conclusion of Fejer et al. (2011) and Park et al. (2012) that SSW event is an amplification of lunar tide that modulates the low-latitude and mid-latitude ionosphere. Liu et al. (2010) proposed that the observed semidiurnal perturbations in the ionosphere are due to the nonlinear interaction between migrating tides and planetary waves. However, significant changes in the tidal winds were found to occur in the low latitude E region where electric fields are generated by the dynamo mechanism, resulting in modulation and enhancement of the vertical drift velocity and electron densities in the ionosphere. According to Pancheva et al. (2009) intensified nonmigrating tides linked with the nonlinear interaction between planetary waves and migrating tides could also be observed in the stratosphere and lower mesosphere temperatures during the 2003/2004 SSW. For further clarification about

SSW, it is important to mention its classification, which are into three categories: major, minor and final warming (SCHERHAG, 1952).

Major SSW occur when the eastward winds reverse, i.e. become westward. A complete disruption of the polar vortex is observed and the vortex will either be split into daughter vortices as shown in Figure 1.1, or it will be displaced from its normal location over the pole. This Figure 1.1 shows the first recorded major warming in the Southern Hemisphere region splitting the vortex and tearing the normally quiescent Antarctic ozone hole into two parts. The event started on 15 September when the vortex was characterized by levels of potential vorticity (PV) with a sharp gradients of PV in the associated strong eastward jet stream. On September 20, a few days prior to the split, the vortex was elongated showing a precondition state to the split. By 25 September the split had occurred leading to two distinct centers of high PV connected by a long thin streamer of air stronger at one end of polar vortex (around Antarctica and Australia) and weaker at the other end (around South Atlantic). Once splitted the individual vortex are rapidly weakened by the shearing out of PV around the split vortexes, as indicated on 30 September. We noted (from the average mean temperature of 30 years) that polar temperature during this period was extremely high, indicating that the event was an unprecedented event of the southern hemisphere at least in the past 24 year.

Minor SSW are similar to major warmings however they are less dramatic, the eastward winds are slowed, but do not reverse. Therefore a breakdown of the vortex is never observed.

Final warming: since atmosphere mean flow is eastward during winter and during summer it is westward, a final warming occur when polar vortex winds change direction for the warming and do not change back until the following winter because the stratosphere has entered the summer westward phase. Therefore another warming cannot take place over the summer, hence it is the last warming of the current winter.

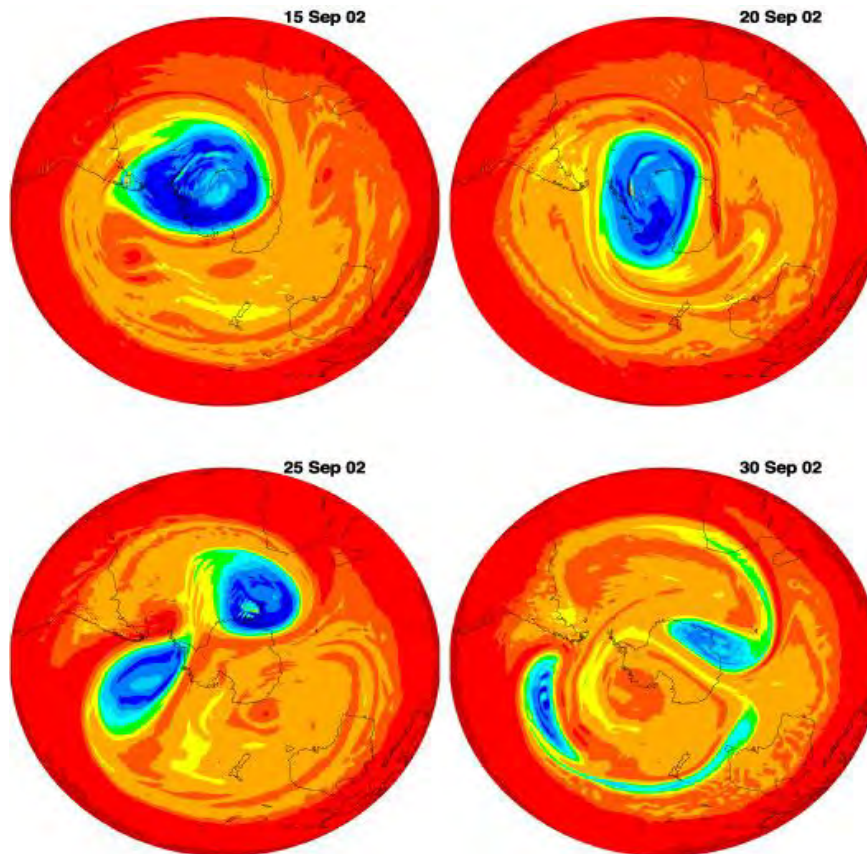


Figure 1.1: Time evolution of the polar vortex for the Antarctica region on the dates shown during September 2002.

Source: http://www.knmi.nl/gome_fd/index.html

1.3 Final Remarks

Most of the literatures reviews suggests many important mechanisms and results which are consistent in our study. However their argument did not take account of the whole of South America region which is the focus of our study. Using GPS-TEC from most of the receivers over South America sector, we intend to provide observational evidence that clearly demonstrates how the ionization phenomena at the EIA and generally over the South American continent is affected by solar flux intensity, by season, by each month of the year, by day-to-day variability as well as by the SSW events of 2008 and 2009 during geomagnetic quiet periods and how these TEC variability could affect the behavior of the EIA, taking into consideration the aforementioned mechanisms.

2. THE EARTH ATMOSPHERE AND THE IONOSPHERE

2.1 Earth's Atmosphere

The envelop of gases surrounding the earth, which is a stable mixture of several types of gases from different origins is known as the atmosphere. It is kept in space by gravitational attractions. Nitrogen and Oxygen make up to 99% of the atmosphere at sea level, with the remainder comprising CO₂, noble gases and traces of many gaseous substances. Based on the temperature changes with height, the Earth's atmosphere can be divided into mainly four distinct regions: troposphere, stratosphere, mesosphere and thermosphere. The ionosphere is bounded in the region of thermosphere, and it is a layer under investigation in the research work and shall be discussed in more detail. Figure 2.1 illustrates atmospheric temperature profile and ionospheric density profiles.

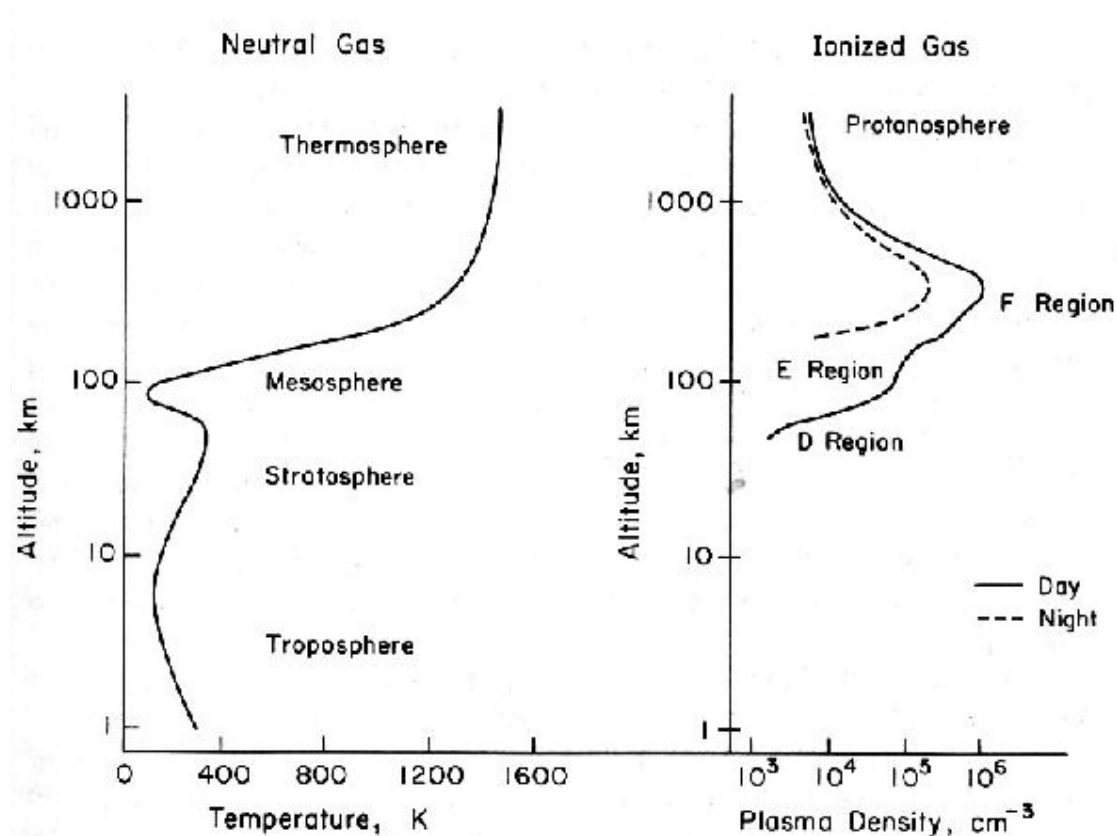


Figure 2.1 - Illustration of the layers of the neutral atmosphere with temperature and the layers depending on the ionospheric electron density profiles.
SOURCE: Rishbeth and Garriott (1969).

2.2 Layers of the Atmosphere

Troposphere: is the lowest part of the atmosphere and extends to the altitude of 8 km above the poles and 18 km over the equator. The temperature generally decreases with height in the troposphere. The troposphere contains 99% of water vapor in the atmosphere which plays a major role in regulating air temperature because it absorbs solar energy and thermal radiation from the planet's surface. The layer is bounded at the top by the tropopause (RISHBETH AND GARRIOTT, 1969)..

Stratosphere: The stratosphere is also an important layer to this research work because this is where the SSW is initiated. It is the second layer of the earth's atmosphere, and it starts at an altitude of 8 km - 18 km and extends up to 50 km. It is so named because the stratified layers within it have a temperature profile that increases with altitude (MOHANNAKUMAR, 2008). The stratosphere holds the ozone that absorbs harmful UV radiation and prevents it from reaching the earth's surface. Every winter the stratosphere over the pole at the winter hemisphere cools, this begins when the sunlight can no longer provide the energy to heat the ozone. Without this energy, the stratosphere cools rapidly, creating a thermal imbalance with the warmer stratosphere further south. This imbalance creates a large pressure difference and combined with the Coriolis effect, creates a large strong jet stream, spring the globe in the stratosphere in the eastwards direction (this is most famous in the Antarctica and Arctic region due to extremely low temperature in this region). This system is known as the polar night jet, and a strong vortex known as the polar vortex is contained within it. The polar vortex increases and decreases in strength depending upon how cold the polar stratospheric atmosphere becomes during winter. The colder the polar stratosphere becomes, the stronger the polar vortex - and vice versa. This action leads to generation of ozone hole and the consequent split of the polar vortex company by a rise in stratospheric temperature. This event is referred to as SSW whose effects on TEC will be analysed in this work. The stratospheric layer is bounded at the top by the stratopause.

Mesosphere: is a layer that extend from 50 to 80 km and characterized by decrease in temperature with increasing altitude. The region is considered to be the coldest of Earth atmosphere reaching a minimum of ~180 K at 80 km altitude. The chemical compositions are fairly uniform and pressures are very low. The layer is bounded at the top by the mesopause.

Thermosphere: is a region of high temperature and density is very low. The thermosphere include the ionosphere and extend out to several hundred kilometers. The temperature increase is due to the absorption of intense solar radiation by the limited amount of molecular oxygen present. The thermopause is the level at which the temperature stops rising with height which depend on the solar activity.

2.3 The Earth Ionosphere and its Variability

The ionosphere is a partially ionized region of the earth's upper atmosphere. It comprises of free electrons and ions, generally in equal numbers, in a medium that is electrically neutral (HUNSUCKER; HARGREAVES, 1995). The ionosphere extends approximately from about 60 to 1000 km. The main sources of ionization are the solar radiations such as extreme ultra violet (EUV) and X-ray radiations. Apart from photoionization, ionization by collisions of energetic particles due to particle precipitation from the magnetosphere at the aurora latitudes is another source of ionization at the topside ionosphere (KELLEY, 1989). The processes explained above lead to the production of plasma which undergoes chemical reactions with the neutrals, diffuses due to the gravitational force and pressure gradients, and it is transported through neutral winds and electric field under the influence of the earth's magnetic field.

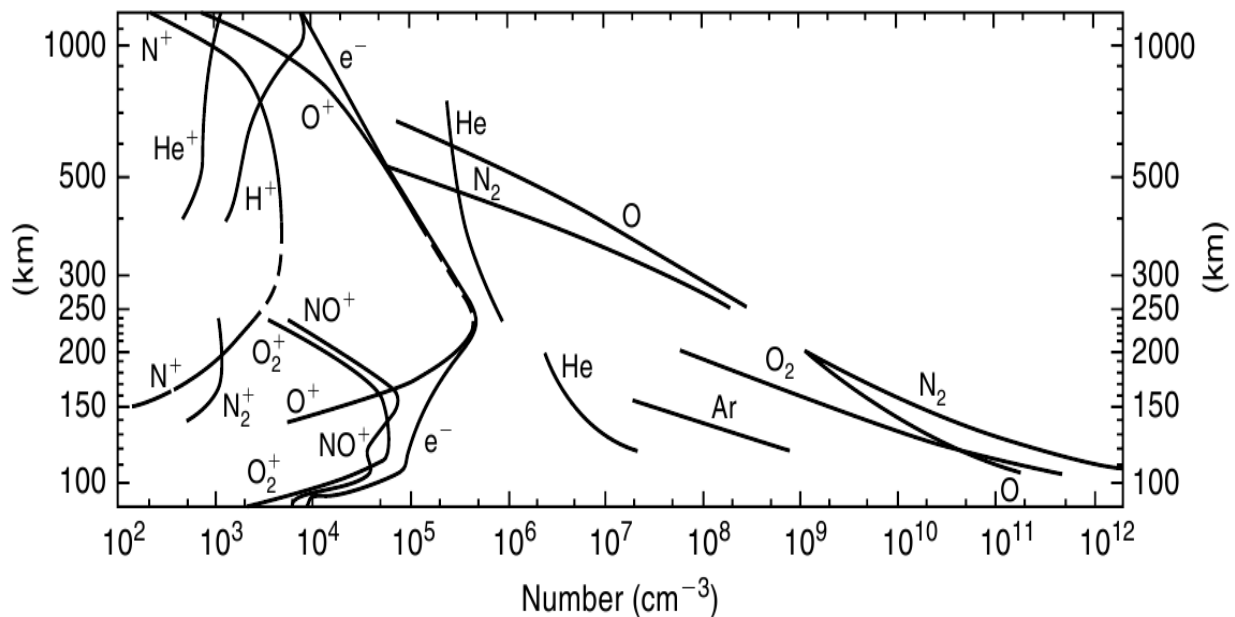


Figure 2.2 - Typical vertical profile of the electron ions and neutral densities in the mid-latitude
Source: Kelley (1989)

As a result of the altitude variations in the atmospheric neutral composition and the production rate with altitude, the plasma density in the ionosphere has vertical layer structures, which are denoted by the D, E, F layers. These layers are controlled by different physical and chemical processes and have different composition of ions. The D and E regions are dominated by more molecular ions (O_2^+ , N_2^+ , NO^+) as shown in the Figure 2.2. The recombination rates at these regions with electrons is higher and hence leads to the disappearance of both layers after sunset. On the other hand, the F region is composed mostly of atomic ions (O^+ and H^+). The recombination rates with electron is much more lesser and therefore part of the layer is sustained during the night. The maximum electron density is obtained in the F region. Above the F2 peak is the topside ionosphere, where diffusion dominates and the chemical composition is H^+ and He^+ . The result of the processes of ionization and ion loss, along with the dynamics of ionospheric region, determine the electron density profile with different behaviors in their vertical structure depending on ionizing radiation, seasons, latitude as well as differences between the day and night, as illustrated in Figure 2.3.

2.4 Ionospheric Layers

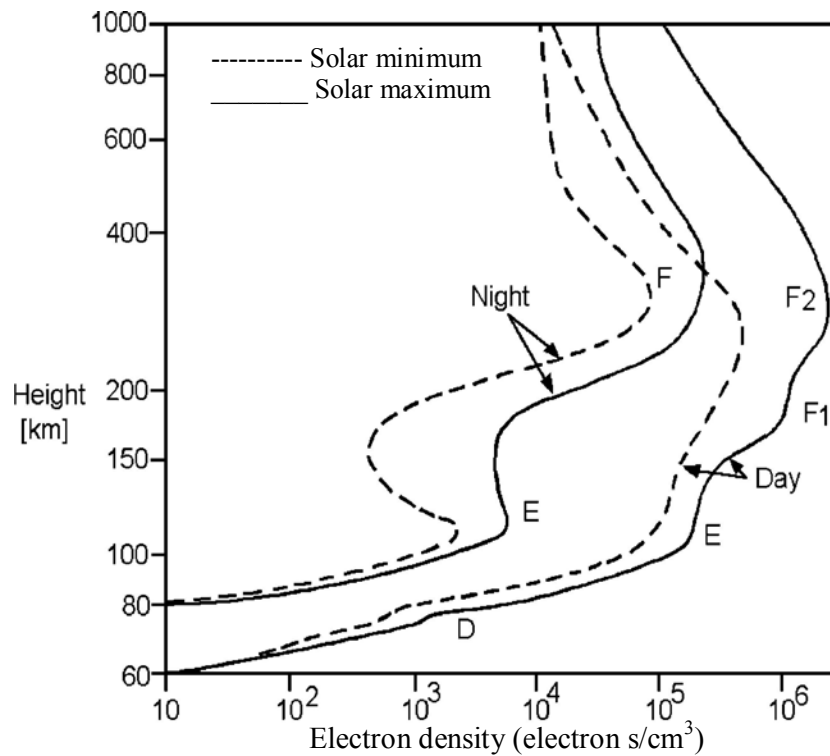


Figure 2.3. Vertical profile of the ionosphere

Source: Hargreaves (1992).

D Layer: Located at the bottom of the ionosphere up to ~ 90 km height. This region presents a complexity in chemical and photochemical processes which may be characterized by low density and high ionization collisions frequency of electrons with ions and neutral particles. There are three ionization sources in this region, these being X-rays, cosmic rays and Lyman- α radiation, which ionize only nitric oxide (NO). The chemical processes present in this region are quite complex and involve O, O₂, O₃, NO, NO₂, CO₂, H₂O and alkali metals. The ionization of this region is however very low ranging from 10^7 to 10^{10} e/m³ and as a result the HF radio waves are not reflected by this region which is then mainly responsible for absorption of high-frequency radio waves. When a radio wave enters the ionosphere, the free electrons are set into motion by the alternating electric field on the wave. The energy that is transferred from the wave to the free electrons is lost when the electrons collide with molecules. Therefore the greatest energy loss is in the D region, where the quantity $N\nu$ (N is the electron density, and ν the collision frequency between electrons and neutral molecules), to which the absorption loss is proportional, reaches its maximum value.

E Layer: Situated between 90-140 km high, is characterized by increased electron density between 90 and 110 km. This region of high conductivity is very important due to the presence of ionospheric electrical currents and the interaction of these currents with the Earth's magnetic field. The main sources of ionization are weak X-rays ($\lambda > 10 \text{ \AA}$) radiation, solar Lyman- β (1025.7 \AA) and EUV ($< 1000 \text{ \AA}$) ionizing the O₂, EUV ($< 900 \text{ \AA}$) ionizing the N₂. Within this region, due to different mechanisms, highly variable dense and thin layers (whose thickness varies from 0.2 to 2 km), called E sporadic (Es) layers, may develop. At mid- and low-latitudes the probability of occurrence of these Es layers is major during the summer daytime hours, while at high-latitudes the probability of occurrence is more pronounced at nighttime hours.

F Layer: Located approximately between 150-1000 km height. Its main sources of the ionization are Extreme Ultraviolet Radiation (EUV) lines and Lyman continuum of hydrogen. The dominant ion is O⁺. The F region can be characterized by two other layers, F1 and F2. In the equatorial region may create a third layer, named F3. The layer F1 is defined based on an inflection or a peak in the curve electron density around 180 km. It is in this region that the transition between the processes of linear and quadratic loss occurs. The F2 layer is located in vicinity of the peak electron density (~ 300 -400 km), and it is the region with higher ionization density of the ionosphere. Its formation is predominantly dependent of the winds and its

concentration varies with solar activity. The highest concentration of free electrons can be observed during the day, especially during local noon. During the night, this concentration decreases, but the layer remains due to low recombination of ion with neutral and wind transport effects. The equatorial meridional wind plays an important role in the nighttime F layer density maintenance. More explanations will be given in following sections.

In addition to the variation of the plasma density with altitude, the ionosphere also shows important changes with time of day, latitude, longitude, season, solar activity and geomagnetic activity. Latitudinal variation has a distinctive behavior due to the geometry of the Earth's magnetic field lines. Hence the ionosphere can be classified by three latitudes controlled by different physical processes: the low and equatorial, middle and high (aurora) latitude regions. In this study, focuses will be limited to the equatorial and low latitudes since the South American sector is located within these latitudes.

2.4.1 Low and equatorial latitudes

The larger fraction of solar energy is absorbed within $\pm 30^\circ$ latitude zone centered on the equator (Abdu, 2005), so it is expected to have larger ionization at the region. However, one of the most prominent features in the ionosphere, known as equatorial anomaly (also called the Appleton Anomaly), occurs at the low latitudes, given origin to a depletion at equatorial latitudes and two ionizations crest at low latitudes as explained below.

The electric field configuration, which is eastward during the day, produces an upward drift ($E \times B$ drift) leading to a plasma fountain. The lifted plasma by the fountain effect then diffuses downward along the geomagnetic field lines due to the gravitational force and pressure gradient, which result in the ionization enhancement on both sides of the magnetic equator at $\pm 15^\circ$ latitude.

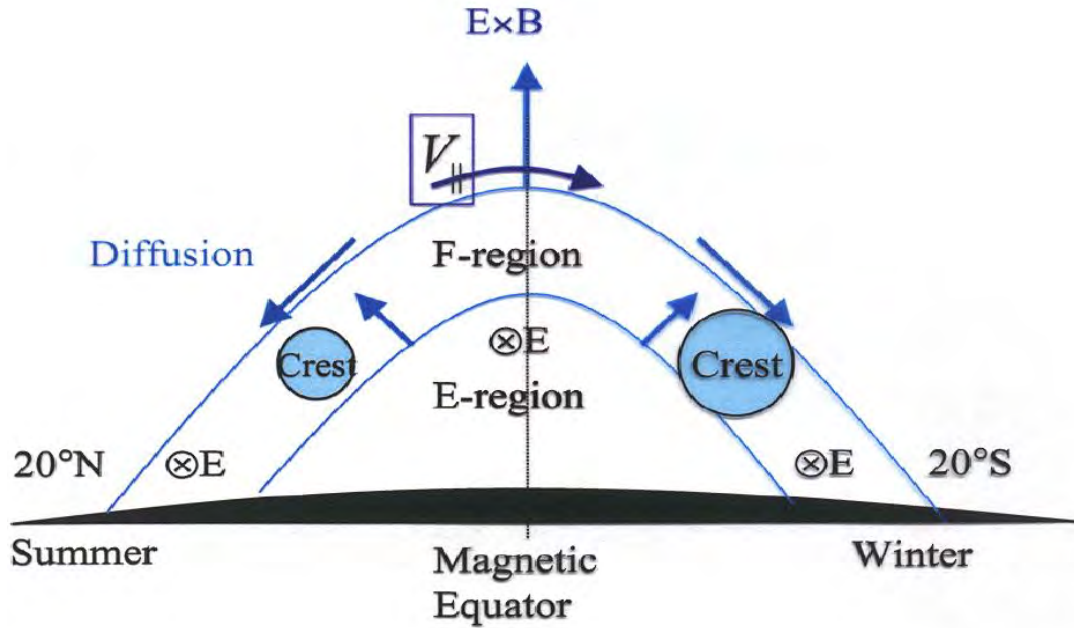


Figure 2.4 - Asymmetry of the Equatorial Ionization Anomaly. E denotes an eastward electric field and B is the northward geomagnetic field Scheme Anderson and Roble (1981).

The low latitude anomaly may exhibit asymmetry behavior between the northern and southern ionization crests due to an inter-hemispheric wind blowing from the summer to winter hemisphere. The behavior is represented in the Figure 2.4. In the summer hemisphere, plasma moves upward along the geomagnetic field lines, while plasma moves downward in the winter hemisphere. Therefore the plasma is transported from the summer hemisphere to the winter hemisphere. As a result, the equatorial anomaly crests in the winter hemisphere are generally larger than in the summer hemisphere (Figure 2.4).

2.4.2 Middle latitude ionosphere.

The middle latitude ionosphere is a relatively less variable and disturbed region and as a result of this, most of the ionosphere sensing instruments, observations and measurements are best obtained at this region.

This latitude is also usually free of the effects imposed by the horizontal magnetic field geometry associated by the equatorial region. The ionospheric plasma is constrained to move along the geomagnetic field lines (Figure 2.5) hence the thermospheric neutral wind effectively transport

plasma along the field lines into higher and lower altitudes regions in which recombination rates are different resulting in changes of the plasma density. The poleward neutral wind move plasma down to lower altitude where recombination rate is large during the day. As a result, the peak height of F2 is reduced and there is a decrease in the peak electron density but during the night the typically equatorward wind move plasma up. Therefore the recombination of the plasma with neutrals decreases, the peak height increases and the night time peak electron density is partially maintained.

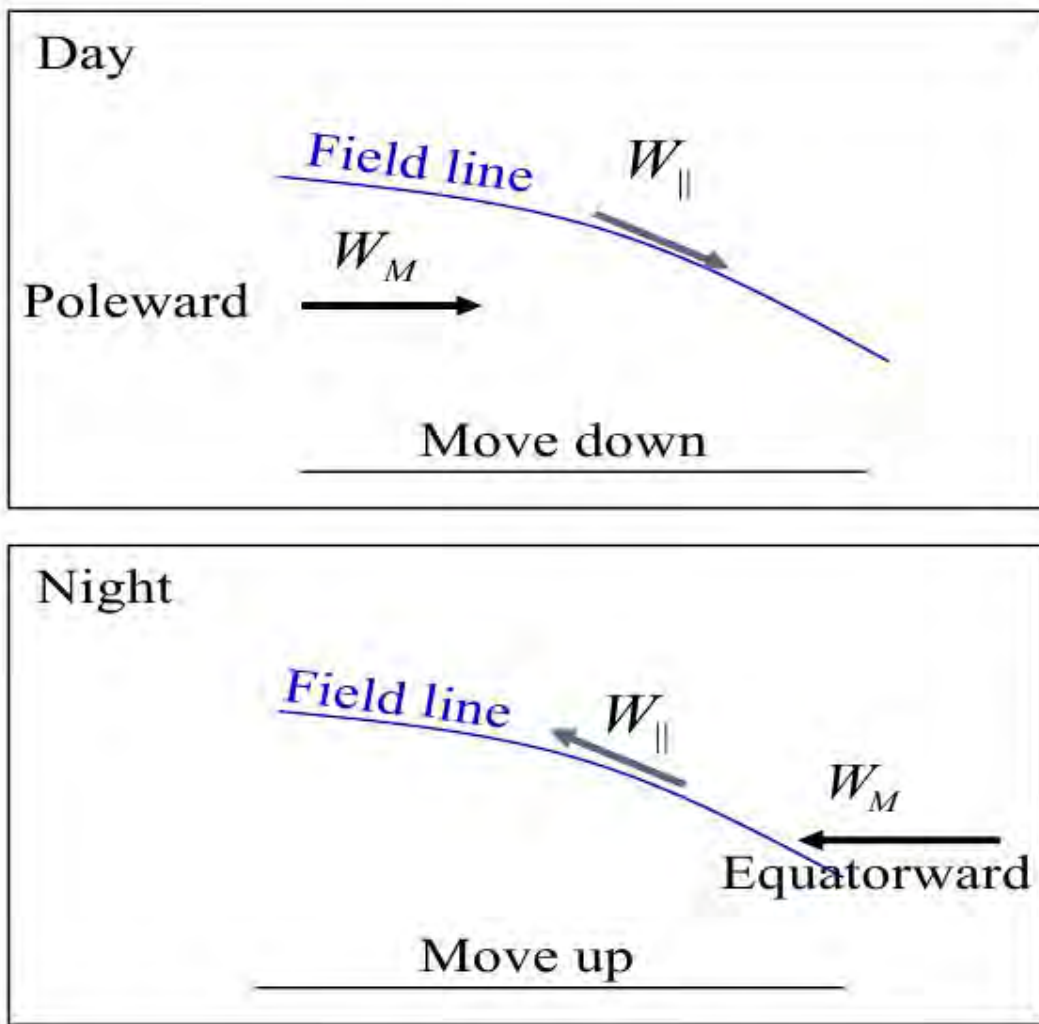


Figure 2.5. Vertical plasma drifts due to the meridional neutral wind (W_M). W_{\parallel} is the meridional wind component along the geomagnetic field line.

2.5 E Region and F Region Dynamo

The ionosphere acts not only as the reflection or absorption layer of the radio wave, but also as an electric current layer. Low latitude electric fields, plasma drifts and ionospheric currents result largely from the dynamo action of E and F neutral winds, but can be significantly perturbed by lower atmospheric gravity and planetary waves during magnetically quiet times. (e.g., Richmond 1994 and Abdu 2005) . The E layer dynamo electric field mapped along the highly conducting magnetic field lines controls the plasma dynamic/transport of the equatorial F-region during the day, whereas the F dynamo electric field can develop only during the night as result of the disappearance of E layer conductivity after sunset.

2.5.1 E Region Dynamo

The electric fields are generated in the E region by ionospheric dynamo driven by atmospheric tidal winds (Heelis et al., 1974). The winds, which are established by the absorption of solar radiation in the stratosphere and troposphere, affect the movement of charged particles. Ions and electrons assumes a cyclotron movement in the present of the magnetic field (\vec{B}). The interaction between the tidal wind (\vec{U}) and \vec{B} gives rise to a relative movement between the ions and electrons which leads to an induced electric field as a result of $\vec{U} \times \vec{B}$. The induced current associated with this is not stationary, i.e. $\vec{\nabla} \cdot \vec{J} \neq 0$. This makes electric field polarization (\vec{E}_p) to be established in the E region without any current divergent. The total electric field in this ionospheric region:

$$\vec{E} = \vec{E}_p + (\vec{U} \times \vec{B}), \quad (2.1)$$

and the total current flowing in the same direction of the field can written as:

$$\vec{J} = \sigma \cdot \vec{E} \quad (2.2)$$

where σ is the electrical conductivity tensor.

Substituting equation (2.1) in (2.2) we have:

$$\vec{J} = \sigma \cdot (\vec{E}_p + \vec{U} \times \vec{B}). \quad (2.3)$$

The current flowing in a conductor, which in this case is the E region, is not divergent, then the divergent of equation 2.3 gives:

$$\vec{\nabla} \cdot \vec{J} = \vec{\nabla} \cdot (\sigma \cdot (\vec{E}_P + \vec{U} \times \vec{B})) = 0 \quad (2.4)$$

According to Kelley (2008), the physics of the dynamo region can be understood by considering it as a conductive thin plate subjected to a constant zonal electric field (\vec{E}_x), perpendicular to \vec{B} as shown in Figure (2.6).

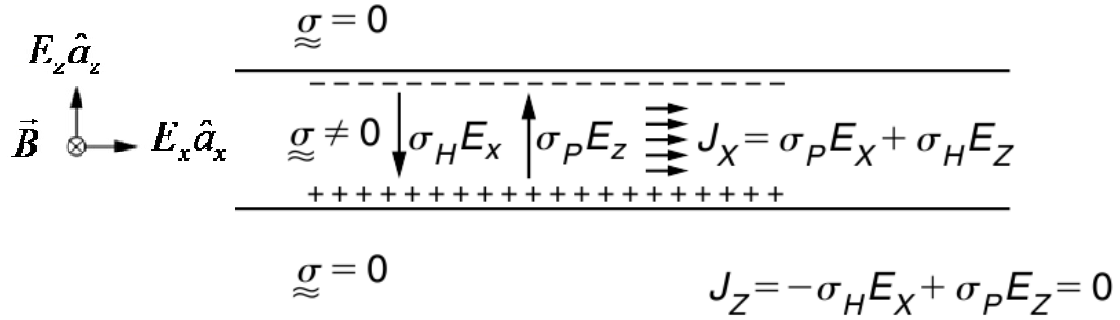


Figure 2.6 - E region electrodynamics.

Source: Kelley (2008).

The \vec{B} and the electric field in the region are perpendicular to each other. There are essentially two types of current in the equatorial E region, which are the Hall and Pederson current. The Hall current ($\sigma_H E_x$) flows in the direction perpendicular to both electric field (\vec{E}_x) and the \vec{B} , while the Pederson current ($\sigma_P E_x$) flows parallel to the electric field (\vec{E}_x) and perpendicular to \vec{B} . The Hall current cannot flow across the boundary and this leads to accumulation of charges at both boundary. These accumulated charges gives rise to upward electric field polarization ($E_z \hat{a}_z$). In response to this polarization, the Hall current ($\sigma_H E_x$) and the Pederson current ($\sigma_P E_z$) are in steady state but no vertical current can flow hence both Pederson and Hall current cancels. This gives:

$$\sigma_H E_x = \sigma_P E_z \quad (2.5)$$

Dividing both side by σ_P :

$$E_z = \left(\frac{\sigma_H}{\sigma_P} \right) E_x \quad (2.6)$$

In the horizontal direction the current add up and then form an intensified field called equatorial electrojet:

$$J_x = \sigma_H E_z + \sigma_P E_x \quad (2.7)$$

Substituting equation (2.6) at (2.7) we have:

$$J_x = \left[\left(\frac{\sigma_H^2}{\sigma_P^2} \right) + 1 \right] \sigma_P E_x = \sigma_C E_x \quad (2.8)$$

Where σ_C is called Cowling conductivity. The equatorial electrojet is determined by tidal winds that create the global component of the daily zonal electric field measured at the equator. It is the strong current around $\pm 3^\circ$ latitude of the geomagnetic equator.

2.5.2 F Region Dynamo

While the E layer dynamo electric fields are generated by winds associated with the tidal waves arising from solar ultraviolet radiation (UV) absorption in the ozone layer and atmospheric water vapor, as well as from lunar gravitational field, the thermospheric winds that are responsible for the F layer dynamo electric fields results from solar thermal tides arising from the solar extreme ultraviolet radiation (EUV) absorption in the thermosphere (ABDU, 2005).

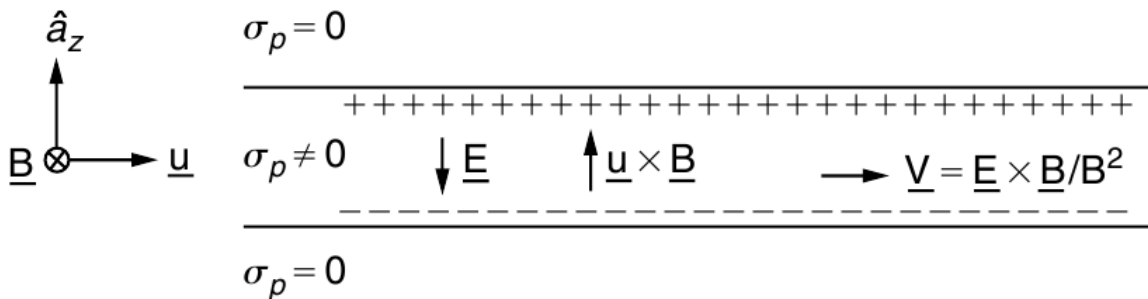


Figure 2.7 - F region electrodynamic.

Source: Kelley (2008).

Figure (2.7) illustrates the electrodynamic of F region as a narrow conducting thin layer. σ_P is constant inside the layer and zero elsewhere and zonal wind U is constant everywhere. The

thermospheric winds cause induced motion of charged particles in the direction of $\vec{U} \times \vec{B}$. The movement perpendicular towards both \vec{B} and the wind itself, gives rise to an electric field which tend to establish a polarization field as a result of accumulated charges at the two boundaries as shown in Figure (2.7).

During the day conductivity is large in the E-region and there is high mobility across magnetic field lines, which behave as good conductors, and then the electric field polarization is discharged by current flowing along magnetic field line through the E region and thus close the circuit between the E and F layer. During night hours when conductivity of E decreases drastically, the circuit is not closed, this give rise to electric field polarization resulting in the movement of plasma along the magnetic field lines (Rishbeth, 1971 and Heelis et al., 1974). The drift velocity of the motion can be represented by the equation:

$$\vec{V} = \left(\frac{\vec{E} \times \vec{B}}{B^2} \right) \quad (2.9)$$

2.6 Altitude Variation of Conductivity

The ionosphere conductivity is due to the drift motion of the electron ($E \times B$ drift) and presents its maximum in the E region where only electron practically drifts to the direction of $E \times B$. The conductivity depends on various parameters such as location, time, season and solar activity. There are three types of conductivity: Parallel conductivity which is usually in the direction parallel to the magnetic field line and denoted as " σ_0 ", Pedersen conductivity which is usually in the direction perpendicular to the magnetic field and parallel to the electric field - it is denoted as " σ_1 ", and Hall conductivity in the direction perpendicular to both the magnetic and electric fields. It is denoted as " σ_2 ". The vertical profiles of these conductivities are presented in Figure 2.8.

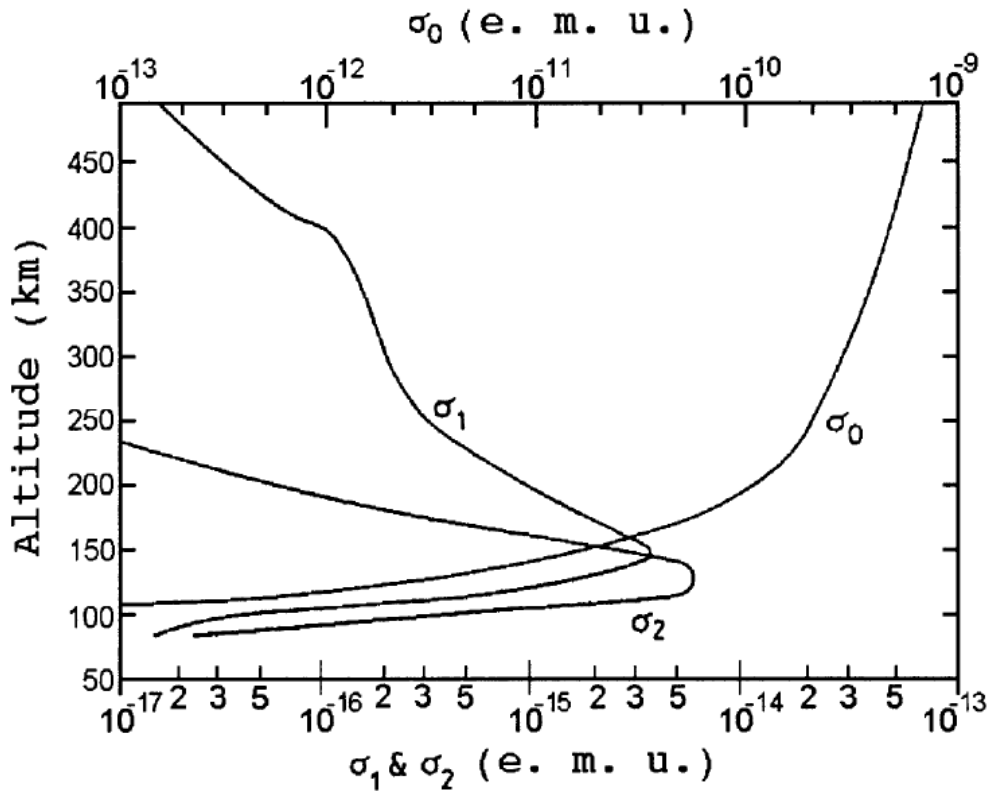


Figure 2.8: Vertical profile of the Parallel (σ_0), Pederson (σ_1) and Hall (σ_2) conductivities.
Source: Abdu (2005)

Figure 2.8 also shows Pederson conductivity peak at around 140 km and the Hall conductivity peak at around 120 km. Their values decrease rapidly above and below these heights (Abdu, 2005).

The conductivity parallel to the magnetic field increases strongly with altitude due to decreasing collisions with the neutral gas. The parallel conductivity is always much higher than the conductivity perpendicular to the magnetic field.

The movement of a class of charged particles perpendicular to the magnetic fields depends on the ratio of the collision frequency (ν) to the gyrofrequency (ω_g). If $\nu \gg \omega_g$ then collisions prevent the particle from gyrating and the particles move in the direction of the electric field, as a Pedersen current. If, on the other hand, $\nu \ll \omega_g$ then the particles predominantly drift perpendicular to the electric field.

3. TEC MEASUREMENTS AND INSTRUMENTATION

Many measuring instruments have been used to measure TEC value for decades. For example the Faraday rotation, Ionosonde and the Incoherent Radar systems located close to the magnetic equator in Peru. However, nowadays TEC measurements are often made using GNSS data because of the improved global coverage of the GNSS observation network. Ionospheric TEC has been widely studied using GNSS observations in recent years (e.g. CAMARGO 2009, BAGIYA et al. 2009, MUELLA et al. 2010, KELLEY et al., 1996; HO et al., 1996; AARONS et al., 1996; BEACH et al., 1997; etc). The related equations and estimation of GPS-TEC are discussed in the next section 4.

3.1 Global Navigation Satellite System (GNSS)

The GNSS is a constellation of satellites which provides global coverage of signals from space transmitting positioning and timing data. Examples of GNSS are the USA's NAVSTAR Global Positioning System (GPS), Russia's Global'naya Navigatsionnaya Sputnikovaya Sistema (GLONASS), and the new Europe's Galileo system. The accuracy and integrity of GNSS can be greatly enhanced by the use of augmentation information derived from various sources such as: Space Based Augmentation Systems (SBAS) (for example the European Geostationary Navigation Overlay Service (EGNOS) in Europe and Asia, Wide Area Augmentation System (WAAS) in USA, Multi-functional Satellite Augmentation System (MSAS) in Japan, as well as the GPS Aided Geo Augmented Navigation (GAGAN) system in India).

3.2 Description of GPS

GPS consist of three segments showed in Figure 3.1: the space segment is formed by the satellite constellation, the control segment is formed by the monitoring stations and the user segment is formed by the GPS receivers.

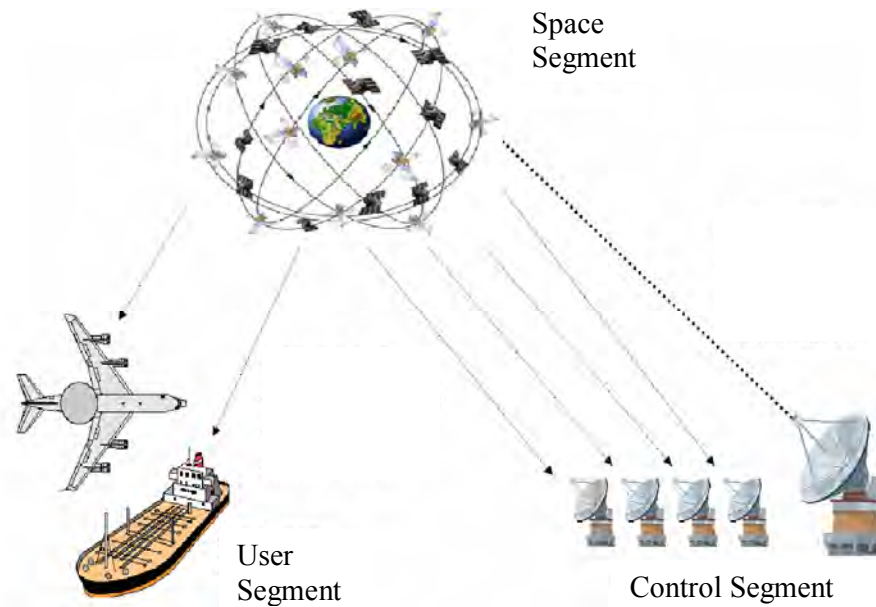


Figure 3.1 - The three segments that make up the GPS

The Space Segment consists currently of 32 GPS satellites (PRN:1 - 11, 13 - 18, 20, 21 and 23 - 32) arranged in 6 orbital planes located at the altitude of 20,200 km inclined at 55° to the equator. The coverage provided by the GPS constellation which provide information for determining the position of the satellite, its distance from the user and satellite clock error, ensures a minimum of 4 satellites and maximum of 11 satellites visible at anytime, anywhere in the world. The orbital period of satellite is approximately 11hr 58min. Therefore a GPS satellite completes 2 revolutions in 23hr 56min as a result of this, the satellite appears over the same geographical location on the Earth's surface every day (i.e. minus 4 minutes).

The Control Segment tracks each satellite and periodically sends the corrections of ephemeris and clock which are analyzed continuously by monitoring stations around the globe, that are in Hawaii, Ascension Island, Kwajalein, and Diego Garcia (Figure 3.2). The monitoring stations are analyzed remotely by a Master Station at Colorado Springs which provides commands and control functions. The monitoring stations are equipped with communication facilities to

transmit data to the master station via terrestrial transmission (S band). Some functions of the Master station include the following:

- monitor the satellite orbits;
- monitor and maintain the health of the satellites;
- keep the GPS time;
- calculate the satellite ephemeris and clock parameters;
- update the navigation messages from satellites, and
- control maneuvers to maintain satellites in orbit and re-allocate satellites.

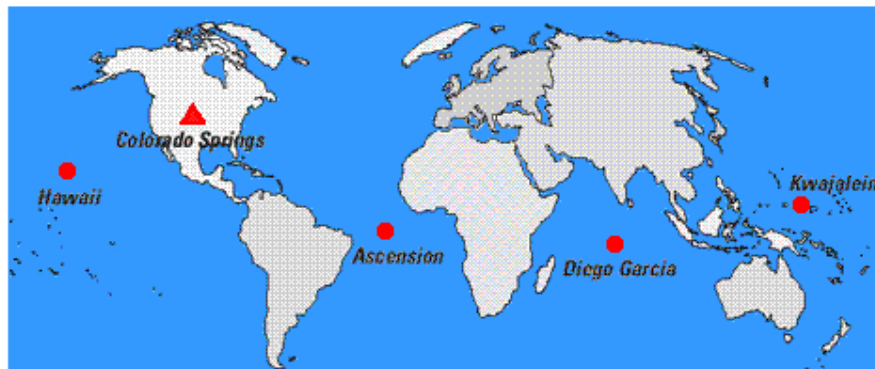


Figure 3.2 - Location of the four unmanned stations (circles) and one Master Station (triangle) of the GPS Control Segment.

Source: Frederic G. and Snider, R.P.G. (2012).

The User Segment: The user segment consists of receivers used by both military and civilians. The receiver is made up of hardware and processing software for positioning in three dimensions, navigation, and timing applications. This is possible by making use of the signals transmitted by the constellation of GPS.



Figure 3.3: IGS network of permanent GPS tracking stations

Source: <http://igscb.jpl.nasa.gov/network/site/wroc.html>

Today there are several hundred of GPS receivers stations around the world. Figure 3.3 represent the distribution of permanent global GPS sites maintain by the International GPS Service, which consists of more than 300 stations. It is clear evidence from the Figure 3.3 that the density distribution of the receivers is more at the northern hemisphere compared to the southern hemisphere. Apart from the IGS global stations, there are also regional GPS network stations. One of these, is the laudable RBMC/IBGE which was implemented by Brazilian Geodetic System (GBS) (Figure 3.4). The network consist of over 80 GPS receiver stations scattered strategically all over Brazilian region. The data used for this study were collected from both IGS and RBMC networks and can be obtained via <ftp://garner.ucsd.edu/pub/rinex/> and <ftp://geoftp.ibge.gov.br/RBMC/dados> respectively. Other developing GPS receiver networks situated in South America are: the Low-Latitude Ionospheric Sensor Network (LISN), Red Argentina de Monitoreo Satellite continuo (RAMSAC), and the Colombia Continuously Observing Reference Frame (MAGNA-ECO).

3.3 GPS Signals Structure

All GPS satellites transmit the same L1 and L2 carrier frequencies. The code modulation (Figure 3.5), however is different for each satellite. The fundamental frequency is 10.23MHz. Two carrier signals are created from this signal by multiplying the frequency and wavelength (frequency of 1575.42 MHz and wavelength of 19.0 cm,) by 154 for the L1, and by 120 for the L2 (frequency of 1227.60 MHz and wavelength of 24.4 cm) (BLEWITT, 1997). The binary digits 0 and 1 are actually represented by multiplying the electrical signal by either +1 or -1, which is equivalent to leaving the signal unchanged, or flipping the phase of by 180° when the code value changes from zero to one or from one to zero.

Information is encoded in the form of binary bits on the carrier signals by a process known as phase modulation. There are three types of code on the carrier signals:

- The C/A code
- The P code
- The Navigation Message

The C/A (“course acquisition”) code can be found on the L1 channels. This is a code sequence which repeats every 1 millisecond. It is a pseudo-random code that appears to be random and generated by a known algorithm. The carrier can transmit the C/A code at 1.023 Mbps (million bits per second). The “chip length”, or physical distance between binary transitions (i.e. between digits +1 and -1), is 293 meters. The basic information that the C/A code contains is the time according to the satellite clock and when the time the signal was transmitted by the satellite. Each satellite has a different C/A code, so that they can be uniquely identified. The C/A code range measurement is relatively less precise compared with that of the P-code. It is, however, less complex and available to all users. It is important to mention that there are new Modern global positioning system signals of L2C and L5 for civilian purpose which, have a new developmental prospect. The principal objective of modernizing GPS signal is to improve the overall performance of the GPS system, in terms of improving the accuracy, providing better immunity to RF interference and multipath and better atmospheric corrections. (interested readers are referred to the second edition of Galera M.J.F., 2008)

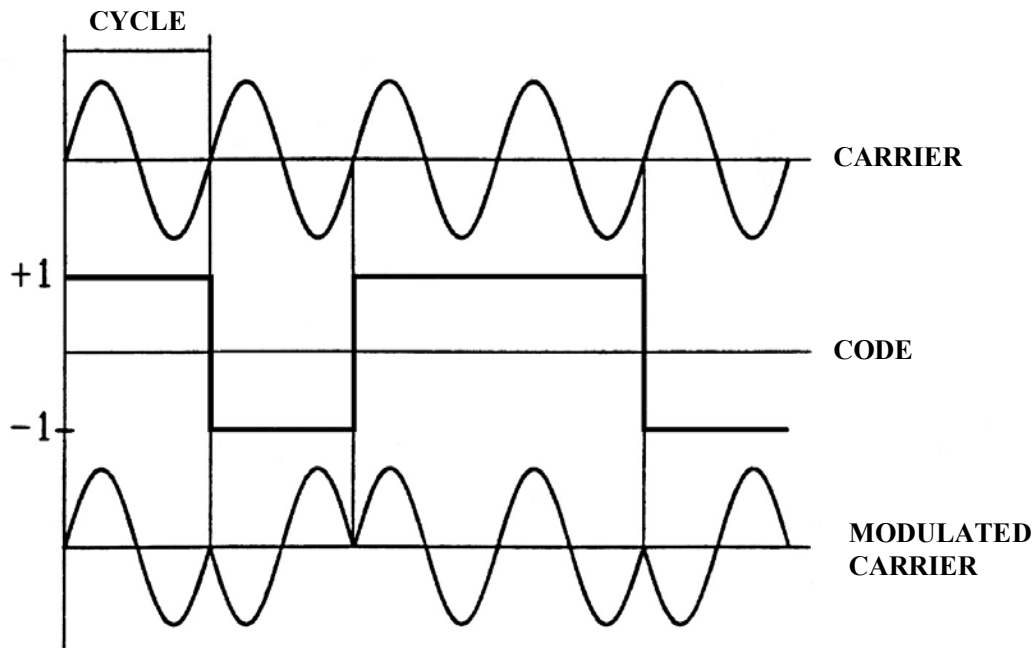


Figure 3.5: Modulation of the code on the carrier wave.

SOURCE: Hofmann-Wellenhof et al. (1994)

The P (“precise”) code is identical on both the L1 and L2 channel. P code is better for more precise positioning. The P code repeats every 267 days. In practice, this code is divided into 28 day segments; each 7days long is designated a “PRN” number, and is designated to one of the GPS satellites. That is, each satellite transmits a unique 1 week segment of the P-code, which is initialized every 7th day at midnight. The carrier can transmit the P code at 10.23 Mbps, with a chip length of 29.3 meters. The basic information is the satellite clock time which is identical to the C/A information, except that it has ten times the resolution. Unlike the C/A code, the P code can be encrypted with W-code by a process known as “anti-spoofing”(A/S) and the resulting code is denoted by Y-code. Thus, when A/S is activated, the P-code on L1 and L2 carrier is replaced by Y code which in turn cause accuracy denial for civilian users. (Hoffmann-Wellenhof et al., 1994). Originally the encryption was intended as a means to safeguarding the signal from being corrupted by interference or falsified signals with the GPS signature. Similarly, selective availability (S/A) is a kind of accuracy denial. It is a type of intentional error imposed on GPS signal. In the presence of S/A, the GPS user may account for position error of up to 100meters (BLEWITT; 1997). S/A is either turned 'on' or turned 'off'. However, when turned 'on' it could be mitigated by differential GPS, where errors in the GPS signal can be computed at a reference station at known coordinates.

The Navigation Message can be found on the L1 channel, being transmitted at a very slow rate of 50 bps. It is a 1500-bit sequence, and therefore takes 30 seconds to transmit. The Navigation Message includes information on the Broadcast Ephemeris (satellite orbital parameters), satellite clock corrections, almanac data (a crude ephemeris for all satellites), ionosphere information, and satellite health status.

3.3.1 Pseudorandom Code

GPS receivers antenna calculate distances to satellites antenna as a function of the amount of time it takes for satellites' signals to reach the ground. To make such a calculation, the receiver must be able to tell precisely when the signal was transmitted, and when it was received. The satellites are equipped with extremely accurate atomic clocks, as a result, the timing of transmissions is always known. Receivers contain cheaper clocks, which tend to be sources of measurement error. The signals broadcast by satellites, which are known as "pseudo-random codes," are accompanied by the broadcast ephemeris data that describes the shapes of satellite orbits.

3.3.2 Ephemeris Data

GPS satellites include ephemeris data in the signals they transmit to GPS receivers. Ephemeris data is a set of parameters that can be used to accurately calculate the location of a GPS satellite at a particular point in time. It describes the path that the satellite is following as it orbits Earth. For a better accuracy calculation of any location, ephemeris data is only usable for a limited time (a few hours or less). Up-to-date data is needed to minimize error that results from minor variations in a satellite's orbit.

3.3.3 Almanac Data

GPS receivers use almanac data to predict which satellites are nearby when they're looking for GPS signals. Almanac data includes a set of parameters for each GPS satellite that can be used to calculate its approximate location in orbit. Using almanac data saves time by letting the receiver skip looking for satellites that are below the horizon. GPS satellites include almanac data in the signals they transmit to GPS receivers. Although variations in satellite orbits can accumulate with time, almanac data doesn't need to be highly accurate to be useful. The ephemeris data are more precise than the almanac data. Whereas ephemeris information is highly detailed and considered valid for no more than four hours, almanac information is more general and is considered valid for up to 180 days.

3.4 Sources of GPS Signal Errors

GPS errors are unwanted variations in position measurements that come from a variety of error sources. Without corrections to the errors, the accuracy of the GPS system is approximately 50 to 100 meters. The electromagnetic wave passing through the ionosphere undergoes refraction or delay (as explained in chapter one), and changes in speed, cause pseudorange error in the GPS signal. Pseudorange error is an approximation of the distance between a satellite and a navigation satellite receiver. Other factors that can degrade the GPS signal and thus affect accuracy include the following:

Ionosphere and troposphere delays — the satellite signal on pseudorange code slows as it passes through the atmosphere. The GPS system uses a built-in model that calculates an average amount of delay to partially correct this type of error.

Signal multipath — This occurs when the GPS signal is reflected by objects such as tall buildings or large rock surfaces before it reaches the receiver. This increases the travel time of the signal, thereby causing errors.

Receiver clock — A receiver's built-in clock is not as accurate as the atomic clocks onboard the GPS satellites. Therefore, it may have very slight timing errors.

Orbital — Also known as ephemeris errors, these are inaccuracies of the satellite's reported location.

Cycle slip — The loss of signal lock between a GPS satellite and the receiver is referred to as cycle slip. Cycle slips occur when the continuous tracking of a satellite is interrupted by an obstruction, or faulty signal processing within the receiver, or even when the ionospheric activity is highly variable. Cycle slips generally occur at a receiver tracking a satellite and rarely are there slips on all satellites at the same time. Slips can occur independently on L1 and L2.

Satellite geometry/shading — This refers to the relative position of the satellites at any given time. Ideal satellite geometry exists when the satellites are located at wide angles relative to each other. Poor geometry results when the satellites are located in a line or in a tight grouping.

3.5 The Effects of the Ionosphere on the GPS Signals

The free electrons in the ionosphere, as discussed in section 2, affect the propagation of radio waves. At frequencies below about 30MHz, the ionosphere acts almost like a mirror, changing the path traveled by radio wave back towards the Earth, thereby allowing long-distance

communication. However at higher frequencies, such as those used by the GPS, radio waves could pass through the ionosphere but are affected (slow down) by it.

The speed of propagation of radio wave at some point in the ionosphere is determined by the electron density present. The phase of the carrier speed is actually increased by the presence of the electrons. The greater the density of the electrons, the greater is the speed of the carrier phase. The overall effects on a radio wave is obtained by integrating the electron density along the whole path that a signal follows from a satellite to a receiver. The result is that a particular phase of the carrier arrives at the receiver earlier than it would have had the signal traveled from the satellite in a complete vacuum. This early arriver is known as phase advance. On the other hand, the modulating signal of the carrier (the pseudorandom noise codes and navigation message) is delayed by the ionosphere which increases the apparent length of the path travelled by the signal. The delay of the modulation is called the group delay.

The size (error) of the phase advance and the group delay are equal in magnitude and opposite in signs. Both are proportional to the TEC and inversely proportional to square of the carrier frequency. The higher the frequency the smaller is the effect.

4. METHODOLOGY AND STATISTICS USED

4.1 Nagoya Model Approach

The Nagoya model provides two-dimensional map of absolute TEC and a binary formatted grid data (when loaded with GPS observation data) as a function of time and location. It is important to mention that apart from the Japan GEONET project, the Nagoya model is also being used in the Brazilian region to produce real time TEC maps. The model is based on new technique which make use of a least square fitting procedure to remove instrumental biases from GPS satellite and receiver (OTSUKA et. al., 2002).

4.1.1 Calculation of TEC from Pseudorange Observation

The pseudorange is a measure of propagation delay time of the satellite signal transmitted to the receiver multiplied by the speed of light in vacuum (c).

The pseudorange observation can be expressed as

$$P_r^s = c\tau_r^s = \rho_r^s + c(\hat{\partial}t_r - \hat{\partial}t^s) + I + T + mp + \varepsilon + br + bs \quad (4.1)$$

where

P_r^s is the pseudorange measurement at receiver from the satellite, τ_r^s is the transmission time from the receiver antenna to the satellite antenna in free space, ρ_r^s is the line-of-sight range between the satellite and the receiver, $(\hat{\partial}t_r, \hat{\partial}t^s)$ are the offsets of the receiver and the satellite clock from GPS time respectively, I is the ionosphere induced error (or the ionospheric delay), T is the tropospheric induced error, br, bs are the receiver and satellite instrumental delay respectively, ε is the noise or random error, mp is the multipath error while $T + mp + \varepsilon + br + bs = E_p$ is the noise generated by the pseudorange measurement.

The error or effect of 1st order due to ionosphere in pseudorange along the satellite direction referred to as the ionospheric delay (I) can be calculated from the refractive index

$$\Delta r = \int_r^s (1 - n) dl \quad (4.2)$$

where Δr is the group delay and n is the refractive index.

The first-order refractive index (n) is given by: $\frac{1-40.3N}{f^2}$ and (4.3)

$$TEC = \int_r^s Ndl \quad (4.4)$$

where N is the electron density and 1 TEC unit = 10^{16} electrons/m². Note that TEC is proportional to the ionospheric differential delay between (1575.42Mhz) and L2 (1227.60MHz) signals.

By equations (4.2), (4.3), and (4.4), the ionospheric group delay is:

$$\Delta r = \frac{40.3}{f^2} \int Ndl = 40.3 \frac{TEC}{f^2} \quad (4.5)$$

For a pseudorange measurement from two different frequencies equation (4.1) becomes:

$$P_1 - P_2 = I_1 - I_2 + E_{p1} + E_{p2} \quad (4.6)$$

where P_1, P_2 are the pseudorange measurement on L1 and L2 respectively, E_{p1}, E_{p2} represents the multipath and noise of the signal.

Applying equation (4.5) and (4.6) relative TEC can be readily calculated by:

$$TEC_p = \frac{f_1^2 f_2^2 (P_1 - P_2)}{40.3(f_1^2 - f_2^2)} \quad (4.7)$$

where P and f are the pseudorange and the corresponding frequency respectively. Substituting f_1 and f_2 :

$$TEC_p = 9.52 \times 10^{16} (P_1 - P_2) \quad (4.8)$$

Equation 4.8 is unambiguous but noisy and therefore is imprecise.

4.1.2 Calculation of TEC from Carrier Phase Measurement

The carrier phase measurements correspond to the phase difference between the received signal (transmitted by the satellite) and the signal generated by the reference oscillator of the receiver.

The observed equation for a carrier phase measurement can be expressed as:

$$\Phi_r^s = \rho_r^s + c(\partial t_r - \partial t^s) + I + T + \lambda N_r^s + mp_\phi + \varepsilon + br + bs \quad (4.9)$$

Φ_r^s is the phase measurement in unit of length, λ is wavelength of the carrier phase, N_r^s is integer ambiguity between satellite and receiver, mp_ϕ is the multipath error. The equation can be reduced to:

$$\Phi_r^s = \rho_r^s + c(\partial t_r - \partial t^s) + E_\Phi \quad (4.10)$$

where E_Φ is the errors.

For carrier phase measurements derived from two different frequencies equation (4.9) can be solved by:

$$TEC_\Phi = -\frac{f_1^2 f_2^2 (\Phi_1 - \Phi_2)}{40.3(f_1^2 - f_2^2)} \quad (4.11)$$

where Φ and f are the carrier phase and the corresponding frequency respectively.

Substituting f_1 and f_2 :

$$TEC_\Phi = -9.52 \times 10^{16} (\Phi_1 - \Phi_2) \quad (4.12)$$

Φ_1, Φ_2 are the carrier phase measurement at L1 and L2 frequencies. The cycle slips are detected as discontinuity in L1 and corrected using an algorithm developed by Belwitt (1990). Although TEC derived from the carrier phase data is precise, it is ambiguous due to unknown initialization constant in phase data.

4.1.3 Leveling of the Carrier Phase with the Pseudorange

Since the code (pseudorange) measurement is unambiguous but noisy and the carrier is very precise but ambiguous, the level of the TEC derived from the carrier is adjusted to that of TEC derived from the corresponding pseudorange difference for each satellite and receiver pair. The level is determined for each set of connected TECs. The data separated over more than 15 minutes in time are not connected.

$$TEC_{combi} = TEC_{\Phi_i} - (TEC_{\Phi_i} - TEC_{pj}) \quad (4.13)$$

where i and j are the ionospheric indices. The ambiguity is removed by averaging $(TEC_{\Phi_i} - TEC_{pj})$ over a satellite pass (phase connecting arc). Nevertheless the result still include instrumental biases of satellite and receivers from the pseudorange and carrier measurements.

4.2 Absolute TEC

In order to estimate the absolute TEC $(I^i(t))$, the biases inherent from the satellite and receiver hardware (i.e. the instrumental biases) are removed by the following steps. The TEC carrier phase and pseudorange which is the composition of slant TEC ($T^i(t)$) and instrumental bias (B^i) is given by:

$$I^i(t) = T^i(t) + B^i \quad (4.14)$$

The slant TEC $I = T^i(t)$ at a given point in the ionosphere shell is related to the equivalent vertical TEC ($V^i(t)$) at that point by:

$$T^i(t) = S(\varepsilon^i(t))V^i(t) \quad (4.15)$$

where $\varepsilon^i = \varepsilon^i(t)$ is the elevation angle of GPS satellite, $S(\varepsilon^i)$ is the slant factor given by $\frac{\tau_i}{\tau_o}$, and τ_i = length of ray path between 300 and 550 km altitude while τ_o is equal to the ionospheric thickness of 250 km for zenith path.

In order to eliminate errors, which increase relative to the slant factor, the cutoff elevation angle was fixed at 30° . The absolute TEC can therefore be obtained by equation:

$$I^i(t) = S(\varepsilon^i(t))V^i(t) + B^i \quad (4.16)$$

where B^i is the instrumental biases of both the receiver and the satellite.

4.3 The Estimation of TEC Map

The construction of the two-dimensional TECMAP is obtained by the following three steps:

Step (1): The hourly averages of TEC for all satellites are estimated by applying a weight least squares fitting procedure to the GPS data from a single receiver.

Dividing equation (4.16) by $S(\varepsilon^i)$, the average of one hour is estimated to a value of vertical TEC, $\overline{V_k}$ where k is the index of time sequence of hourly TEC average. Hence the equation below can be obtained from equation (4.16).

$$\frac{\overline{I_k}}{\overline{S(\varepsilon_k^i)}} = \overline{V_k} + \left(\frac{1}{\overline{S(\varepsilon_k^i)}} \right) B^i \quad (4.17)$$

for $k = 1, 2, \dots, Nt$ and $i = 1, 2, \dots, Ns$, where Nt and Ns are number of hourly TEC average and number of satellite observed by the receiver respectively. The over line on some variables denote average values.

The unknown values $\overline{V_k}$ and B^i are determined through least squares fitting procedure minimizing the following residuals:

$$E = \sum_i^{N_s} \sum_k^{N_i} W_k^i \left[\frac{\overline{I_k}}{S(\varepsilon_k^i)} - \left(\overline{V_k} + \left(\frac{1}{S(\varepsilon_k^i)} \right) B^i \right) \right]^2 \quad (4.18)$$

where W_k^i is the weighting function. Equating the equation to zero and taking the partial derivative of E with respect to $\overline{V_k}$ and B^i , the $(\overline{V_k}$ and $B^i)$ can be solved to reduce error of hourly TEC average caused by assumption of thin shell model, partial uniformity of the hourly TEC average and setting W_k^i as inverse of slant factor:

$$W_k^i = \frac{1}{S(\varepsilon_k^i)} \quad (4.19)$$

Step (2): Using the hourly average obtained in the step1 above, the instrument biases can be computed. The ionospheric shell is assumed to be located at 400 km altitude. The receivers however should be closely distributed. So the overlapped provided by the receiver TEC could be smoothed to obtain the hour TEC average spatially. Substituting the hourly averaged and spatially smoothed TEC in equation (4.17) the instrumental biases B^i is determined. This new B^i is more accurate due to spatially smoothing of the hourly TEC average than the previous B^i obtained from the least square fitting method in step (1).

Step (3): The biases are removed from the measured TEC to obtain absolute TEC. Absolute vertical TEC is obtained by substituting B^i in equation (4.16) and is mapped in the ionospheric shell height at 400 km altitude with a spatial resolution of $0.15^\circ \times 0.15^\circ$ latitude and longitude for every 30 sec time resolution

4.4 Statistical Method

Having obtained the absolute vertical TEC of several stations (as shown Figure 4.2 and Table 4.1) with time resolution of 10 minutes and spatial resolution of 1° (in latitude and longitude) using the Nagoya model by following the procedure explained in section 4.1 - 4.3, we intend to use the following solar and magnetic indices and methodology to accomplish our objectives:

- **F10.7 Index:** The F10.7 index is a measure of emission of solar radiation at a wavelength of 10.7 cm (2800MHz) received on Earth's surface. Determinations are made with F10.7 flow monitors stream (satellite dishes) which are equally sensitive to all points of solar disk, and are equipped to measure emissions linearly polarized in north to south. It has been used as a proxy for solar activity in the ionospheric model like International Reference Ionosphere (IRI). Figure 4.1 upper panel shows the F10.7 cm flux for the period of 2000 to 2010. The vertical dash lines show the 2001 (when F10.7 was larger than 120) and 2009 (when F10.7 was smaller than 120) F10.7 values. According to Liu et al. (2006), F10.7 is a better solar proxy than the Sunspot number (SSN), because in a statistical sense it represents the intensity of solar EUV fluxes fairly well. From the same figure, it can be seen that the F10.7 cm flux of 2001 shows an oscillating increase and the highest F10.7 was observed during this year. On the other hand 2009 F10.7 cm flux exhibits the lowest and consistent radio flux which makes it a proper low solar activity period for study. The monthly mean F10.7 for 2001 and 2009 is also shown in Table 4.2.
- **Kp index:** is a number proportional to the degree of disturbance of the Earth's magnetic field. The values of Kp represent an average of values obtained from an interval of three hours, therefore, one day represents eight values of Kp. The classification between calm days and disturbed can be determined according to the sum of these eight values. If the daily sum of Kp exceeds the 24, the day is classified as disturbed, otherwise the day is classified as calm (the Kp data is available at: <http://wdc.kugi.kyoto.ac.jp/wdc/Sec3.html>). Daily Kp index of less or equal to 24 was used to specify quiet geomagnetic periods (Figure 4.1)
- The diurnal and monthly variation of TEC for both solar minimum (2009) and maximum (2001) is analyzed by plotting mass plots of TEC for each month of each year.
- The seasonal variation of TEC for both solar minimum (2009) and maximum (2001) is studied by grouping data into three seasons and taking the hourly average and standard deviation. The months of November, December, January, February are considered as summer solstice, the months of May, June, July, August as winter solstice while the months of March, April, September and October as equinox. (Scherliess et al., 2008)

- The tracing of magnetic field line for fixed longitudinal position was carried out using the IGRF Earth's magnetic field from International Geomagnetic Reference Field (IGRF) model. This enable us to obtain TEC (along a selected magnetic field line) and the data were used to observe the latitudinal variation and the EIA as shown in Figure 4.2.
- Wavelet analysis will be used to check TEC periodicities as well as meridional and zonal wind periodicities at the height of 100 km (the winds were obtained from the meteor radar located over Cachoeira Paulista and Santa Maria), which could be responsible for the day-to-day variability. Notwithstanding, to study extensively the day-to-day variability of TEC many parameters are involved. For example the thermospheric neutral wind data for both meridional and zonal components which were not available at the time of this study. Therefore the extensive studies on day-to-day variability could be an interesting study in the nearest future.
- To study the SSW effects, we apply the methodologies of Goncharenko et. al. (2008) and Chau et al. (2009) by observing TEC data before (control days) and comparing them with TEC data around days under the SSW effect of January 2009 and September 2008.

4.5 Data Used

In order to study the variation of TEC due to local time, season and solar activity over South America sector, we have obtained data from the following data bases:

1. SOPAC: Scripts and Permanent Array Centre Garner GPS archive (known as SOPAC GARNER) contains files of observation and navigation from the GPS global network. The data base belong to the International GNSS Service (IGS). It is available at <ftp://garner.ucsd.edu/pub/rinex/>.
2. RBMC/IBGE: Brazilian Network for Continuous Monitoring of the Institute of Brazilian Geography and Statistics. The data of this database can be accessed at <ftp://geofp.ibge.gov.br/RBMC/dados/>.

Data of 2001 and 2009, representing maximum and minimum solar activity respectively are collected from the aforementioned data bases and analyzed. On average the total number of stations that were used for the study is represented in the Table 4.1. The number of stations that is being used is very dynamic because some stations had technical problems and therefore these stations are unusable for the period of study. It is important to mention that less than 15 RBMC GPS stations in 2001 increased to 70 GPS receiver station in 2009. With this development, our statistics for 2009 analyses were also improved.

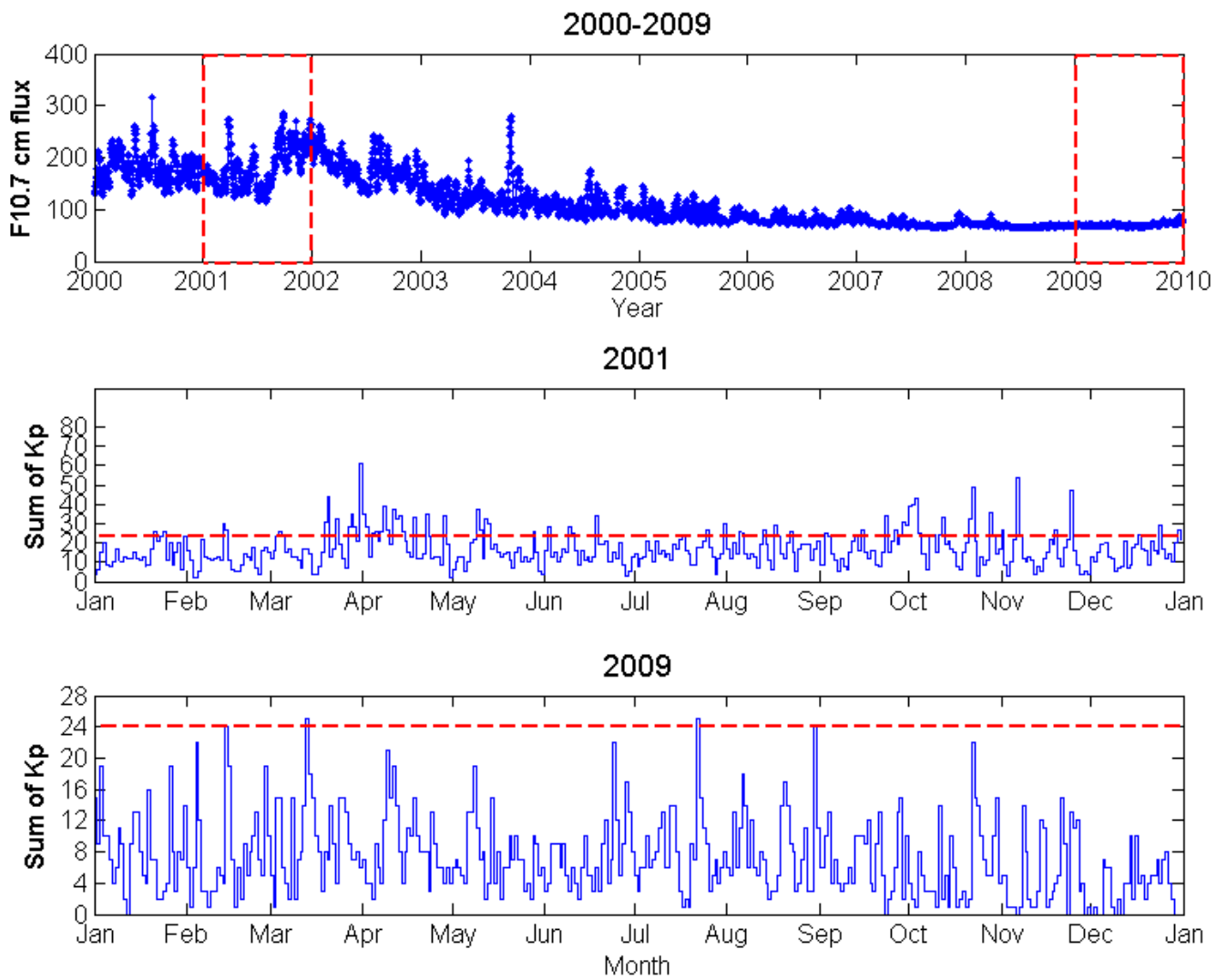


Figure 4.1 - F10.7 cm flux and sum of Kp index. The red dash lines indicate the period of data used. The data were collected from <http://www.ngdc.noaa.gov/nndc/struts/form>.

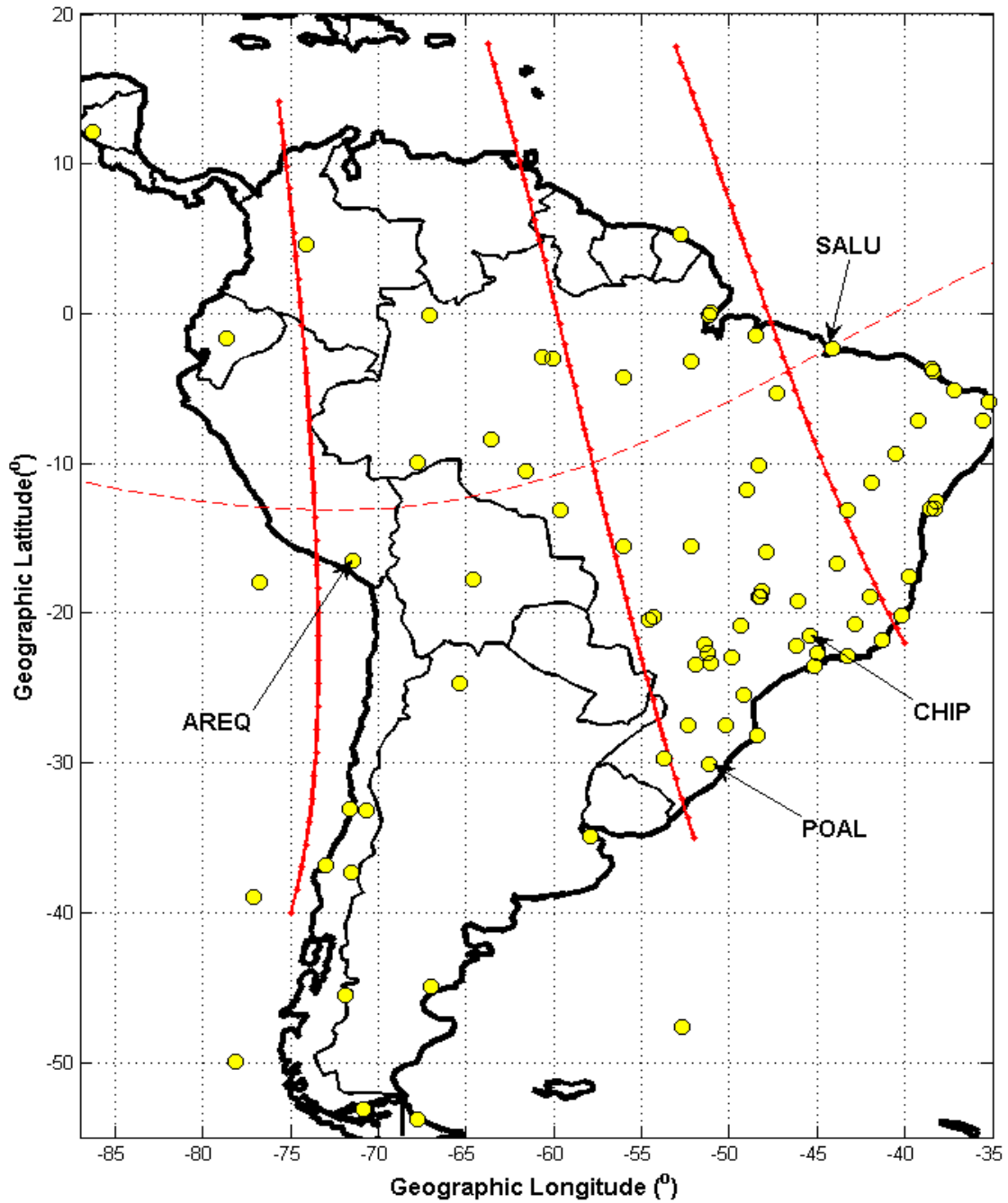


Figure 4.2 - Locations of RBMC and IGS stations that were used. The red lines indicate the magnetic field lines traced using the IGRF model.

TABLE 4.1 - LIST OF RBMC AND IGS STATION USED.

CITY	ABBREVIATION	LATITUDE	LONGITUDE
RBMC STATIONS			
ALTAMIRA	PAAT	-03.12°	-52.10°
ARAPIRACA	ALAR	-09.44°	-36.39°
BARRA DO GARÇAS	MTBA	-15.53°	-52.15°
BELÉM	BELE	-01.24°	-48.27°
BELO HORIZONTE	MGBH	19.56°	-43.55°
BOA VISTA	BOAV	-02.50°	-60.42°
BOM JESUS DA LAPA	BOMJ	-13.15°	-43.25°
BRASÍLIA	BRAZ	-15.56°	-47.52°
CACHOEIRA PAULISTA	CHPI	-22.41°	-44.59°
CAMPINA GRANDE	PBCG	-07.12°	-35.54°
CAMPO GRANDE	MSCG	-20.26°	-54.32°
CAMPOS DOS GOYTACAZES	RJCG	-21.45°	-41.19°
CANANÉIA	NEIA	-25.01°	-47.55°
CHAPECÓ	SCCH	24.08°	-52.35°
CRATO	CRAT	-07.14°	-39.24°
CRUZEIRO DO SUL	CRUZ	-07.36°	-72.40°
CUIABÁ	CUIB	-15.33°	-56.04°
CURITIBA	PARA	-25.26°	-49.13°
CURITIBA UFPR	UFPR	-25.26°	-49.13°
FORTALEZA	BRFT	-03.52°	-38.25°
FORTALEZA	CEEU	-03.52°	-38.25°
FORTALEZA	FORT	-18.51°	-41.57°
GOV. VALADARES	GVAL	-10.47°	-65.19°
GUAJARÁ-MIRIM	ROGM	-11.44°	-49.02°
GURUPI	TOGU	-07.30°	-63.01°
HUMAITÁ	AMHU	-07.30°	-63.01°
IMBITUBA	IMBT	-28.14°	-48.39°
IMPERATRIZ	IMPZ	-05.29°	-47.29°
INCONFIDENTES	MGIN	-22.19°	-46.19°
IRECÊ	BAIR	-11.18°	-41.51°
JATAÍ	GOJA	-17.52°	-51.43°
JI-PARANÁ	ROJI	-10.51°	-61.57°
LAJES	SCLA	-27.47°	-50.18°
MACAPÁ	MAPA	00.03°	-51.06°
MANAUS	MANA	-03.07°	-60.03°
MANAUS	NAUS	-03.01°	-60.03°
MARABÁ	MABA	-05.21°	-49.07°
MONTES CLAROS	MCLA	-16.43°	-43.52°
MONTES CLAROS	MGMC	-16.42°	-43.51°
MOSSORÓ	RNMO	-50.12°	-37.19°
NATAL	RNNA	-05.50°	-35.12°
PALMAS	TOPL	-10.10°	-48.19°
PETROLINA	PEPE	-09.23°	-40.30°
PORTO ALEGRE	POAL	-30.04°	-51.07°

PORTO VELHO	POVE	-08.42°	-63.53°
PRES. PRUDENTE	UEPP	-22.07°	-51.24°
PRES. PRUDENTE	PPTE	-22.07°	-51.24°
RECIFE	RECF	-08.03°	-34.57°
RIO BRANCO	RIOB	-09.57°	-67.48°
RIO DE JANEIRO	RIOD	-22.49°	--43.18°
RIO DE JANEIRO	ONRJ	-22.54°	-43.13°
SALVADOR	SALV	-13.00°	-38.30°
SALVADOR INCRA	SAVO	-12.56°	-38.30°
SALVADOR CAPITANIA	SSA1	-12.58°	-38.30°
SANTA MARIA	SMAR	-29.43°	-53.42°
SÃO GABRIEL DA CACHOEIRA	SAGA	-00.08°	-67.03°
SÃO FÉLIX DO ARAGUAIA	MTSF	-11.37°	-50.39°
SÃO LUÍS	SALU	-02.35°	-44.12°
SÃO PAULO	POLI	-23.33°	-46.43°
TEIXEIRA DE FREITAS	BATF	-17.33°	-39.44°
UBATUBA	UBAT	-23.33°	-45.07°
UBERLÂNDIA	UBER	-18.55°	-48.15°
UBERLÂNDIA	MGUB	-18.55°	-48.15°
VARGINHA	VARG	-21.32°	-45.26°
VIÇOSA	VICO	-20.45°	-42.52°
VITÓRIA	CEFE	-20.18°	-40.19°
IGS STATIONS			
AREQUIPA	AREQ	-16.47	-71.49
BOGOTA	BOGT	04.64	-74.08
BRASÍLIA	BRAZ	-15.94	-47.88
CACHOEIRA PAULISTA	CHPI	-22.29	-44.99
CONCEPCION	CONZ	-36.84	-73.03
EUSEBIO	BRFT	-03.88	-38.43
FRENCH GUYANA	KOUR	05.25	-52.80
LA PLATA	LPGS	-34.91	-57.93
LOS ANGELES	ANTC	-37.34	-71.53
PUNTA ARENAS	PARA	-53.14	-70.88
RIO GRANDE	RIOG	-53.79	-67.75
SALTA	UNSA	-24.73	-65.41
SANTIAGO	SANT	-33.15	-70.67

TABLE 4.2- MONTHLY MEAN SOLAR INDEXES

Month	F10.7 (cm)		EUV (0.1 - 50nm)		SSN	
	2009	2001	2009	2001	2009	2001
January	69.8	166.6	1.81E+10	5.17E+10	60.8	145.2
February	70.0	146.7	1.8E+10	5.06E+10	61.5	128.8
March	69.2	177.7	1.78E+10	5,32E+10	61.7	158.5
April	69.8	178,1	1.75E+10	5,49E+10	63.2	161.4
May	70.5	147.9	1.85E+10	4.96E+10	64.9	136,1
June	68.6	173.7	1.8E+10	5.34E+10	63.7	161.3
July	68.2	131.3	1.76E+10	4.67E+10	63.4	122.0
August	67.4	163.1	1.72E+10	5.11E+10	62.1	150.4
September	70.5	233.8	1.79E+10	6.86E+10	64.1	212.6
October	72.3	208.1	1.86E+10	6.35E+10	64.7	185.9
November	73.6	212.7	1.93E+10	8.3E+10	64.8	187.3
December	76.8	235.6	1.98E+10	6.57E+10	66.9	205.4
Summer	72,6	191,3	1,88E+10	6,31E+10	63,5	167,4
Equinox	70,4	199,3	1,8E+10	6E+10	63,4	179,5
Winter	68,7	153,8	1,78E+10	5,02E+10	63,5	142,3
Yearly average	70.6	181.38	1,81E+10	5.77E+10	63.5	162.9

4.6 RINEX Format

The result of TEC that is being used for this study is obtained from dual GPS frequencies, available in receiver independent exchange format (RINEX) files. RINEX was developed by "Astronomical Institute of the University of Berne" for the purpose of facilitating the exchange of data collected in the campaign European Reference Frame 1989 (EUREF 89), which involved

more than 60 GPS receivers from various manufacturers (Gurtner et al. 1997). This patterning has become necessary due to the different shapes and programs for processing the data obtained in different types of receivers. The second version of RINEX was published in 1990 and subsequently has undergone some minor revisions. Currently, the RINEX format is used by most of the international community users and receiver manufacturers. The RINEX version 2.10 consists of six RINEX ASCII files; each having a header and a data sections: (1) observation data file, (2) navigation message file, (3) meteorological file (4) GLONASS navigation message file, (5) geostationary satellite (GPS signal payloads) data file, and (6) satellite and receiver clock data file. (More information about RINEX format can be found in Hofmann-Wellenhof et al. (1994). The Nagoya model makes use of only the observation data files. This observation file contains in its header information about the file's contents such as the station name, antenna information, the approximate station coordinates, number and types of observation, observation interval in seconds, time of first observation record, L1 and L2 frequencies, P1 and P2, represent phase measurement and pseudorange measurement respectively. Table 4.3 shows a typical example of RINEX file. The data section consists of two epoch each containing the time tag of observation, the number and list of satellites, the various types of measurements as given in the header, the signal strength, loss of lock indicator and some the receiver clock offset in seconds.

Table 4.3 : RINEX OBSERVATION FORMAT

2		OBSERVATION DATA				G (GPS)	RINEX VERSION / TYPE							
RGRINEXO	V2.4.2	LH	IfAG-Wetzzell			11-MAR-96	09:05			PGM / RUN BY / DATE				
IfAG-Wetzzell										COMMENT				
BIT 2 OF LLI (+4)	FLAGS	DATA	COLLECTED	UNDER "AS"	CONDITION					COMMENT				
0.000000000000				HARDWARE	CALIBRATION (S)					COMMENT				
-0.000000004329				CLOCK	OFFSET (S)					COMMENT				
OHIG										MARKER NAME				
ARW										OBSERVER / AGENCY				
319			TurboRogue	SNR-8000	3.2					REC # / TYPE / VERS				
414			DORNE MARGOLIN	T						ANT # / TYPE				
1525874.9925		-2432483.3348		-5676151.9662						APPROX POSITION XYZ				
0.0010		0.0000		0.0000						ANTENNA: DELTA H/E/N				
1	1									WAVELENGTH FACT L1/2				
5	C1	L1	L2	P2	P1					# / TYPES OF OBSERV				
30										INTERVAL				
1996	3	7	0	6	0.000000					TIME OF FIRST OBS				
										END OF HEADER				
96	3	7	0	6	0.0000000	0	6	27	16	17	28	18	22	
21255525.459					-0.53219								21255526.1004	
21606880.941					-1.04819								21606881.7354	
24963237.216					-0.67216								24963240.1474	
					-0.53816								23868688.375	
21902124.704					-0.57919								21902125.1884	
24390657.759					-0.67616								24390659.4404	
96	3	7	0	6	30.0000000	0	7	27	31	16	17	28	18	22
21234706.079					-109406.529	9							21234706.5474	
25172918.270					-0.35616									
21591402.449					-81338.881	9							21591403.3324	
24941720.616					-113072.535	6							24941723.0254	
					-103190.384	6							23849052.136	
21908739.751					34760.073	9							21908740.0554	
24400301.778					50681.700	6							24400302.9894	

5.0 RESULTS AND DISCUSSION

In this chapter we present the analysis of the results obtained using the RBMC and IGS data over South America and the estimation techniques as presented in the previous chapters. The results are presented in four sections. In the first section we discussed ionospheric TEC variation such as: the diurnal, monthly and seasonal variations. Second section is about equinoctial asymmetry during both low and high solar activity and the latitudinal variation and transition of TEC variation from month to month as a function of latitude. In the third section we try to figure out the possible mechanisms that could be responsible for these variations in TEC. The parameters used include the meridional and zonal wind velocity at 100 km over Cachoeira Paulista and Santa Maria which is a station close to Porto Alegre (wind data were not available for other stations) and the solar flux F10.7 cm. We made use of the Morlet wavelet power spectra to determine the periodicity in the TEC data and as well as in the other parameters. The last section in this dissertation is about the SSW events of 2007/2008 and 2008/2009 as observed in the GPS-TEC data of the geographic longitudinal range traced between -52° to -60° (the declination is -17° to -14°) and the magnetic latitudinal range was $\pm 20^\circ$ as shown in Figure 4.2.

5.1 Diurnal Variability

Each value of VTEC is obtained by mapping the ionospheric shell height at 400 km altitude in the satellite to receiver path. Two dimensional maps of VTEC with time resolution of 10 minutes and spatial resolution of $1^\circ \times 1^\circ$ in latitude and longitude were constructed using the procedure described in section 4.0. In order to reduce the errors associated with our mapping procedure, as well as to reduce a possible multipath contamination of the TEC data, we have excluded data with elevation angle below 30°

To observe monthly diurnal, solar activity, longitudinal, latitudinal, seasonal TEC variation and the behavior of EIA, data of the following locations were obtained from the map grid: Arequipa (16.5°S , $71,6^\circ\text{W}$) and São Luís (2°S , 44°W) located close to the dip equator and at both longitudinal ends of the South America region and Cachoeira Paulista (23°S , 45°W), and Porto Alegre (30°S , 51°W) located at low latitude region close to the anomaly crest. The TEC obtained from the mapping were in universal time and were converted to local time by using the equation:

$$T_z = \frac{LONG}{15}, LT = UT + T_z \quad (6.1)$$

where T_z = time zone, LT = local time, LONG = longitude, UT = universal time. Both low solar activity and high solar activity of 2009 and 2001 respectively were analyzed.

5.1.1 Diurnal variation in TEC for Solar Minimum of 2009

Figure 5.1 shows mass plots for typical quiet days ($K_p \leq 3$) of diurnal monthly variation of TEC for a period of 12 months from January to December 2009. The diurnal curves are obtained by the procedure explained above. The blue and green plots represent stations close to dip equator and low latitude stations close to the crest of the EIA respectively. It is clear from the figure that day minimum in TEC is obtained around 0600LT while day maximum occurs around 1300 to 1700LT. Almost similar TEC patterns are observed for all months of different seasons. In general, the diurnal variation of TEC shows a pre-dawn minimum, a steady early morning increase, followed by an afternoon maximum and gradual fall after sunset. Larger variations of TEC are observed in daytime for different stations while nighttime variations are observed only for some stations. The enhancement of TEC particularly at the low latitude stations during daytime can be associated with the upward drift of plasma caused by the fountain effect as a result of $\vec{E} \times \vec{B}$ drift and the consequent gravity force and gradient pressure which form two peaks known as the EIA (Abdu et al. 2007). The low latitude stations exhibits lower value of TEC during May, June, July and August compared to the same months of the equatorial stations. This implies that the formation of EIA is weaker during these months which represents winter solstices. The EIA strength and characteristics can be observed between the Cachoeira Paulista and Porto Alegre stations. In almost all the months, TEC enhancement is larger at the Cachoeira Paulista station than at Porto Alegre station. This is expected because 2009 is a low solar activity period and anomaly is restricted to lower latitudes. Longitudinal variation was observed between São Luís and Arequipa. The Arequipa station shows slightly larger TEC enhancement in almost all the months than the São Luís station. This is expected because São Luís is closer to the equator than the Arequipa station and there is always a trough at the equator due to fountain effect as explained above. However larger magnetic declination effect over São Luís can cancel out the difference and even make São Luís to exhibit larger TEC than Arequipa. This phenomenon is observed in the 2001 solar maximum period.

It is important to mention that the negative TEC value that appeared in some of our result is due to the underestimation of delay code bias by the Nagoya model which has no effect on our studies of ionospheric behavior.

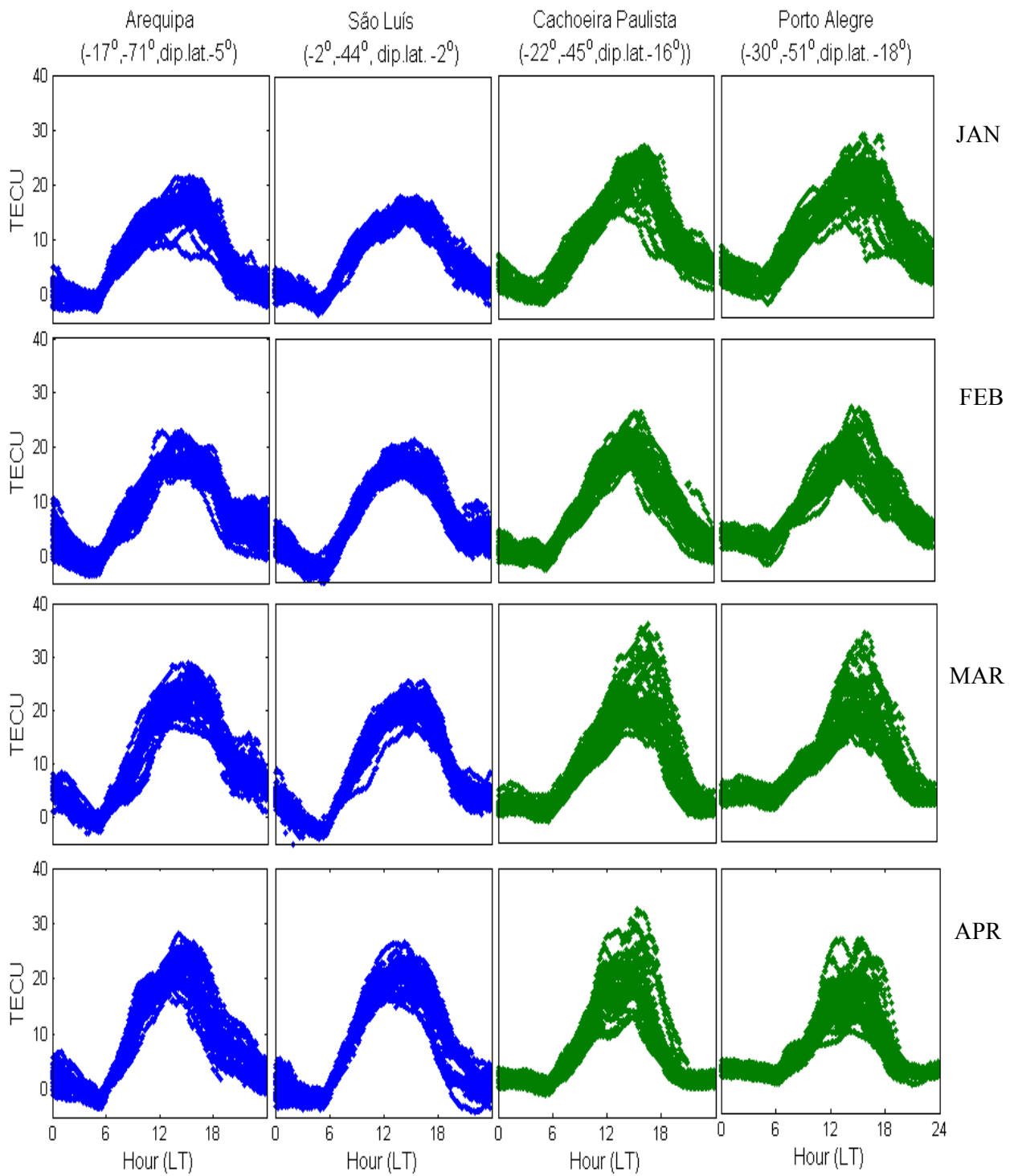


Figure 5.1 - Monthly diurnal TEC variation during 2009

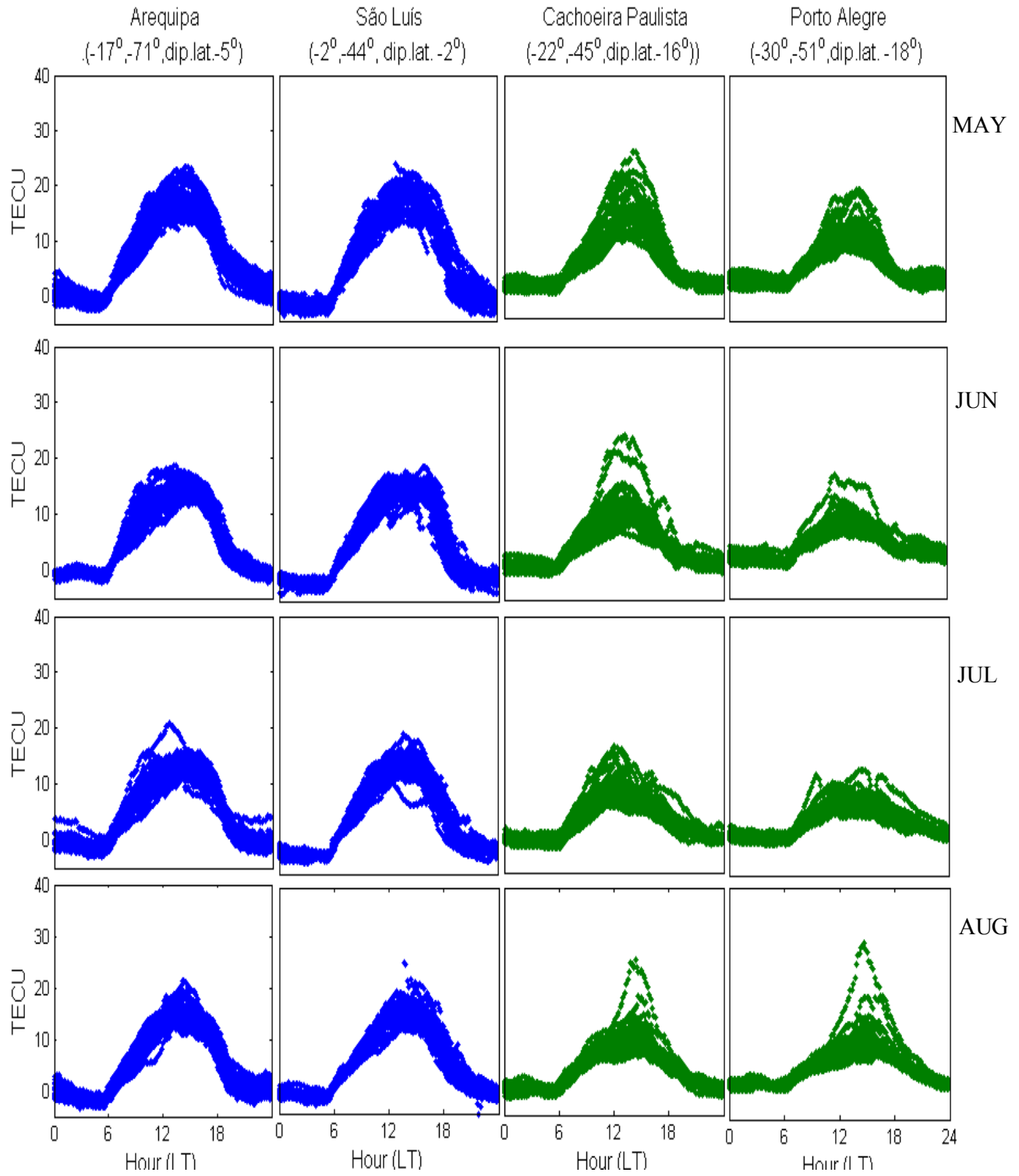


Figure 5.1 - Monthly diurnal TEC variation during 2009

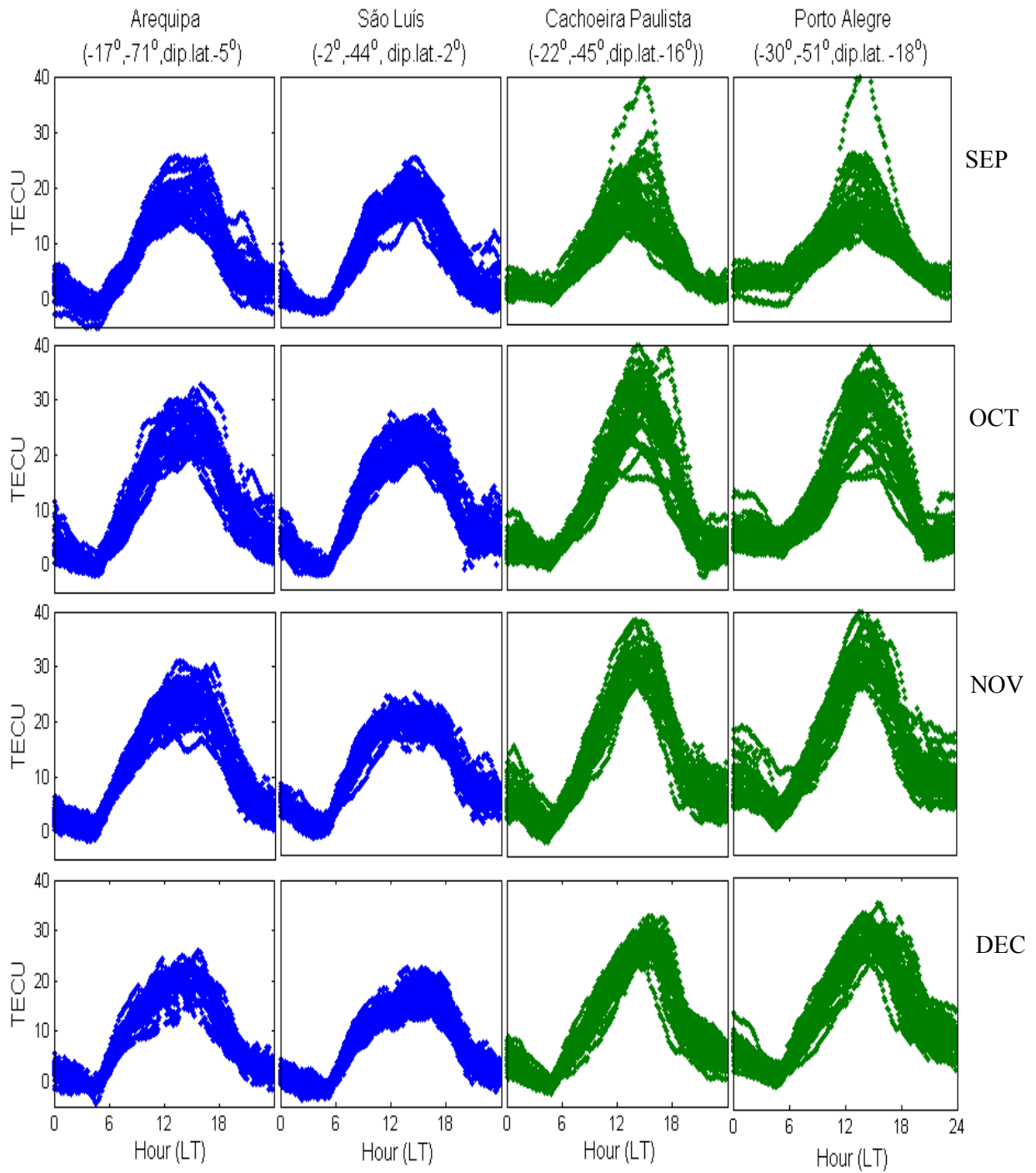


Figure 5.1 - Monthly diurnal TEC variation during 2009

5.1.2 Diurnal Variation in TEC for Solar Maximum of 2001

Figure 5.2 shows the mass plots of diurnal monthly variation of TEC from January to December 2001. Similar diurnal patterns are observed for all months as compared to 2009 except that the rate of nighttime increase are different due to the prereversal enhancement that is prominently associated to solar maximum period. It is important to note that the scale was changed from 40 to 150 TECU and values of TEC increased drastically by more than 200% from solar minimum to solar maximum for all stations. This increase is mainly due to the corresponding increase in the solar flux represented by F10.7 which declined from 235.6 (highest in 2001) to 76.8 (highest in 2009).

Apart from the daily anomaly peaks observed from the 2009 low solar activity, some late anomaly peaks can also be observed after sunset in the months of January to May and October to December for Cachoeira Paulista and Porto Alegre low latitude stations during 2001 high solar activity. It is clearly seen from Figure 5.2 that the weakened EIA at sunset around ~1800-1900LT become intensified during the post-sunset hours. Anderson and Klobuchar (1983) affirmed that the primary source of the enhancement at equatorial anomaly latitudes after sunset is the evening increase of the equatorial fountain. The strength of the EIA at sunset that is intensified by the prereversal electric field enhancement (PRE) is dependent on the solar flux values F10.7 and corresponding increase in the zonal wind and of the ratio between the magnetic field average Pederson conductivity in the F and E regions (Fejer et al. 1991). This will be discussed in more detail later in this section.

Furthermore, some differences were observed between Arequipa and São Luís equatorial stations in 2001 high solar activity, São Luís showing the largest TEC throughout the year as shown in Figures 5.3 and 5.4. However the opposite is the case for solar minimum of 2009 where Arequipa station shows slightly higher values of TEC than São Luís particularly in months of Jan to Apr while the months of May to Dec show the same level of TEC. One of the reasons for this longitudinal difference could be as a consequence of a higher magnetic declination at São Luís station compared to the Arequipa station.

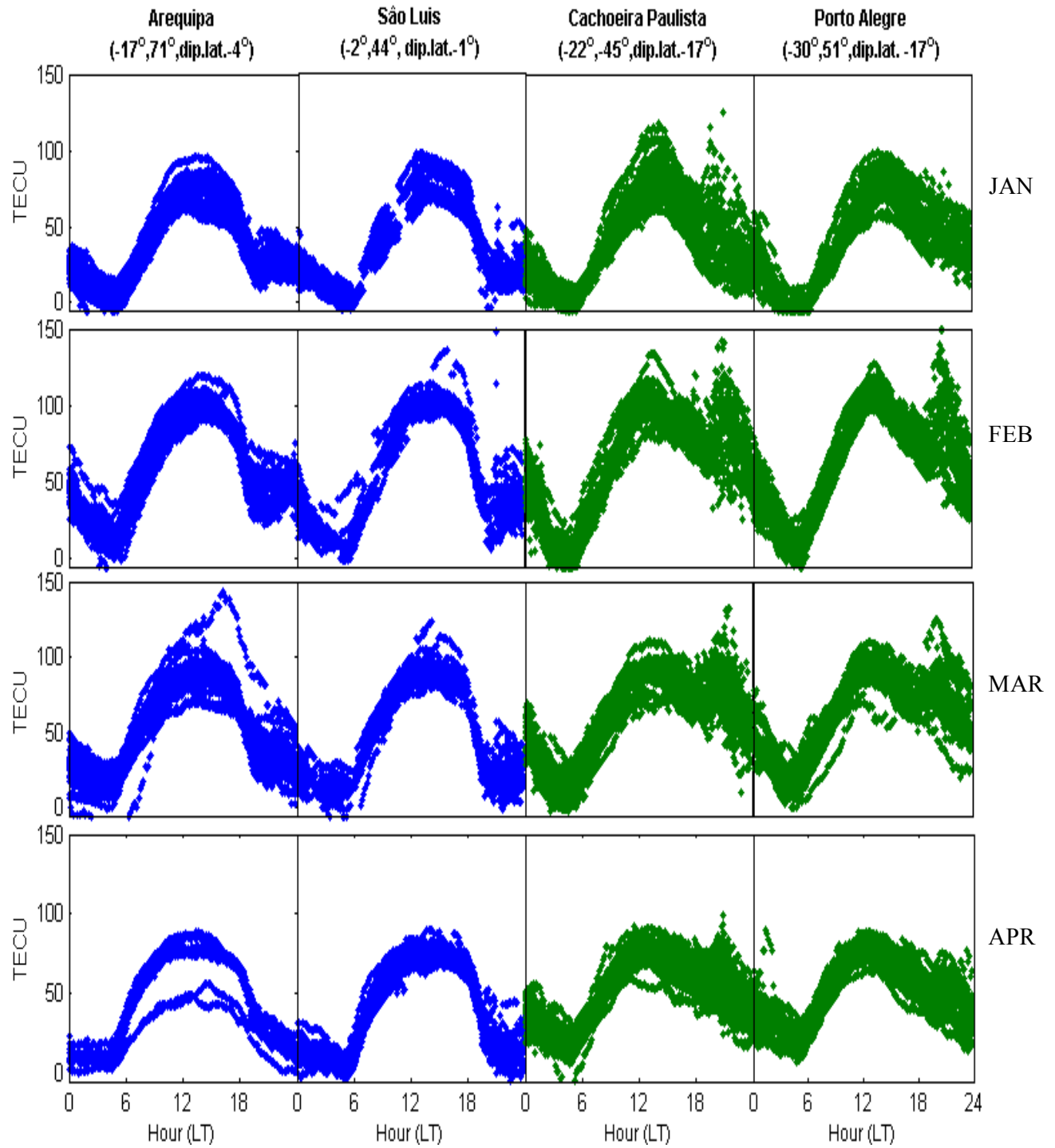


Figure 5.2 - Monthly diurnal variation during 2001

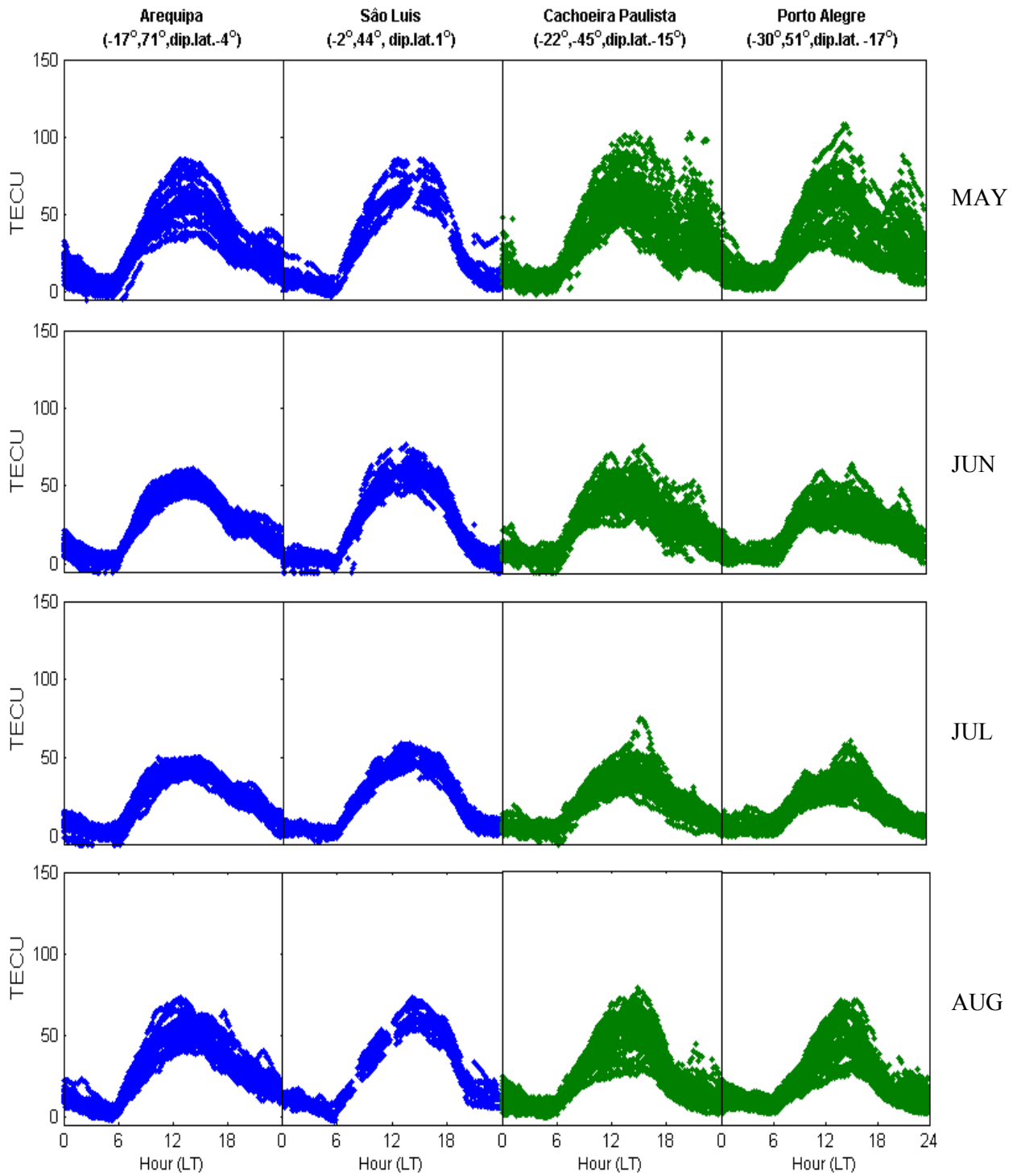


Figure 5.2 - Monthly diurnal variation during 2001

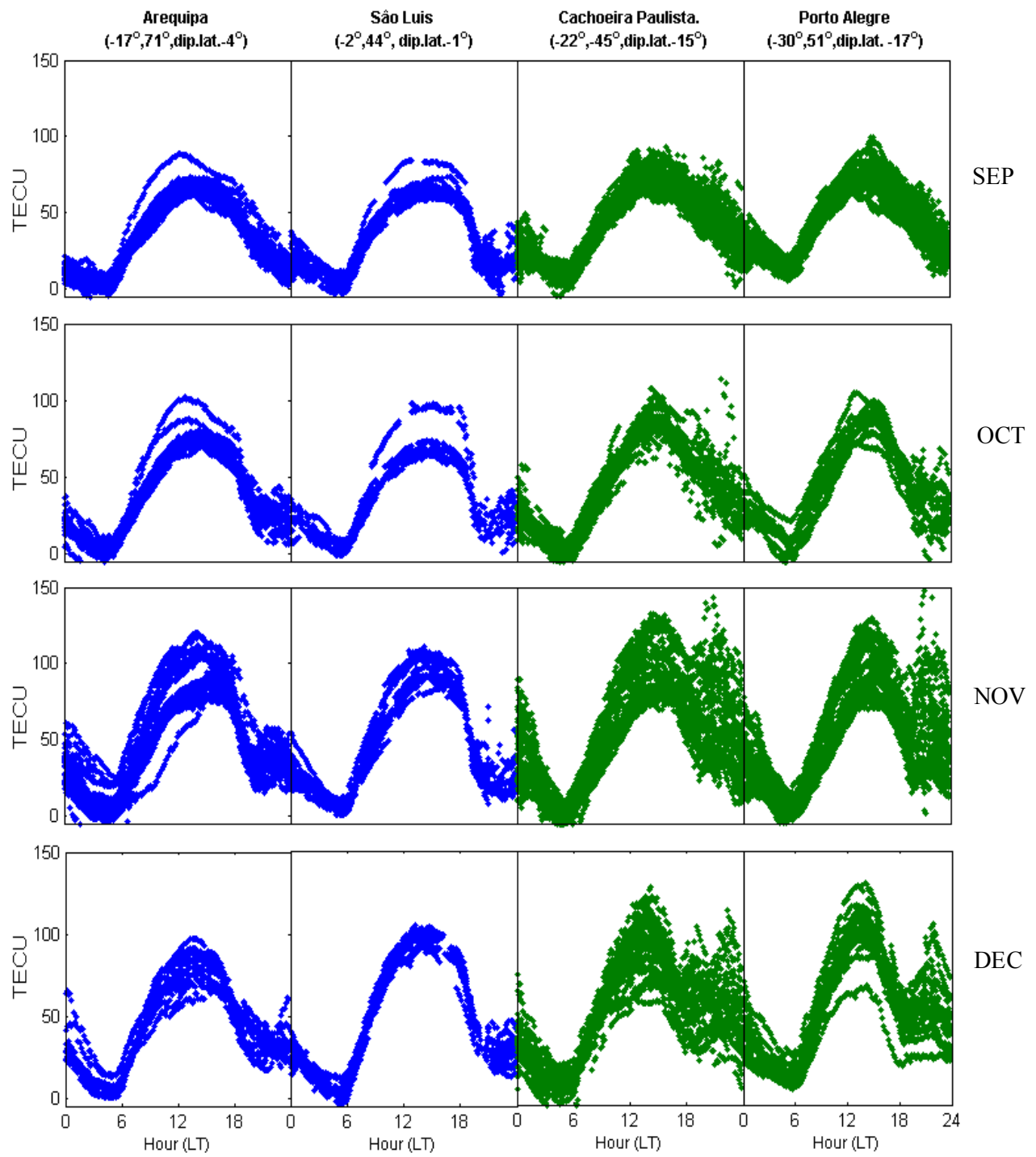


Figure 5.2 - Monthly diurnal variation during 2001

5.1.3 TEC Monthly Variability for 2009

In order to clearly observe the variability exhibited by the diurnal TEC variation shown in Figures 5.1, the monthly average values (TEC) and the standard deviation (STD) values were deduced from the hourly values and plotted on the same axes to give a summary measure of the hourly variability of TEC for each month. The monthly F10.7 is also indicated with the corresponding months at the right side of the plot.

Generally, it is possible to see clearly from the STD in Figure 5.3 that the importance of these plots lies in the fact that they show TEC variations as it changes from one month to another and show the actual variability values of TEC at different local time in different months of different seasons, longitudinally and latitudinally. The STD was found to vary according to the diurnal variation, exhibiting low and steady STD between 1 to 2 TECU during predawn and morning hours, a buildup of up to 4 TECU in daytime and reaches 6 TECU after sunset. It is interesting to see that during winter the diurnal TEC variations are lower at low latitude than at the equator while during summer and equinox the diurnal TEC variations at the low latitude are larger than during winter. This is expected because the fountain effect is more developed at the equator during summer than during winter. Another interesting fact that can also be observed is that diurnal TEC/STD at Cachoeira Paulista is larger than at Porto Alegre. This is due to low photoionization associated with the period of low solar activity which could result to weak diurnal EIA strength hence very low diurnal anomaly get to higher latitudes like Porto Alegre.

The nighttime highvariability is observed only at stations under the anomaly crest during the months of January to April and October to December while the equatorial stations maintain low and steady TEC variability (as indicated by the STD) following the average TEC diurnal pattern. In general, the figures illustrate that the day-to-day variability in 2009 low solar activity is low (highest F10.7 = 76.8).

2009

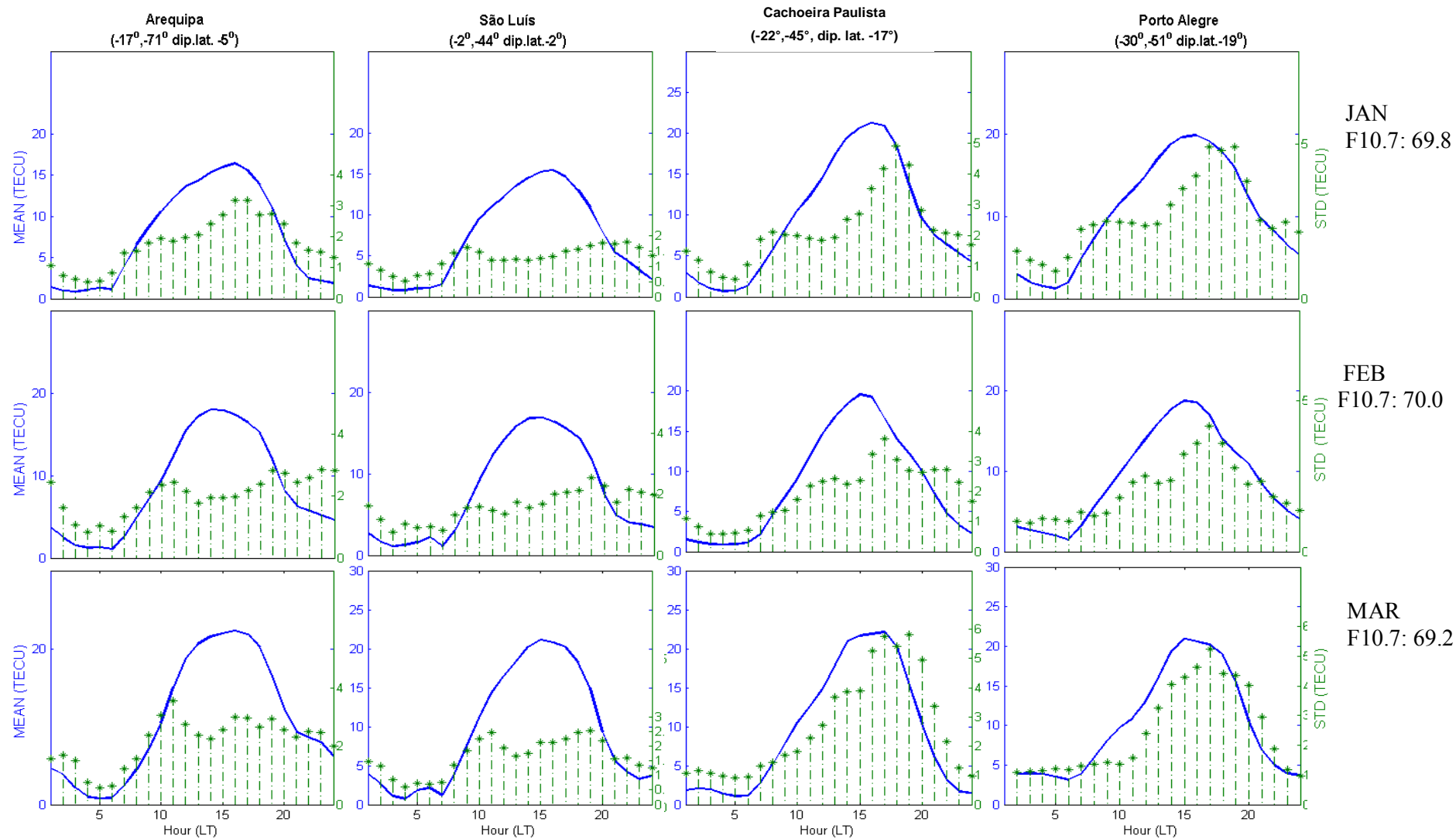


Figure 5.3 - Monthly average together with standard deviation for each month in 2009

2009

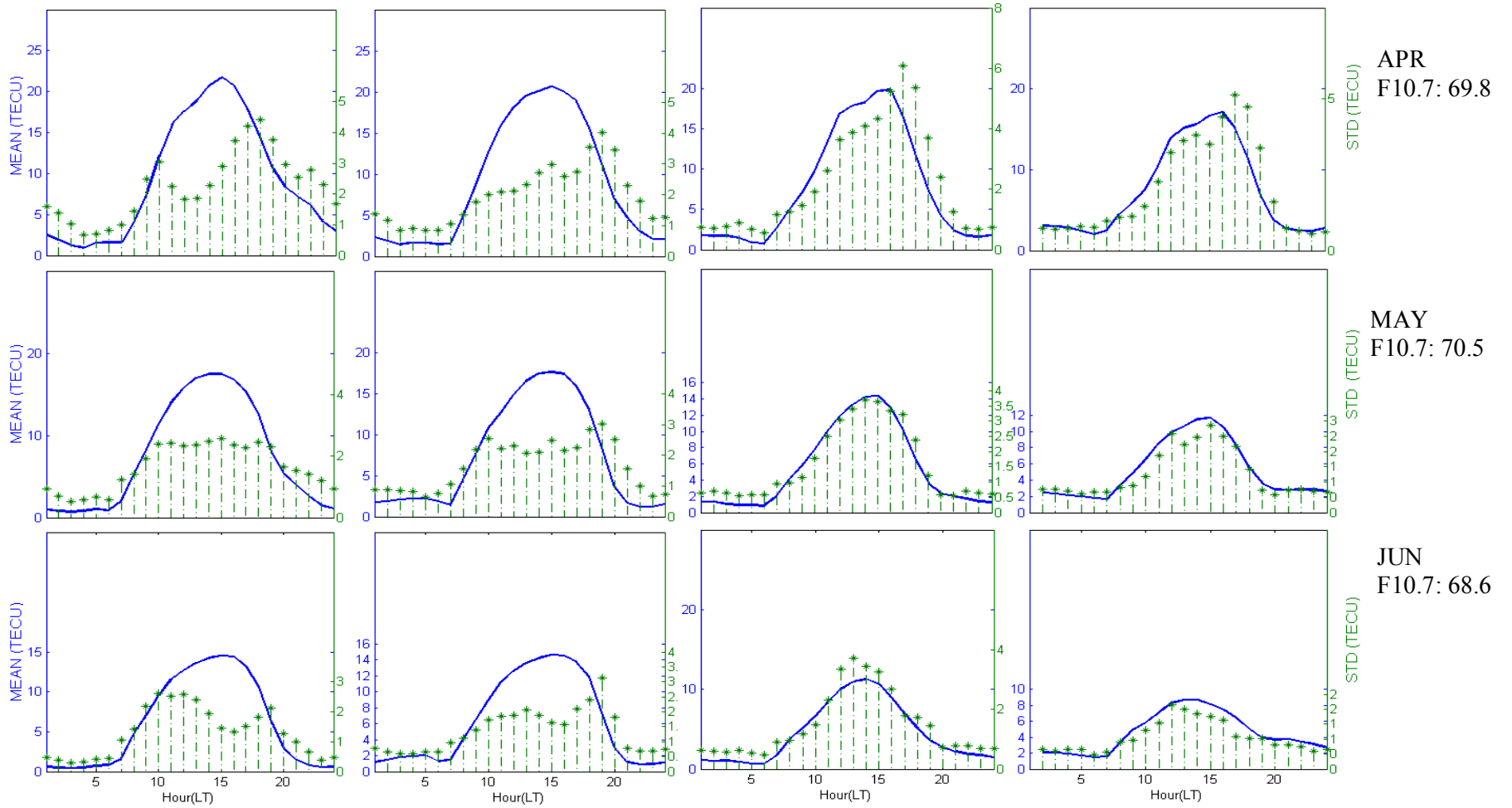


Figure 5.3 - Monthly average together with standard deviation for each month in 2009

2009

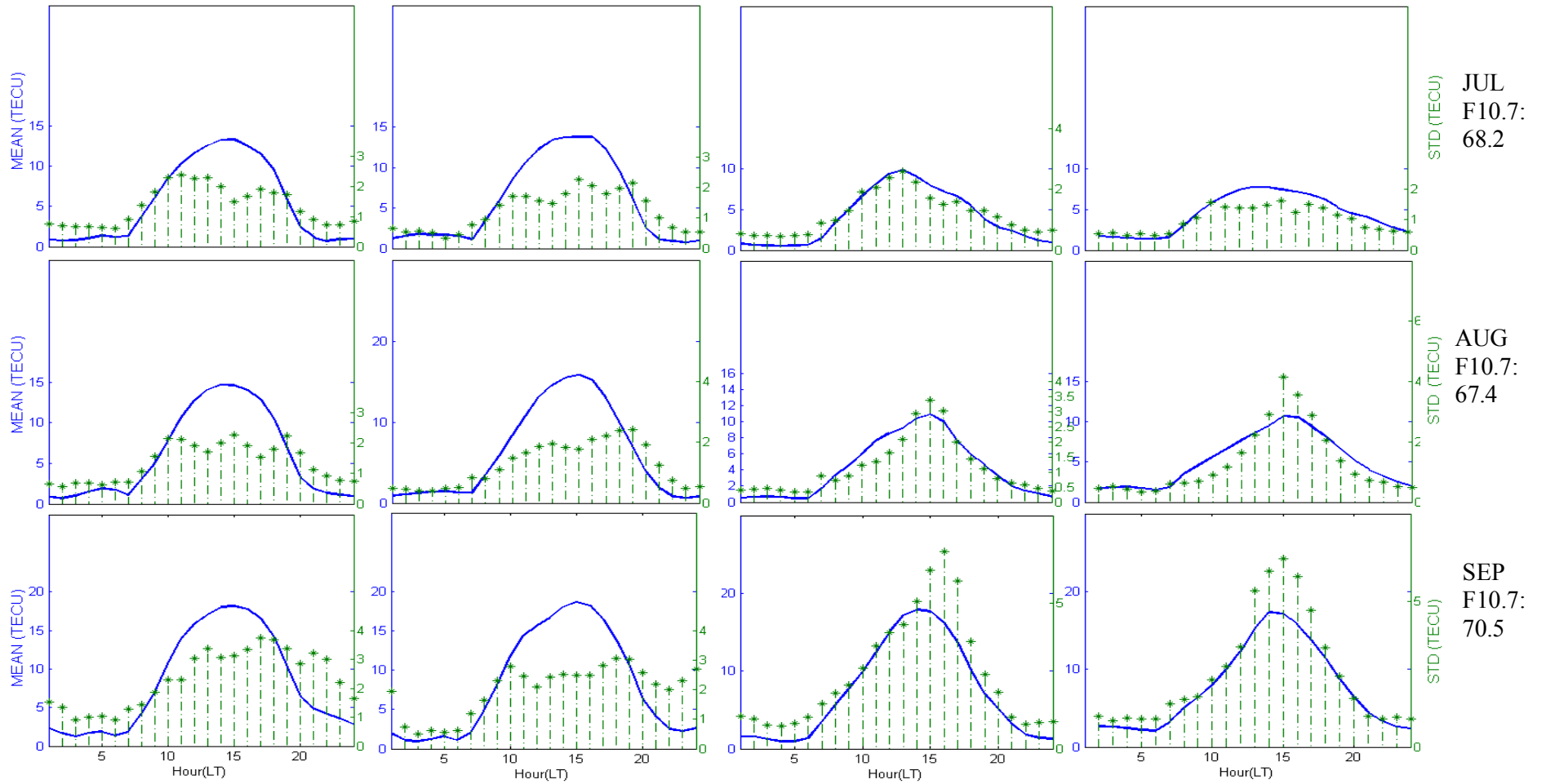


Figure 5.3 - Monthly average together with standard deviation for each month in 2009

2009

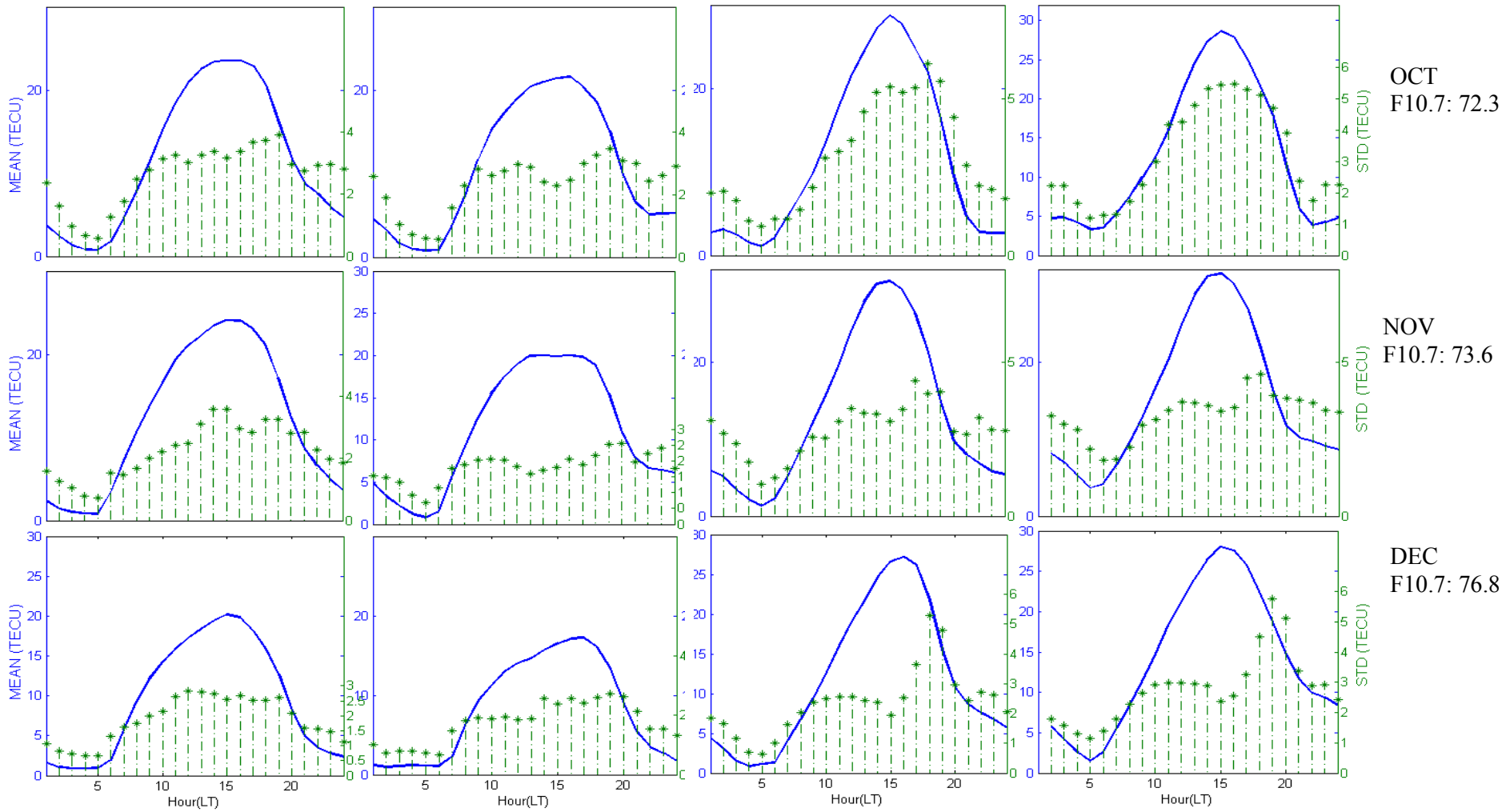


Figure 5.3 - Monthly average together with standard deviation for each month in 2009

5.1.4 TEC Monthly Variability for 2001

Separate figures were plotted for 2001 solar maximum activity using the same analytical method as section 5.1.3 above. The standard deviations were found as well, to vary according to the diurnal variation in some cases for example in June to August, however, the months of March to April and September to October exhibit high post sunset variability in TEC as seen from the STD. The STD increased from 5 TECU (highest observed in the 2009 solar minimum) to 30 TECU in 2001 (highest observed in the high solar period) and it is dominant after sunset during months with relatively high F10.7. This behavior is found mostly at stations located in low latitude region. **This indicates that day-to-day variability from monthly basis of TEC is larger during solar maximum.** A similar variation was been reported by Abdu et. al. (2007) using foF2 data measured by digisondes in the equatorial and low latitude locations in Brazil in 1996 to 2003.

Unlike what was observed in 2009 low solar activity (Figure 5.3) the TEC/STD during day time and nighttime at both Cachoeira Paulista and Porto Alegre exhibits different levels of EIA amplitude. This is because there is higher photoionization effect and more prereversal enhancement effect that could make the fountain effect to be well developed during this period. As a result, the EIA reached much more higher latitudes. Therefore it is logical to conclude that the characteristic of EIA depend largely on solar activity.

High variability in TEC as seen in the STD were observed between 19 and 23LT. The months of March- May, September and October exhibited the largest nighttime variation in STD during post sunset followed by February and November months and the months of June, July and August months indicate lowest nighttime variability and at the low latitude stations as seen in Cachoeira Paulista and Porto Alegre. (Figure 5.4). Generally, a day-to-day analysis revealed that the month of January had very few nighttime variations, which increased through February and had maximum values during the months of March, September and October (Figure 5.4).

Besides the clear evidence from Fejer et. al. (1991) and Abdu et al. (2007) that solar flux plays a principal role in the vertical prereversal drift enhancements and late high peaks in TEC respectively, another important factor that could be responsible for the evening prereversal enhancement and the consequent nighttime variations in TEC as seen in Figure 5.4 could be from the faster decrease of the E region ionospheric conductivity after sunset relative to the F region ionospheric conductivity.

In summary, the variability in TEC as seen from the STD of Figure 5.3 of 2009 low solar activity exhibits a close proportion compared with 2001 high solar activity. Also, the increase in solar flux represented by F10.7 has a substantial increase in TEC from low activity to high solar activity. This behavior is also demonstrated by the VTEC of Figure 5.1 and 5.2.

2001

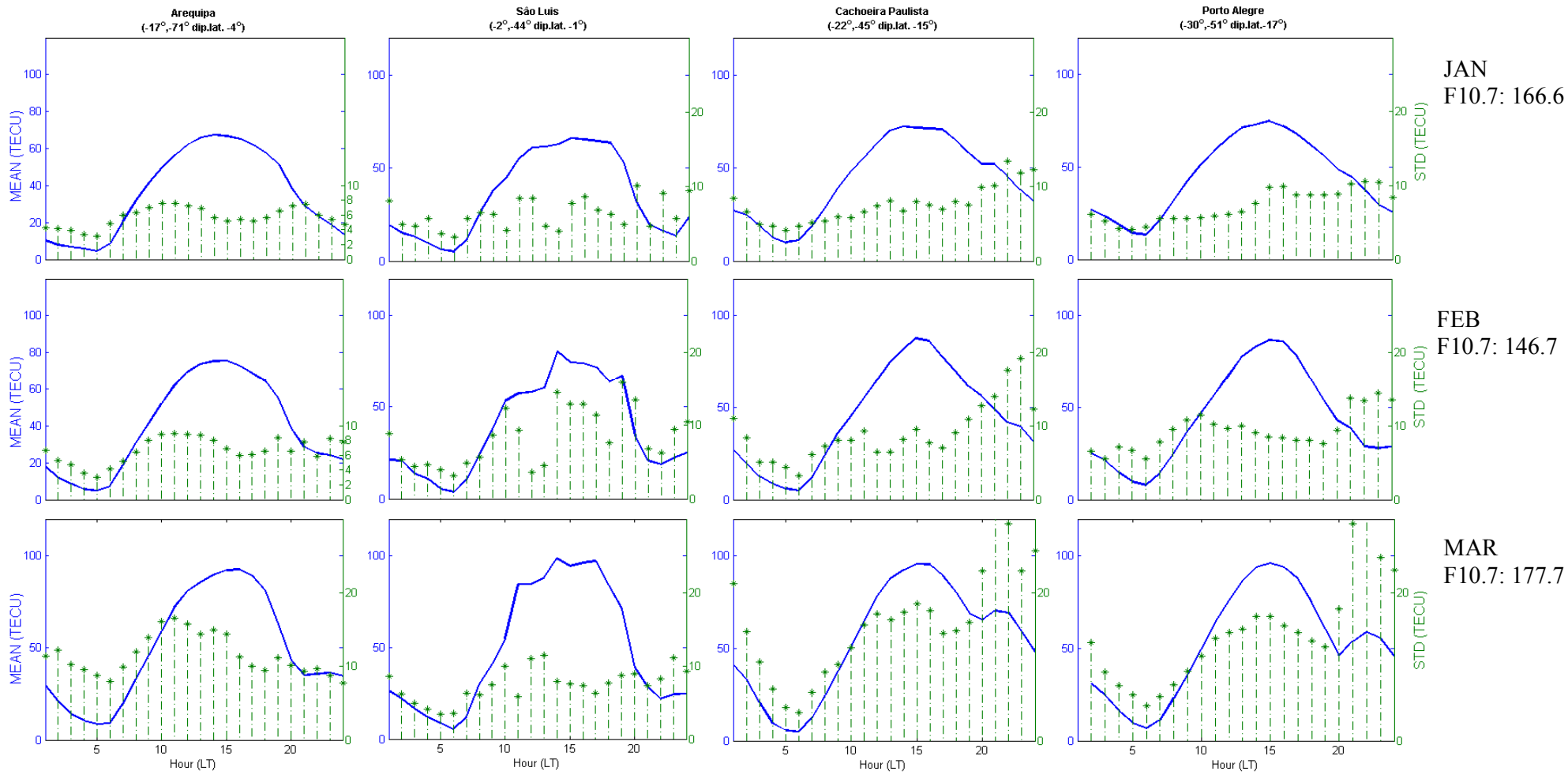


Figure 5.4 - Monthly average together with standard deviation for each month in 2001

2001

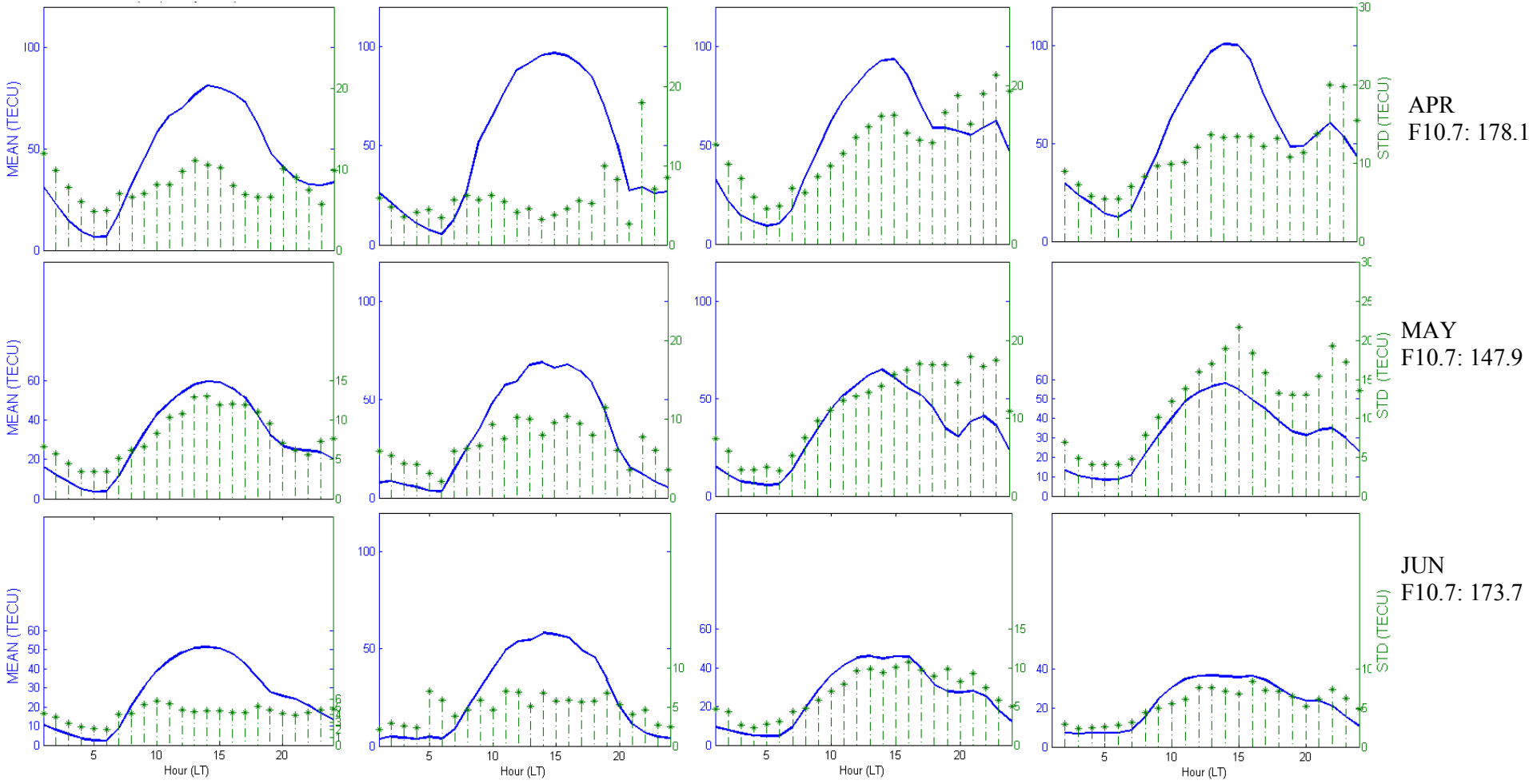


Figure 5.4 - Monthly average together with standard deviation for each month in 2001

2001

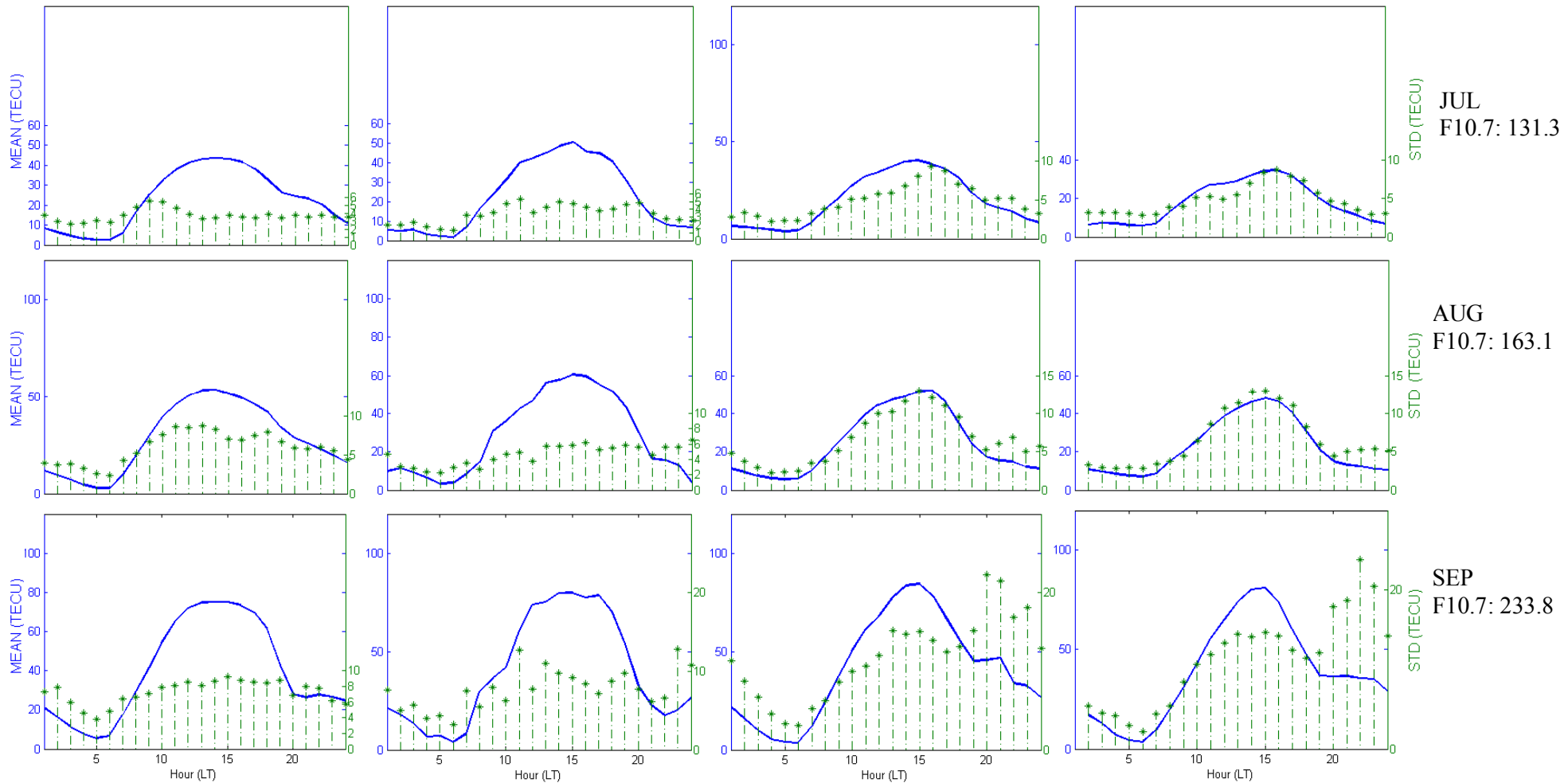


Figure 5.4 - Monthly average together with standard deviation for each month in 2001

2001

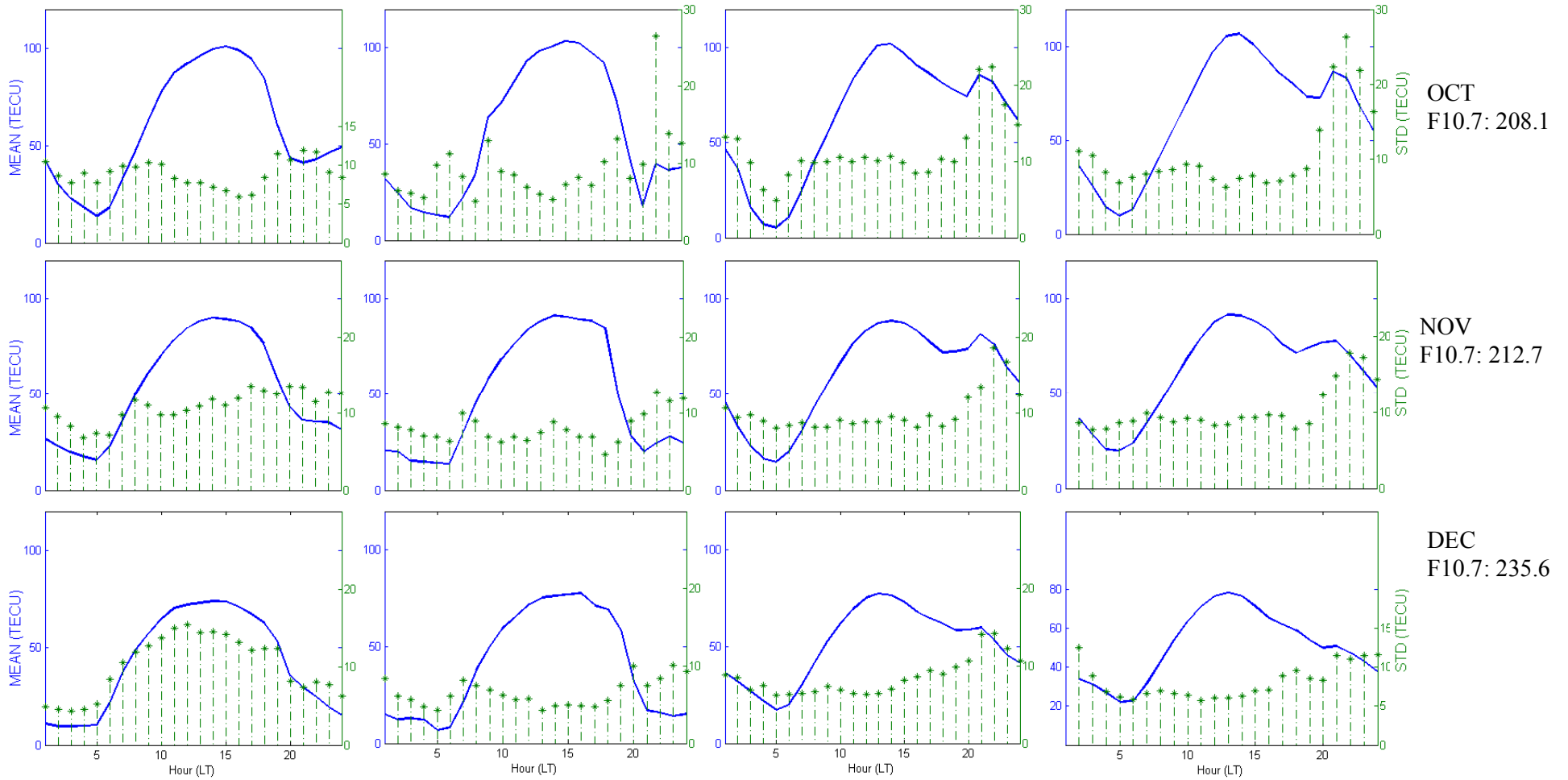


Figure 5.4 - Monthly average together with standard deviation for each month in 2001

5.1.5 Seasonal Variability in TEC

The mean and the standard error bar for hourly seasonal variation in TEC for both 2009 and 2001 as shown in Figure 5.5 and Figure 5.6 respectively, were plotted to show the seasonal hourly dispersion of TEC. The blue color represent winter solstice, green represent equinox and red represent summer solstice. There are important seasonal and long term variations in the ionosphere and therefore each season is represented by groups of four months as stated at section 4.4 in order to study these variations. The average F10.7 for each season is also indicated at the right hand side of the figure.

Generally, the winter solstice shows the lowest value of TEC over all stations for both minimum and maximum solar activities. This is expected because in winter solstices the photoionization at the equator decrease because the sun overhead moves to summer hemisphere and fountain effect is expected to be weak.

However, it is clearly seen that TEC from (figure 5.5 and 5.6) summer solstice is higher than the equinox during 2009 solar minimum activity (figure 5.5). On the hand, during 2001 solar maximum activity, equinox exhibits higher TEC values compared to the summer of the same year (figure 5.6). This phenomena could be because of the following reasons.

Explanations for 2009 (Summer Solstice TEC Larger than Equinox)

It is well known that photoionization caused by EUV radiation has a big contribution in the formation of the EIA apart from the fountain effect and vertical drift that also play a major role. Photoionization can result to more production of electron and therefore enhances the background electron density, hence larger peaks of EIA can be observed during summer solstices. The seasonal effect is clearly seen particularly between December solstice and June solstice of our results during both solar activities (Figure 5.3 and 5.4). The seasonal effect describes the fact that TEC during December solstice conditions is on the average larger than during June solstice conditions. Figure 5.3 and 5.4 also indicates that the TEC variability (showed by the STD) is reduced by about 30% (for stations at the equator) and 200% (for stations at the crest of the EIA) from December to June solstice conditions for both solar activities. The Sun-Earth distance between June and December period could be a causative factor (JEE et al., 2004).

Explanations for 2001 (Equinox TEC Larger than Summer Solstice)

On the other hand, during the equinoxes, the sun overhead is around the equator and the temperature at the equator is hotter than at the pole therefore thermospheric meridional wind blows towards the poles from the equator. This meridional wind changes the neutral composition and O/N₂ increase at equatorial and low latitude stations (due to stronger effect of wind transport during high solar activity). The increase will be maximum at F2 region, and N₂ dissociation is the major process which removes ambient electrons. Hence the increase in O/N₂ ratio will result in higher electron density and therefore during equinoxes, EIA is expected to be more developed than during the solstices. This is referred to as semiannual variation. This mechanism may not work for solar minimum because of low wind effectiveness due to low ionization. The semiannual variation of the EIA could also be due to the combined effect of the solar zenith angle and magnetic field geometry (Wu et al., 2004). TEC diurnal peak show semiannual variation with peak during the equinox of 2001 solar maximum (Figure 5.6) while the diurnal peak TEC variation is observed during the summer of 2009 solar minimum (Figure 5.5) and troughs are observed during winter solstice for both solar activities. This implies that equinoctial semiannual variation depend largely on solar flux.

Generally, the seasonal and semiannual variation vary from one station to another. During 2009 low solar activity, the low-latitude stations illustrate higher TEC daily peaks during summer and equinox while stations close to the equator (São Luís and Arequipa) exhibits low anomaly peaks. On the hand, during winter solstice TEC daily peaks are larger at equatorial stations than at low latitude stations. The reason for this has been explained in section 5.1.4. However taken a close look on Figure 5.6, it can be observed that during summer solstice the equatorial stations presents slightly larger TEC daily peaks than the low latitude station while during equinox period larger TEC daily peaks are observed at the lower stations than at the equator. This is because wind is effective during solar maximum and it blows increase O/N₂ towards the equator during summer (hence low TEC value is observed at low latitudes) and towards the low latitudes during equinox (hence low TEC values are observed at equator). It is important to mention that unlike 2009 low solar activity that exhibited low F10.7 seasonal variation, 2001 high solar activity was associated with high F10.7 seasonal variation. Therefore further observation is needed to clarify our result of 2001 TEC seasonal variation.

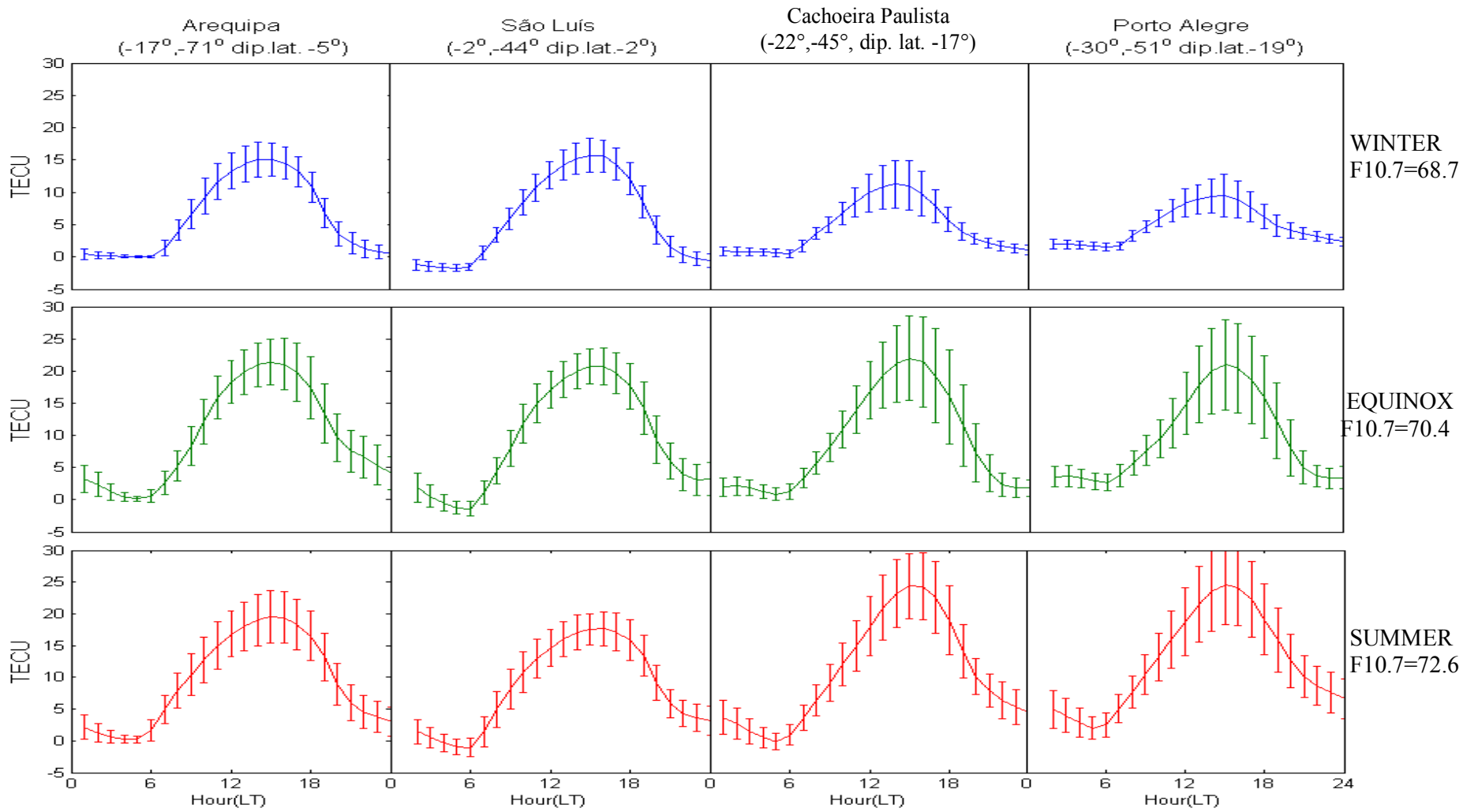


Figure 5.5 - Seasonal variability during 2009

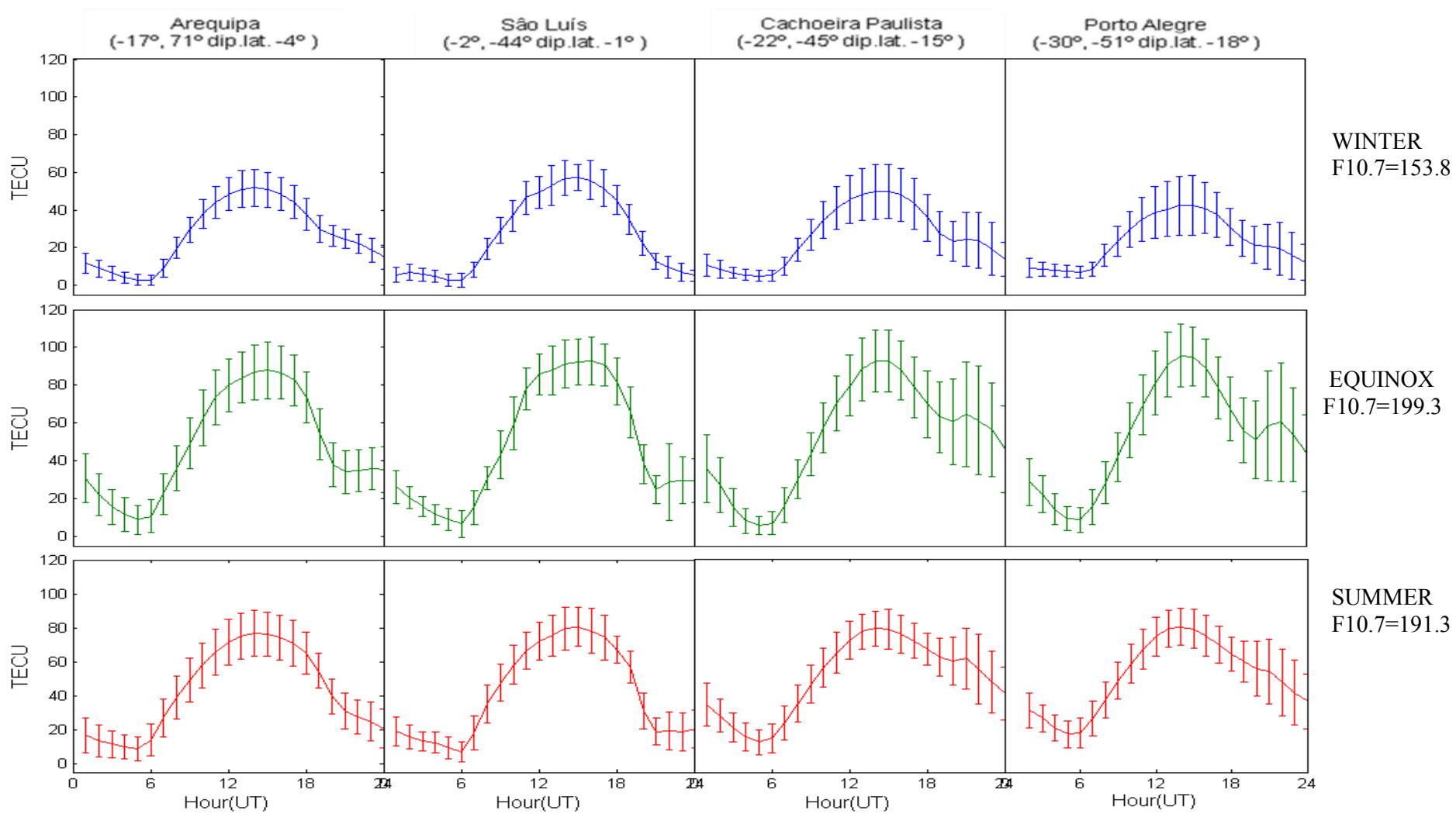


Figure 5.6 - Seasonal variability during 2001

5.1.6 Monthly and Seasonal TEC Variations.

Figure 5.7 shows color contour plots of monthly average of TEC for the low solar activity (left panel) and high solar activity (right panel) as a function of day and local time, longitude (between Arequipa and São Luís) and latitude (between São Luís, Cachoeira Paulista and Porto Alegre). In order to have the same scaling system for both solar activity plots, we used:

$$20 \log_{10} \left(\frac{TEC}{TEC_{ref}} \right) \quad (5.2)$$

where $TEC_{ref} = 1 \text{TECU}$.

Solar cycle 23 is characterized by both extreme minimum (2009) and extreme maximum (2001) activity period that is unique in many ways and it is therefore important to observe the extent of the effect on TEC variation.

The interesting facts in Figure 5.7 is that we can clearly observed that the daily, monthly, seasonally, longitudinal and latitudinal variation as function of time. Most of our discussion before are reflected in these two figures. The most important TEC features are:

- ✓ Nighttime prereversal enhancements peaks are observed at Cachoeira Paulista and Porto Alegre stations particularly during high solar activity (2001), but not at São Luís because it is very close to the equator and very little peaks are shown in Arequipa station because it is relatively further way from the equator compared to São Luís station.
- ✓ The prereversal peaks are dominant during equinoxes for 2001 solar phase, which signifies a semidiurnal variation.
- ✓ Generally, in both 2009 and 2001 solar phases we can observe the seasonal peaks between summer and winter (annual variation) and the equinox maximum compared to the solstices (semiannual variation).
- ✓ The figure shows that there is no much longitudinal difference between Arequipa and São Luís for 2001, and São Luís exhibiting slightly larger TEC in 2001 period than Arequipa of same period and Arequipa shows smaller peaks at sunset compared to São Luís during equinox of 2001.
- ✓ The solar flux variations between the two extreme solar activity is clearly reflected by the value of TEC between the two periods.

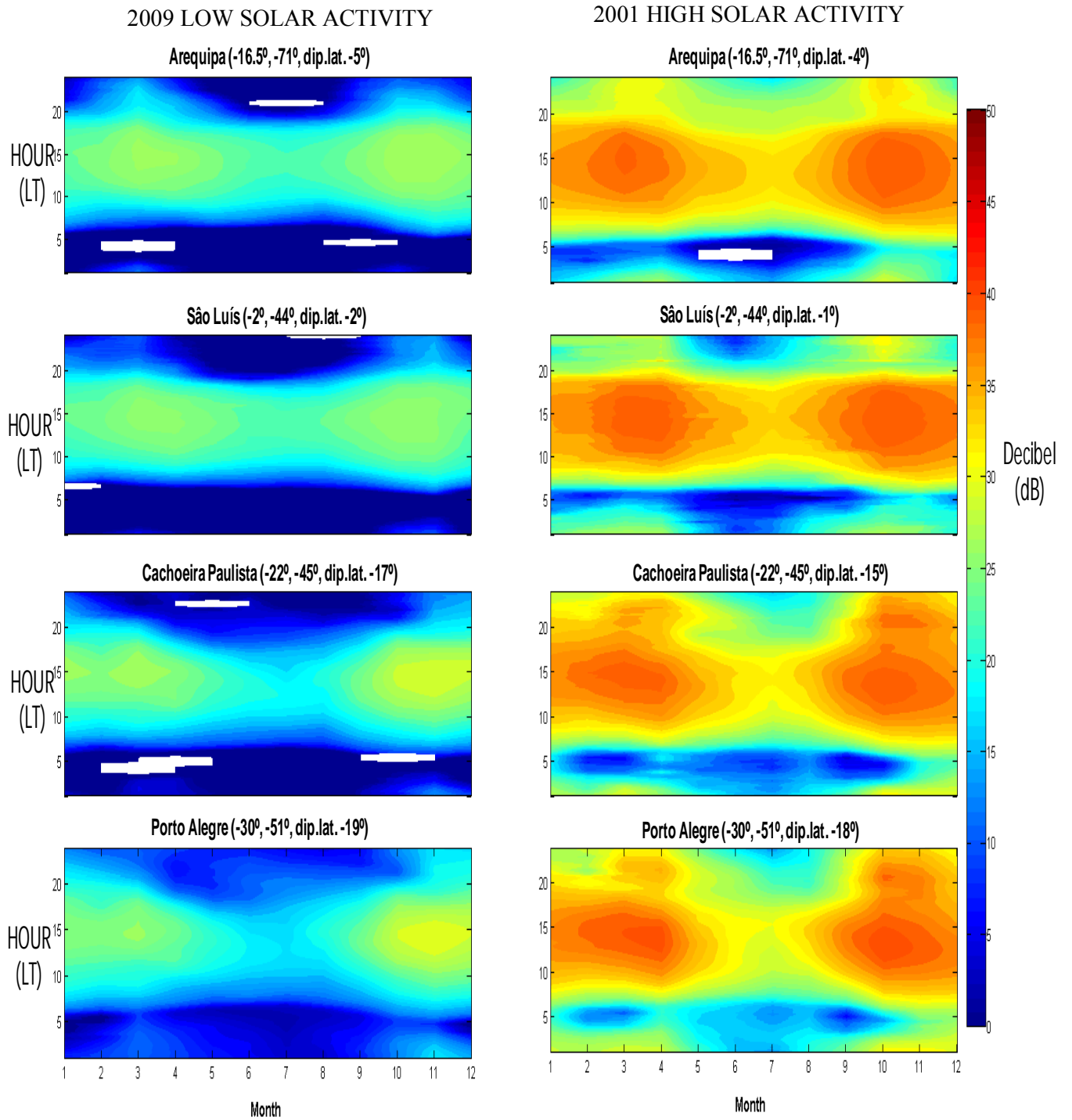


Figure 5.7 - The monthly TEC average contour plots for low (left) and high (right) solar activity.

5.2 TEC Equinoctial Asymmetry

The TEC around equinox during both low and high solar activity is represented in Figure 5.8. Our analyses of data brings out clear existence of an equinoctial asymmetry between TEC values of March and September and how it varies with local time, longitude (Areq and Salu) and latitude (Salu, Chpi, and Poal).

Generally, we observe that TEC during March equinox is larger than TEC during September equinox. In Figures 5.3 and 5.4, we also observed that although the F10.7 cm increases (insignificant increase) from 69.2 to 70.5 in March to September 2009 and increases (significant increase) from 177.7 to 233.8 March to September 2001, TEC values in September does not show the correspondent expected increase with solar flux increase particularly in 2001.

To further investigate this behavior, we made plots of daily correlation (Figure 5.9) of the solar flux parameters F10.7, EUV, and SSN as a function of TEC and for the low latitude receiver stations of Cachoeira Paulista and Porto Alegre for both solar minimum and maximum activities. The plots show positive correlations for all stations for both solar activities. Hence it is certain that TEC increase actually corresponds normally with daily solar flux increase, therefore there could be other factors responsible for TEC asymmetry between March and September. Fejer and Scherliess (1995) and Scherliess and Fejer (1999) had earlier pointed out that during daytime when the equinoctial asymmetry is larger, the equatorial vertical drift which is the main driver of the EIA, is nearly independent of solar flux conditions.

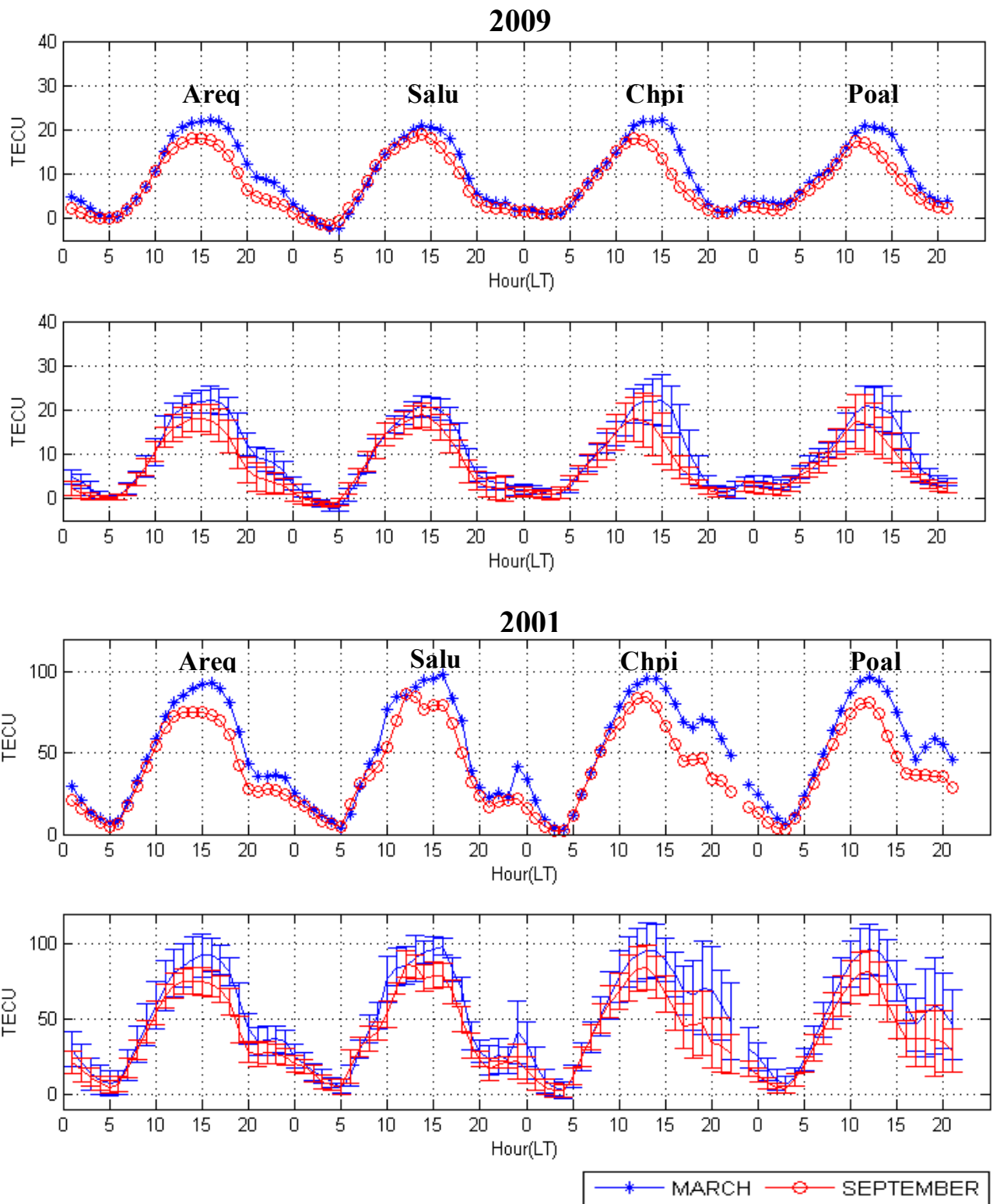
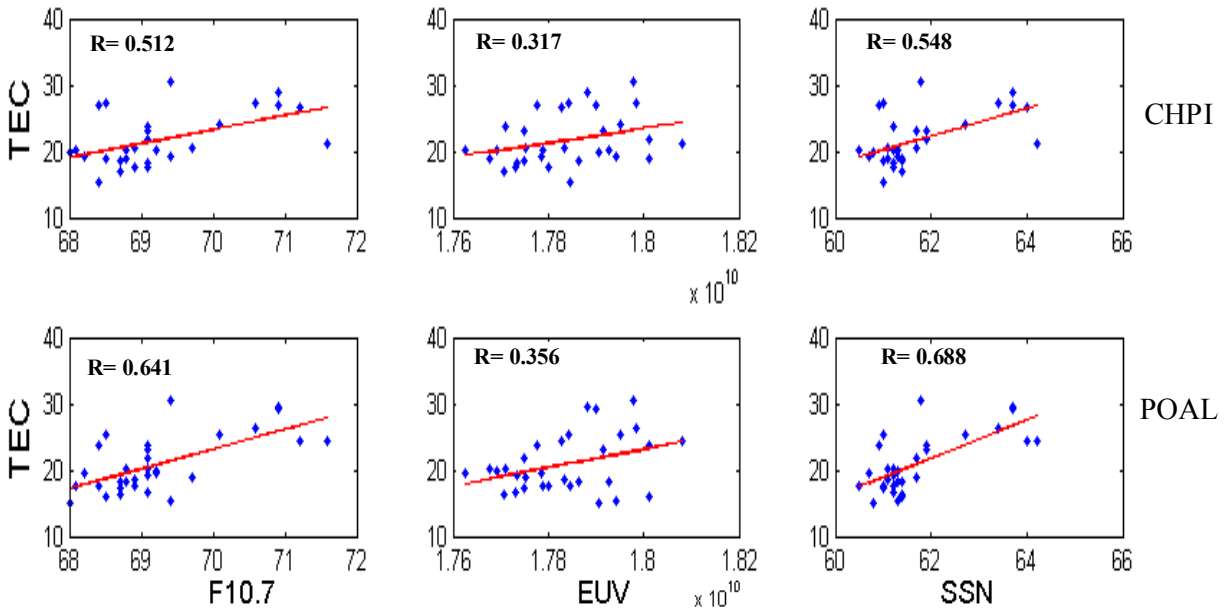


Figure 5.8 - TEC for March and September Equinoxes for 2009 (top panel), and 2001 (bottom panel)

MARCH EQUINOX 2009



SEPTEMBER EQUINOX 2009

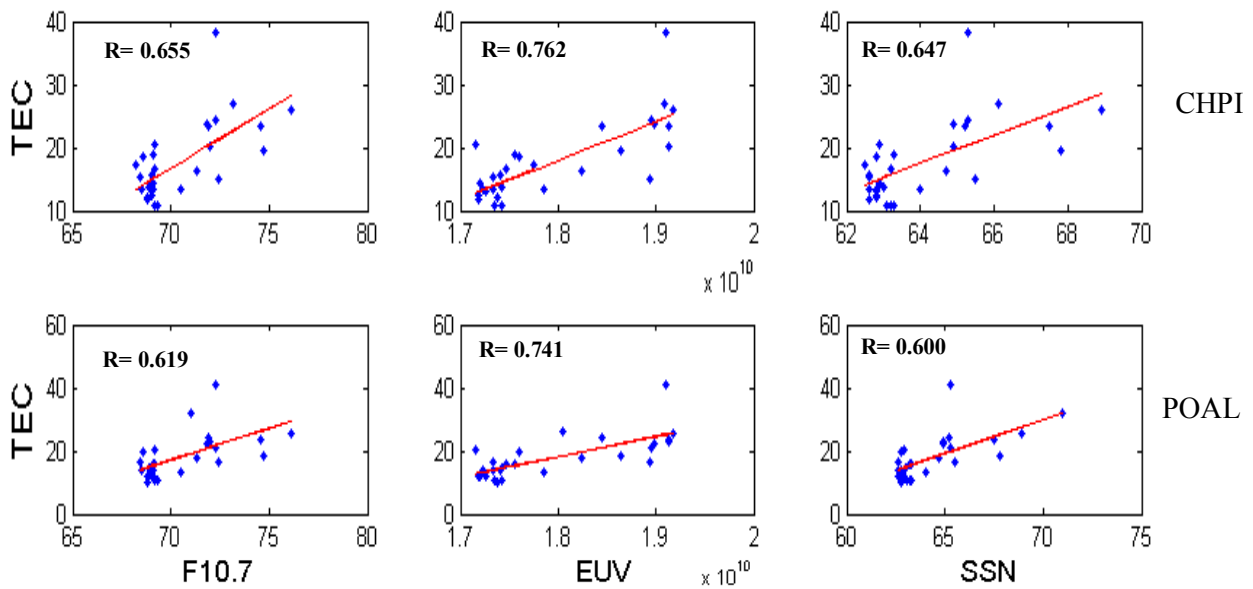
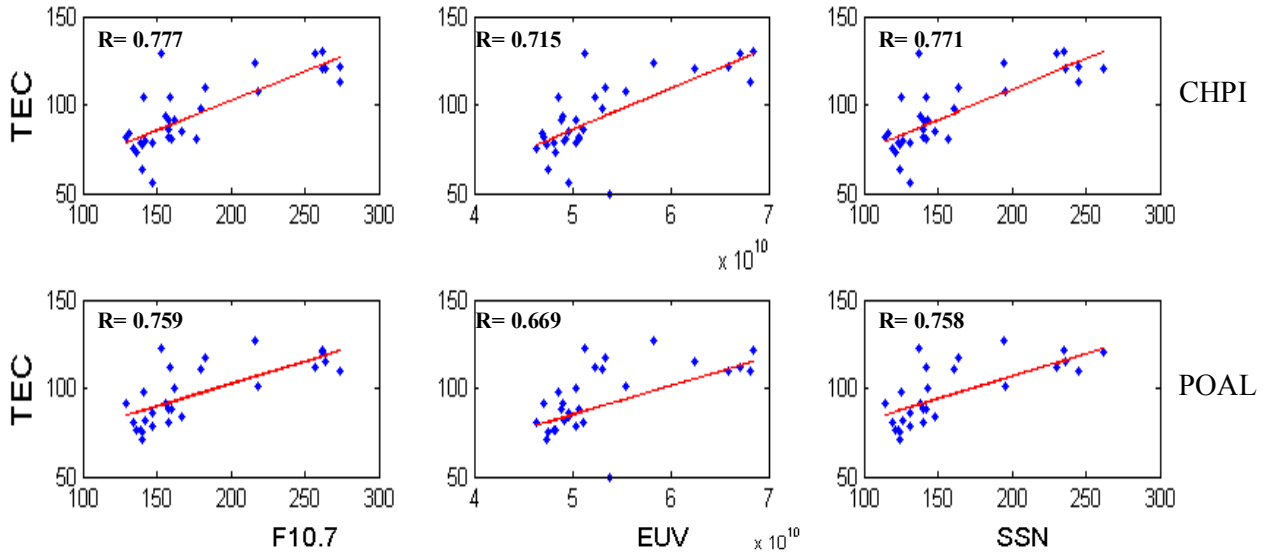


Figure 5.9 - Correlation of daily average of TEC with solar flux for March and September Equinoxes

MARCH EQUINOX 2001



SEPTEMBER EQUINOX 2001

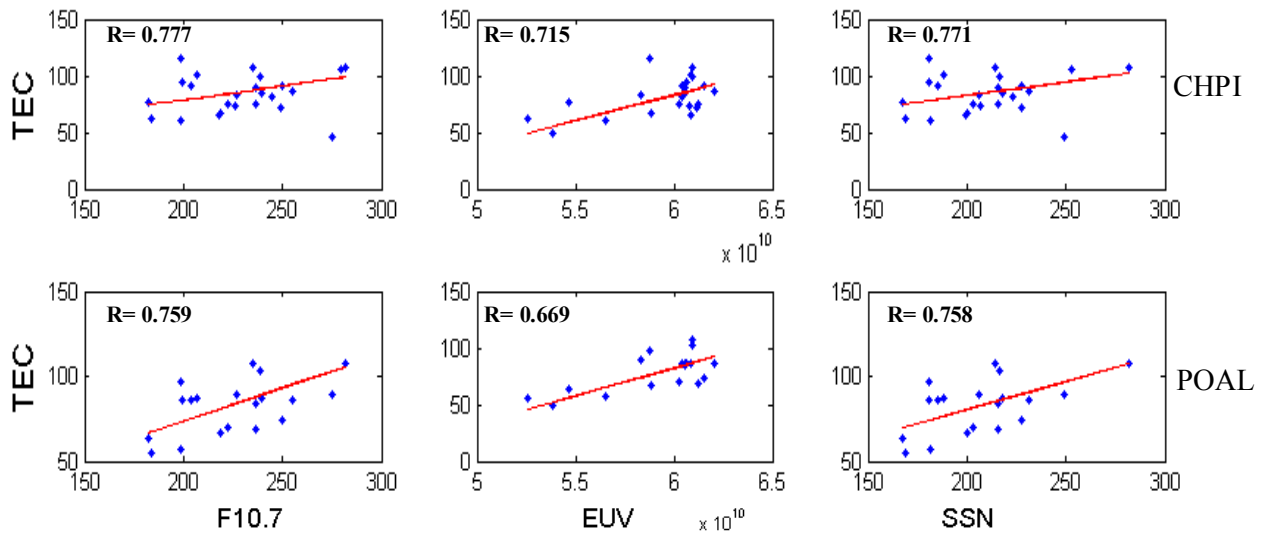


Figure 5.9 - Correlation of TEC with solar flux for March and September equinoxes

The $E \times B$ drift could be an important factor since the equatorial F region vertical drift is controlled also by the $E \times B$ drift arising from an east-west electric field. Batista et al. (1986) using statistically ionosonde measurements at Fortaleza showed that the electric field around sunset during March equinox is larger than electric field during September equinox. Ren et al. (2011) using observations from ROCSAT-1 (at the 600 km) during the period of 1999 to 2004 (as seen in Figure 5.8) found that vertical $E \times B$ drift is higher at March-April than at the September-October. Figure 5.10 shows the local time and longitudinal variations of vertical drift

for March-April (left) and September-October (right). The March-April $E \times B$ drift has more intensity than the September-October. The vertical drift values in the two equinoxes show some similarities. It can be noted that the diurnal variation in the drift of all longitudinal sectors in both equinoxes are all similar with the diurnal variation presented by Fejer et al. (1991) observed at Jicamarca in Peru. The vertical drift in both equinoxes are upward in the dayside and downward at night. But around 1700 - 1900LT there is a sharp increase in upward drift known as prereversal enhancement. In another research, Balan et al. (2000) proposed that, during daytime, the equinoctial asymmetry in the thermospheric composition causes the asymmetry in the bottomside ionosphere, while the asymmetry in the field-aligned component of the neutral wind is responsible for the maximum electron density near the F peak region.

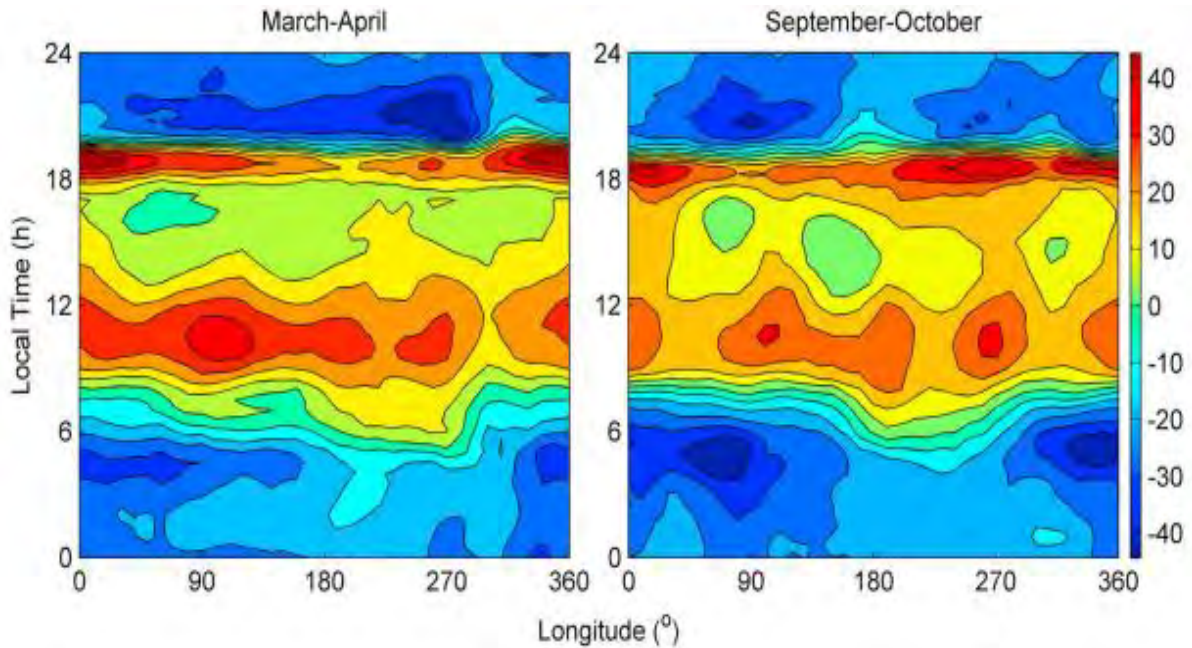


Figure 5.10: Local time and longitudinal variations of vertical drift (m/s) in two equinoxes.

Source: Ren et al. (2011)

Even though the unaccounted diurnal TEC asymmetry between March and September by solar flux could emerge from the combined effects of the aforementioned mechanisms, it is impossible for us to conclude that these results can completely explain our observation because most of the parameters used in the literatures were not during the same period and location with our study. Therefore in order to clearly investigate the mechanisms responsible, we employed the SAMI2 model as explained below.

5.2.1 TEC Diurnal Variation using the SAMI2 Ionospheric Model.

SAMI2 (Some another ionospheric model) is a physics-based model of the ionosphere which solves hydromagnetic equations describing ionospheric plasma. It is a 2-D (latitude and altitude) ionospheric model developed by the Naval Research Laboratory (NRL) (Huba et al., 2000). It models the mid and low-latitude ionosphere, including the geomagnetic equator, along a hemispheric grid from 90 to 20,000 km. It is freely available for modification from NRL, and the 2-D nature of the model allows more realistic evolution of the plasma than a 1-D model. It models the plasma and chemical evolution of seven ion species (H^+ , He^+ , N^+ , O^+ , NO_2^+ and O_2^+) in the altitude range mentioned above. The ion temperature equation is solved for three ion species (H^+ , He^+ , and O^+) as well as the electron temperature equation. The neutral composition and temperature are specified using the empirical NRLMSISE00 model and the neutral winds using the HWM07 model. The dynamics of the SAMI2 model enable us to incorporate many parameters to obtain various desired results.

To understand the daily variation of TEC asymmetry between March and September as we noted from Figure 5.8, we run the SAMI2 model including photochemistry, transport due to the electric field, and transport due to wind. The results are shown in Figure 5.11. There is symmetry during early morning hours and asymmetry during both afternoon and evening time. March equinox clearly showed larger TEC values compared to September. The daily variations over equator is different from off equator which is mainly owing to fountain effect. Prereversal enhancement peaks are also clearly observed in both March and September at the Cachoeira Paulista station around the same time that is was as observed in 2001 activity from the data observation in Figure 5.8.

This result pointed out that photoionization and chemical compositions could plays an important role in the asymmetry between the two equinoxes months during 2009 as well as 2001 solar activities. This will be discussed more in section 5.2.3.

At this point, it is important to mention that, the investigation of Liu et al. (2010) pointed out that the equinoctial asymmetry in the ionospheric plasma density during low solar activity is mainly a low-latitude phenomenon. In our study, however, we have indicated with evidence using both data and simulation that the equinoctial asymmetry (between March and September diurnal TEC variations) is also present around the magnetic equator (São Luís) during both low and high solar activities.

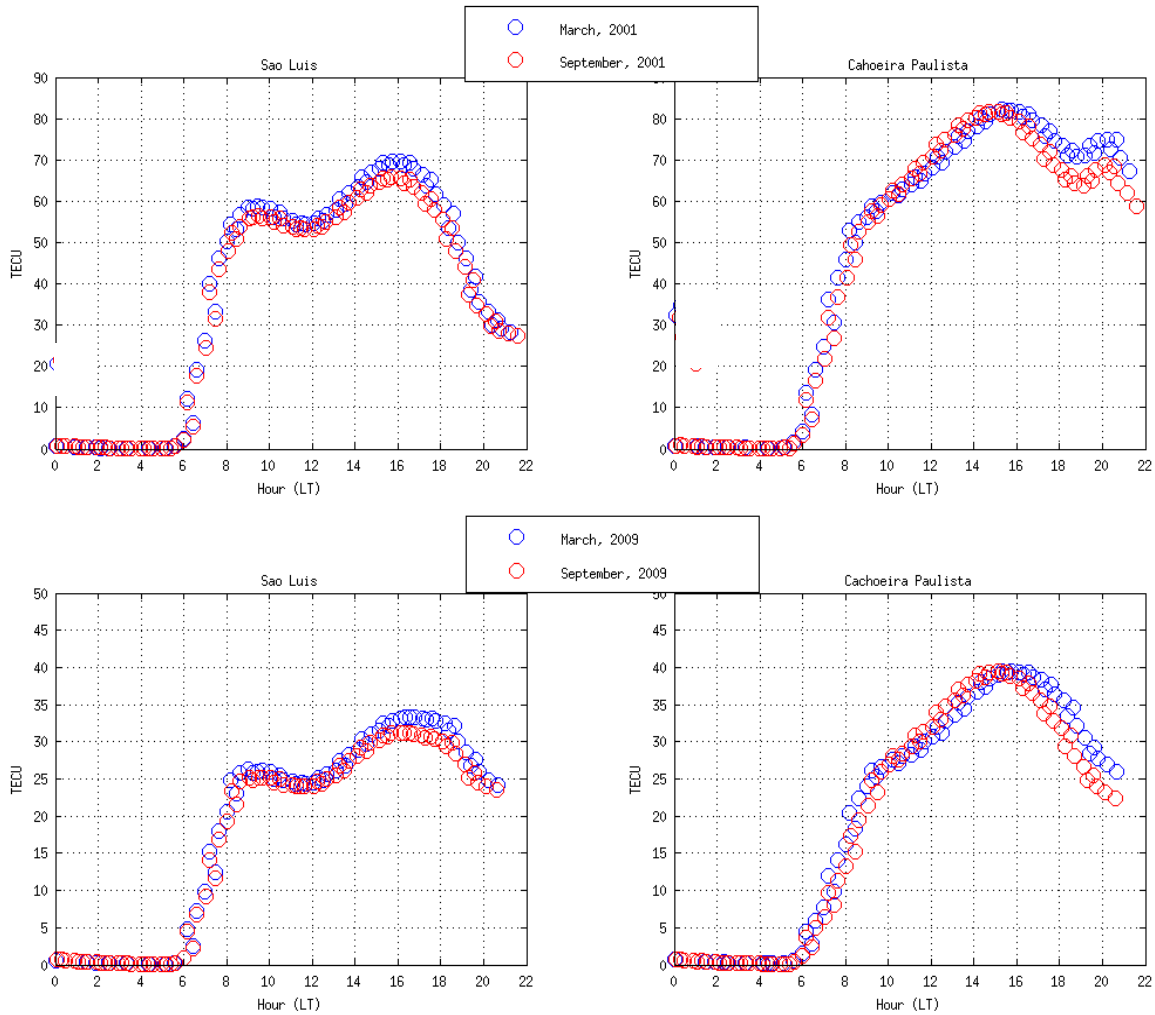


Figure 5.11: Diurnal TEC variation using SAMI2 model for March and September Equinoxes for 2001, (top panel) and 2009 (lower panel). The red circles represent September equinox and the blue circles represent March equinox.

5.2.2 Latitudinal TEC Variation Asymmetry between March and September

To observe the latitudinal behavior between March and September equinox, data for 2001 was not used since the statistic was poor due to lack of many receivers stations during this period. Therefore only 2009 low solar activity data were analyzed latitudinally. Figure 5.12 shows mean TEC along the magnetic dip latitude of $\pm 20^\circ$ traced along the magnetic field line within the geographic longitudinal range of -52° to -60° determined using the International Geomagnetic Reference Field (IGRF) model at 1400 hour local time during March equinox (blue line) and September equinox (red line). A close observation from the figure shows that latitudinal distribution of TEC during 2009 presents asymmetry around the low latitude and about the

magnetic equator for both March and September. The TEC values in March is larger than September. The interhemisphere pattern also shows slight asymmetry. It can also be observed that the trough for both months are shifted away from 0° (magnetic equator) towards the southern hemisphere. This could be a combined effect of interhemispheric wind and large separation between the geographic and geomagnetic equator along 60°W. The wind at this large separation could be the cause of TEC trough shift from the magnetic equator. To make more clarifications we also employed the SAMI2 model and the results are shown in Figure 5.13 and 5.14.

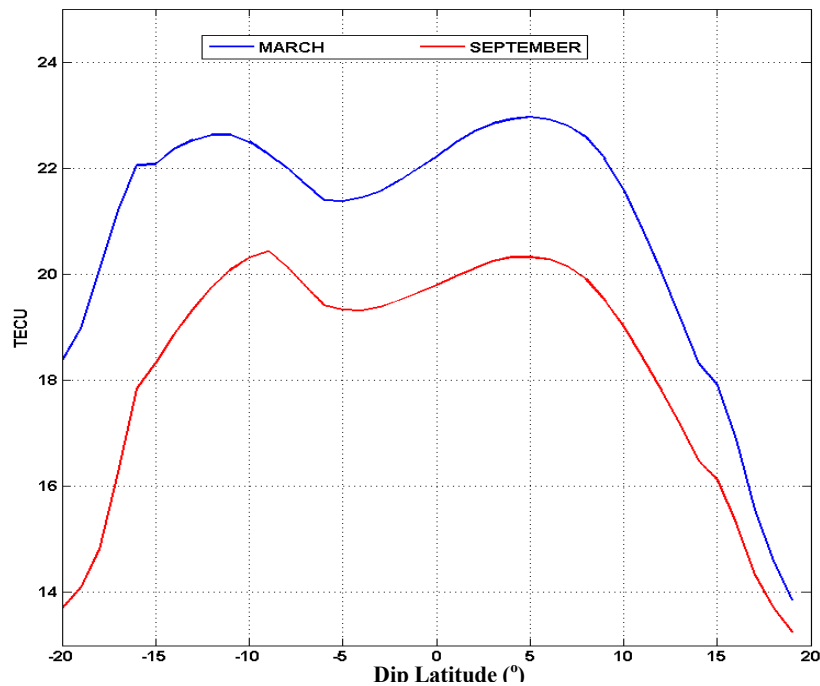


Figure 5.12 - Latitudinal distribution of TEC for March and September Equinoxes, at 1400LT for 2009.

The basic required input parameter for SAMI2 model for example in 2009 are as follow:

- Time for the run - 48hours.
- Altitude - ≥ 300 km.
- Geomagnetic Latitude - $\pm 20^\circ$.
- Geomagnetic Longitude - $- 60^\circ$.
- 3 months average of F10.7 - 70 (2009).
- Value of daily F10.7 - 75 (2009).
- Ap index - 21 (2009).
- Year - 2009.
- Day - 14-15.

Maximum ion specie	-	$H^+ He^+ O^+ N^+ O_2^+ N_2^+ NO^+$.
Neutral wind speed	-	Obtained from the Hedin Wind Model (HWM93).
$E \times B$ drift velocity	-	Obtained from Fejer /Scherliess 1999 empirical model.

For better understanding, we made use of different parameters by enabling and disabling each parameter per time and the TEC measurements in each case were plotted. The results are shown in panels A-E of Figure 5.13 and 5.14. In each panel red cycles represents September and blue cycles represents March. Panel A shows TEC with only photoionization, B represents photoionization plus transport due to the electric field, C represents photoionization plus transport due to electric field and wind, D represents temperature (at ≥ 300 km) of the ions and E is the ratio of O/N₂.

Panel A presents a case where only photoionization is added as input. The result shows that ionization in March is more than in September and equatorial ionization anomaly was not developed. This shows that the model is reliable. However, after including transport due to electric field in panel B, the anomaly developed and symmetry can be clearly observed at both hemisphere but asymmetry is observed between March and September equinox. This alone with some examples literatures discussed in section 5.2.1 are pointers to the fact that transport owing to electric field could be responsible for the March and September asymmetry. Again, in panel C, we include photoionization, plus transport owing to electric field and wind, and we noticed that hemispheric asymmetry appeared with March exhibiting the larger TEC at both southern and northern hemisphere. To have a more complete knowledge of what is happening, we used the model to calculate the temperature of the ions and the ratio of O/N₂. Panels D and E represent temperature and O/N₂ ratio respectively. It is evident that O/N₂ and temperature are larger during March than during September. The large O/N₂ implies less recombination which leads to more TEC as found during March. Also, the larger temperature implies more photoionization that leads to more TEC as found during March.

The same simulation was made for 2001 as shown in Figure 5.14 and similar results were observed. Although there are not enough statistics for 2001 latitudinal variation, the result shows that the model and the simulation are consistent.

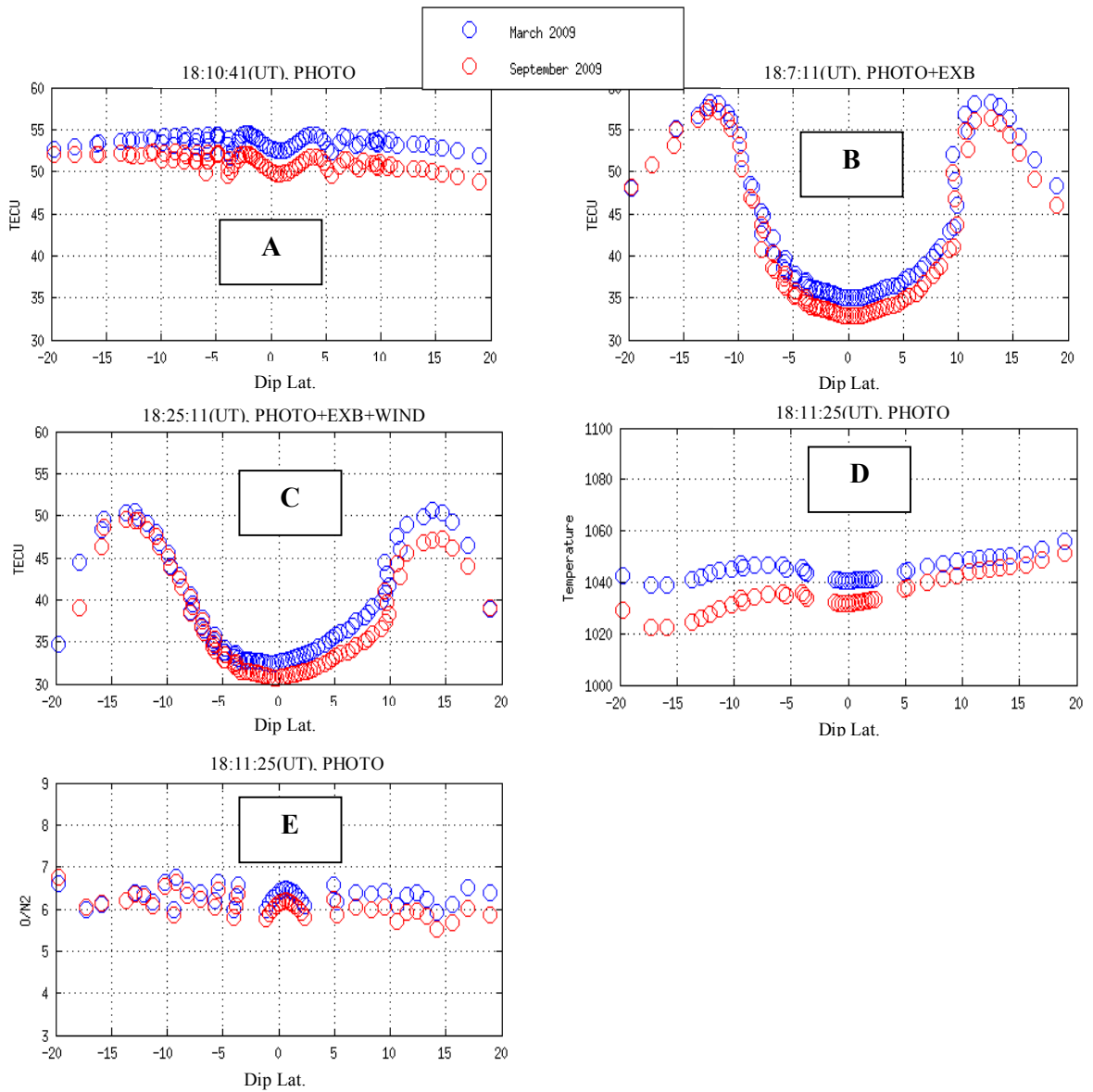


Figure 5.13 - Latitudinal TEC variation, temperature and O/N2 ratio output for 2009 from typical SAMI2 model. Panel A, represents photoionization, B, represents photoionization, Electric field, C, represents photoionization, Electric field and wind, D, represents temperature of the ions and E is the ratio of O/N2

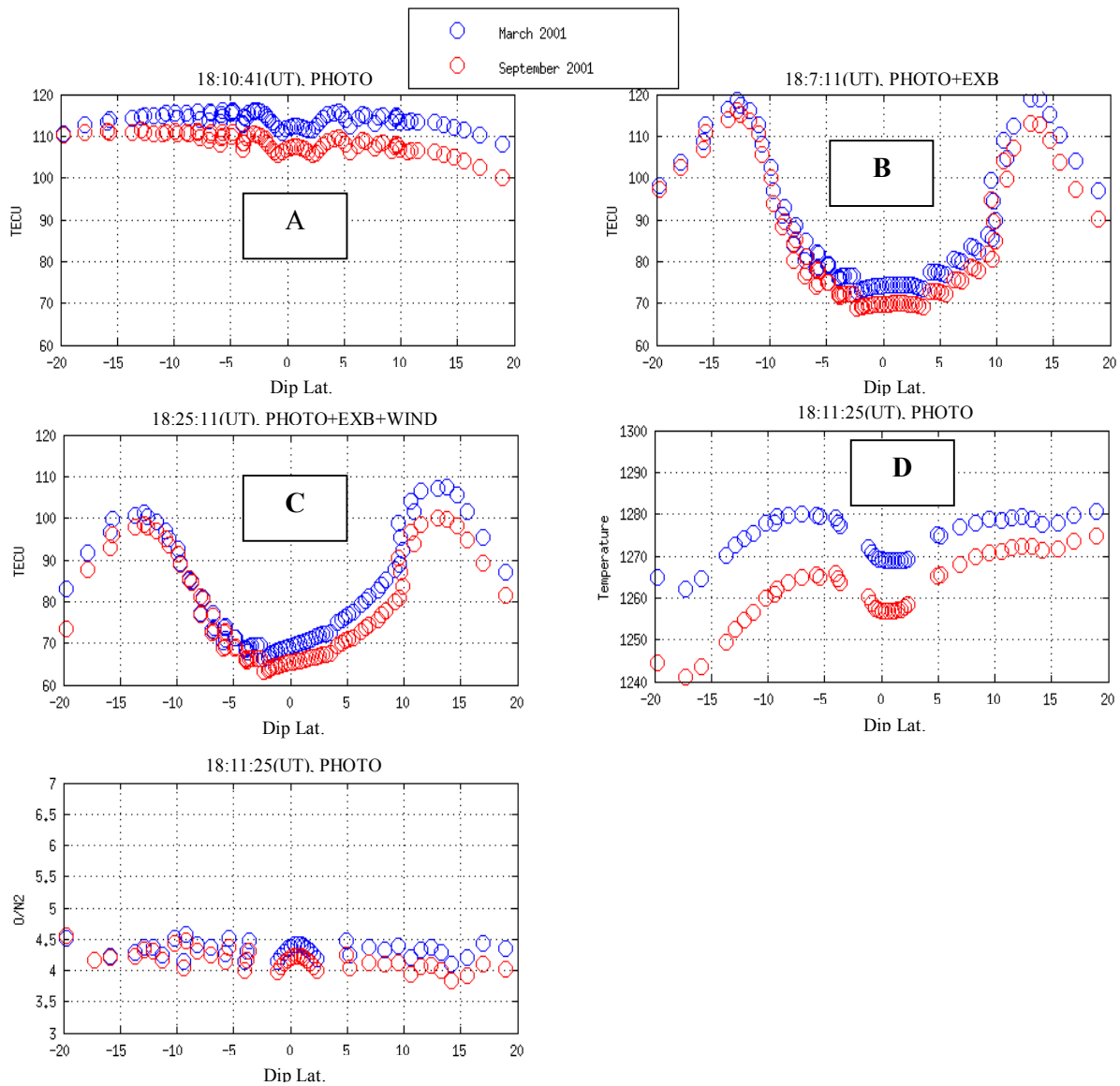


Figure 5.14 - Latitudinal TEC variation, temperature and O/N2 ratio output for 2001 from typical SAMI2 model. Panel A, represents photoionization, B, represents photoionization, and Electric field, C represents photoionization, Electric field and wind, D, represents temperature of the ions and E, is the ratio of O/N2

5.2.3 Latitudinal Variation and Seasonal Evolution of TEC

In order to study the TEC monthly seasonal evolution (for data observation) along magnetic field line of 60°W (magnetic longitude), the IGRF Earth's magnetic field from International Geomagnetic Reference Field (IGRF) model was used with the same specifications given in previous section 5.2.1 and the TEC data along this field line were collected and grouped month by month. The time difference between extreme values of the longitudinal range is less than 40 minutes which can be considered negligible depending on the temporal scale of the physical phenomenon under consideration.

Figure 5.15 shows TEC as function of magnetic dip latitude for the equinox (green), summer solstice (red) and winter solstice (blue) for minimum solar activity. The scaling are the same in all.

The mechanisms responsible for large differences of TEC values and interhemisphere asymmetry between March and September in Figure 5.12 has been given in section 5.2.3. We believe that same mechanism can be used to explain the inter-hemisphere asymmetry and the large TEC between October and April.

Also from Figure 5.16, we observed asymmetries particularly during summer and winter which can be reasonably associated with photoionization. Generally during solstices periods photoionization at the equator decrease because the subsolar point moves to higher latitudes and the fountain effect is expected to be weak.

In solstices periods, Figure 5.15 (b) (summer solstice) and Figure 5.15 (c) (winter solstice), we observed that EIA is not well developed in both seasons. Taking Figure 5.16(b) for example, there is a large asymmetry between the southern hemisphere (which represent summer) and the northern hemisphere (which represent winter). This shows that photoionization is more prominent and give rise to more ionization and larger TEC value in the summer hemisphere than in the winter hemisphere as shown in Figure 5.15 (b). The same conditions apply to Figure 5.16(c) where the summer hemisphere also shows larger TEC principally because of photoionization effect. This observation is in contrast to the well-known winter anomaly (Jee et al., 2004 and Rishbeth et al., 2000). The winter anomaly refers to the observation that during daytime ionization peak of F2 layer is larger during winter than during summer condition particularly during solar maximum periods at midlatitudes as explained earlier. However, our results indicate that winter anomaly is absent or opposite in the month to month TEC changes analysis during the solstices of 2009 solar minimum. Codrescu et al (1999 and 20001) and Jee et al (2004) have also reported that the winter anomaly was not evident in their global TEC analysis. This winter

anomaly could be a phenomenon of solar maximum during some specific hours of the day (SCHERLIESS et al., 2008).

Regarding the seasonal TEC evolution, one fact that is clearly indicated in the Figure 5.15 (a) to (c) is the TEC pattern showing the smooth transition from summer to equinox and from winter to equinox. This is clearly seen in the latitudinal pattern of summer solstice to equinox (February - March) and the transition from winter solstice to equinox, (August to September). Similar patterns were also observed during these transitions. This implies that there is consistency in our data and that photoionization is the main ionization mechanism. Furthermore, there is larger enhancement in the relative TEC variation that exhibits significant latitudinal variations during December and November months compared to the February and January months of summer solstice. This could be because of the relatively higher solar flux represented on F10.7 cm flux which is indicated in Table 4.1. Lastly, we can also observe the semiannual variation indicated in the relatively large value of TEC in equinox compared to the solstices and the seasonal variation in the summer solstice which indicating larger TEC value than in the winter solstice. The reason for this has been explained above.

An interesting point that could be drawn from our discussion so far, is that besides the electric field and wind parameter that have been showed to be factors responsible for diurnal TEC variation, asymmetry in equinoxes and summer and winter behavior, we can also conclude that the ionosphere from summer to equinox responds differently (more ionization) during the February to March transition (Figure 5.16) than from winter to equinox during August to September transition (less ionization). Therefore equinox as represented by March exhibits larger TEC values despite the fact that it has low F10.7 (particularly in solar maximum) compared to September, and September shows low TEC despite its higher F10.7.

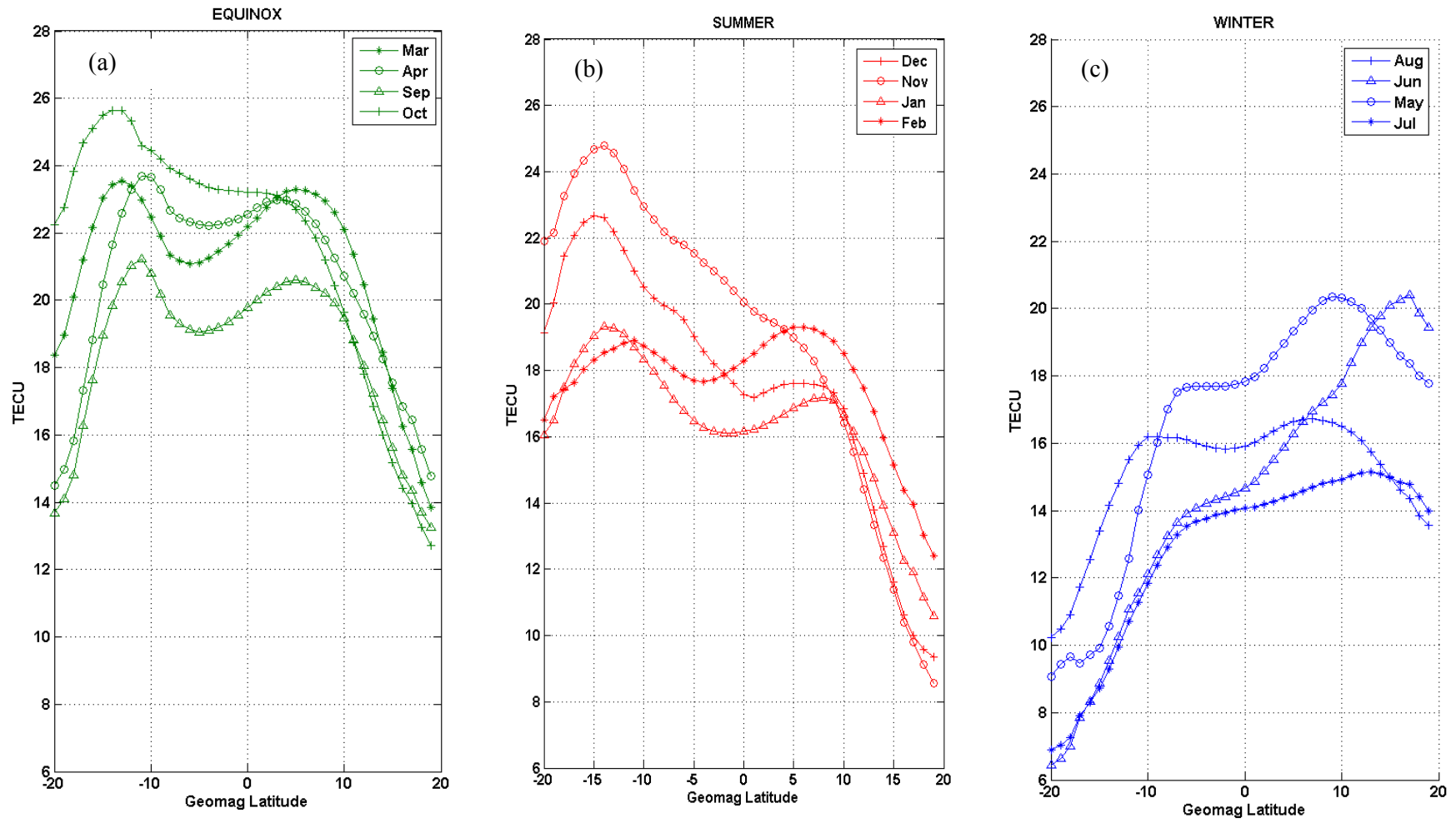


Figure 5.15 - The latitudinal variation of mean TEC during all seasons of 2009 at 1400LT.

5.2.4 Analysis of general TEC distribution

Figure 5.16 illustrates the residual TEC (ΔT) distribution of average seasonal pattern (\overline{TECs}) for each station was calculated and subtracted from each data ($\Delta T = (TEC - \overline{TECs})$). The vertical axis stands for number of occurrence and the horizontal axis stands for residual TEC. The blue color represent low solar activity and the red represent the high solar activity. The low solar activity of 2009 and high solar activity of 2001 show a TEC distribution ratio of 1:4 TECU during equinox and summer solstice and a ratio of 1:3 during winter solstice.

Generally low solar activity exhibits high kurtosis around zero, which confirms the low standard deviation observed in Figure 5.3 during this period. Also during low solar activity period, TEC distribution pattern exhibit a form of Gaussian distribution around zero mean indicating that on average TEC experience as many increase as decrease. This is observed for all the stations.

However, during high solar activity the opposite is the case. The kurtosis is flat confirming the high standard deviation that was observed during the period in Figure 5.4. The TEC patterns skew left but spread out to the right during winter indicating more decreases than increases in TEC and during summer solstice TEC pattern skew right and also spread out to the right in most of the plots indicating more increases than decreases in TEC. While in equinox data form a close normal distribution in all stations showing as much increase as decreases in TEC except in Arequipa station.

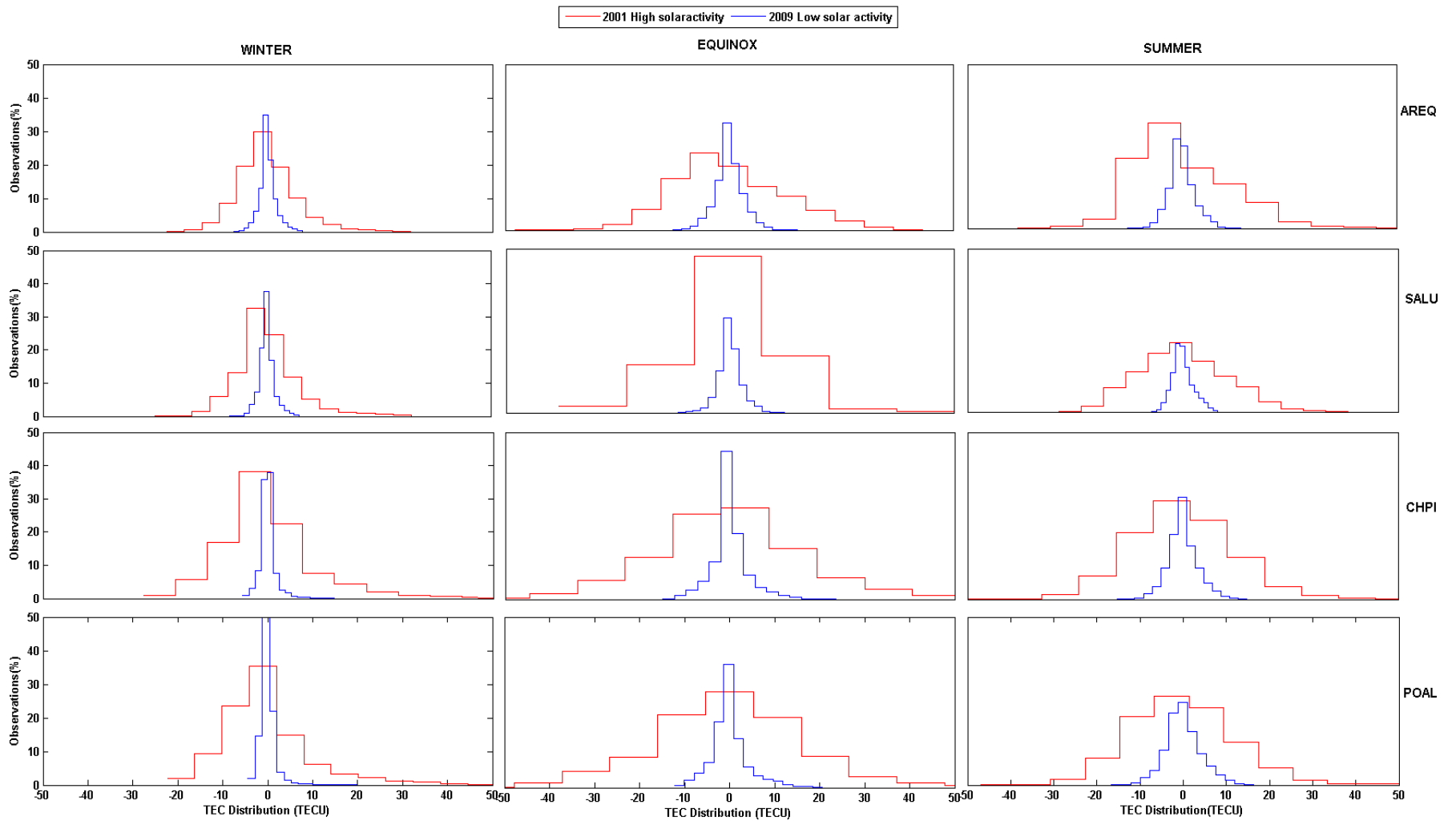


Figure 5.16- Distribution of TEC variation as function of season and location.

5.3 Wavelet Analysis

In this section we show other mechanisms responsible for TEC variation during quiet periods apart from the well known daily peaks and annual and semiannual periodicities using the wavelet spectra distribution for both the daily mean of TEC and daily mean of meridional and zonal wind at 100 km altitude measured by meteoric radars.

It is a well known fact that the ionosphere varies readily with solar radiation and geomagnetic activity. The portion of ionospheric variability not yet accounted for by these drivers is up to ~20% of the F region ionospheric electron density at daytime and ~33% at nighttime (Rishbeth and Mendillo 2001, Forbes et al., 2000 and Mendillo et al., 2002). A number of studies have shown that meteorological processes such as planetary wave, gravity wave, tides etc. can directly or indirectly have impact on the ionosphere electron density (Rishbeth, 2006).

The nonlinear interaction of quasi-stationary planetary waves that are trapped below the mesopause can give origin to large changes in both migrating and non-migrating tides (Goncharenko et al., 2010b). These tides are known to exhibit an amplitude maximum at low-latitudes and can propagate into the lower thermospheric region. Moreover, the propagating tides can modulate electric fields through the ionospheric wind dynamo at E region and consequently they map along magnetic field lines to high altitudes of F region height and then influence ionospheric variability.

Jee et al. (2005) used a one dimensional middle-latitude ionospheric model to study the sensitivity of quiet-time TEC to the atmospheric and ionospheric parameters including the neutral wind and found out that during both day and night, the magnetic meridional component of the neutral wind significantly affect TEC, and the geographic zonal wind can cause noticeable longitudinal variation in TEC due to the longitudinal variation in the declination angle, which is more prominent in the South American sector (the region in focus).

On these evidences and since we are working with only geomagnetic quiet period, it is important to observe the effect of upward propagating waves on the E layer of which may have consequent effect on TEC as explained above. To carry out this investigation we applied wavelet spectral analysis distribution of the daily means of meridional and zonal winds at the altitude of 100 km and compared their periodicities with the daily means of TEC data over Cachoeira Paulista, Porto Alegre, São Luís and Arequipa stations.

Figure 5.17 is the wavelet spectral analysis plots of hourly mean TEC for a period of one solar minimum year of 2009. The 1 day peak period with an annual period and the half day peak period with a semiannual anomaly period can be clearly seen in the figure particularly over Cachoeira Paulista and Porto Alegre. However the semiannual period is not so obvious over São Luís and Arequipa stations. Other periodicities are well shown in the preceding figures and they are compared with meridional and zonal wind.

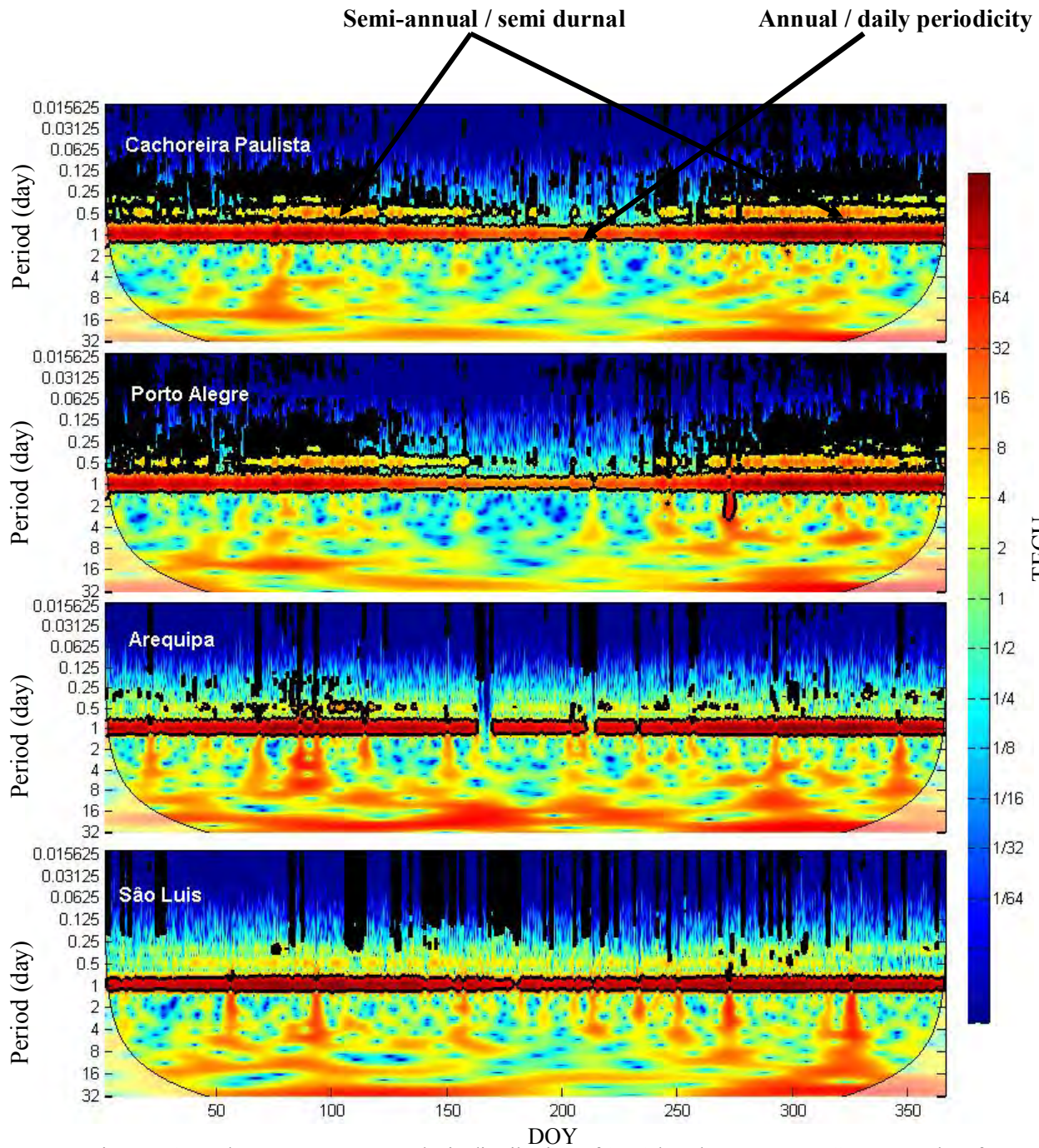


Figure 5.17 - The Power spectra analysis distribution of 2009 hourly average TEC contour plots for Cachoeira Paulista, Porto Alegre, Arequipa and São Luís from top to bottom respectively. The vertical axis represent the daily period and the horizontal axis represent the day of the year.

For clear observations and to see clearly the other periodicities, we eliminated the daily and the semiannual periodicities by using only the daily averages in the following analysis. The remaining periodicities are clearly shown Figure 5.18 which shows the wavelet analysis distribution of daily average of TEC for 2009. Periodicities of 1 to 5 days are stronger at Arequipa and São Luís stations, 16 days and 27 days are also observed at Cachoeira Paulista and Porto Alegre. Likewise, in a tentative effort to explain the TEC periodicities plotted in the Figure 5.19, we made the wave analysis for the zonal and meridional wind (Figure 5.20). From up, the first two panels in Figure 5.19 show the daily average zonal and meridional winds at 100 km and the last panel shows daily mean of F10.7 for 2009. The periods with the black line contour have 95% confidence level and we used the Morlet function (wave number of 6) as a mother wavelet. It can be clearly seen that besides that 27 days solar periodicity that is indicated by the F10.7 power spectra as well as in the TEC, other periodicities are also prominent. For example the 16 days periodicity which is also corresponding to the same period in both zonal and meridional winds around the same days. This 16 days can be associated with lunar tide effect which causes strong enhancement on the semidiurnal variations observed during SSW events (Fejer et al., 2010). A strong 1 to 5 and 7 day periods is also common to all the stations but not so strong at both Cachoeira Paulista and Porto Alegre stations. Most of periods are corresponding with what are observed in the zonal and meridional wind spectra analysis (Figure 5.20). Therefore, the day-to-day variation in TEC do seem to contain a component driven by planetary waves enhanced by tides as they propagate upward (Abdu and Brum 2009).

2009 STATIONS

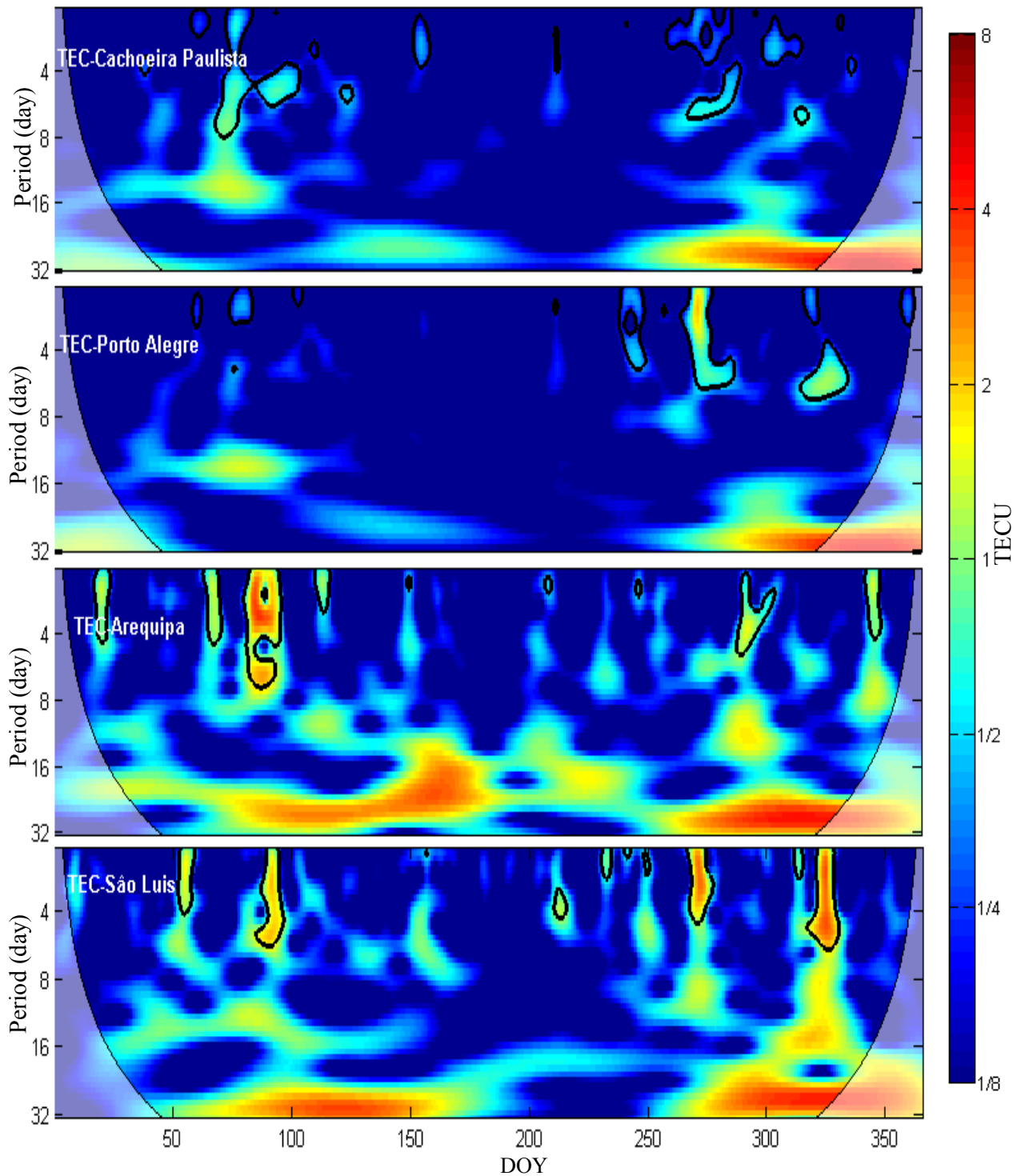


Figure 5.18- The Power spectra analysis distribution of 2009 solar minimum daily average TEC contour plots of Cachoeira Paulista, Porto Alegre, Arequipa and São Luís from top to bottom respectively not considering the daily and semiannual periodicities. The vertical axis represent the daily period and the horizontal axis represent the day of the year.

2009 PARAMETERS

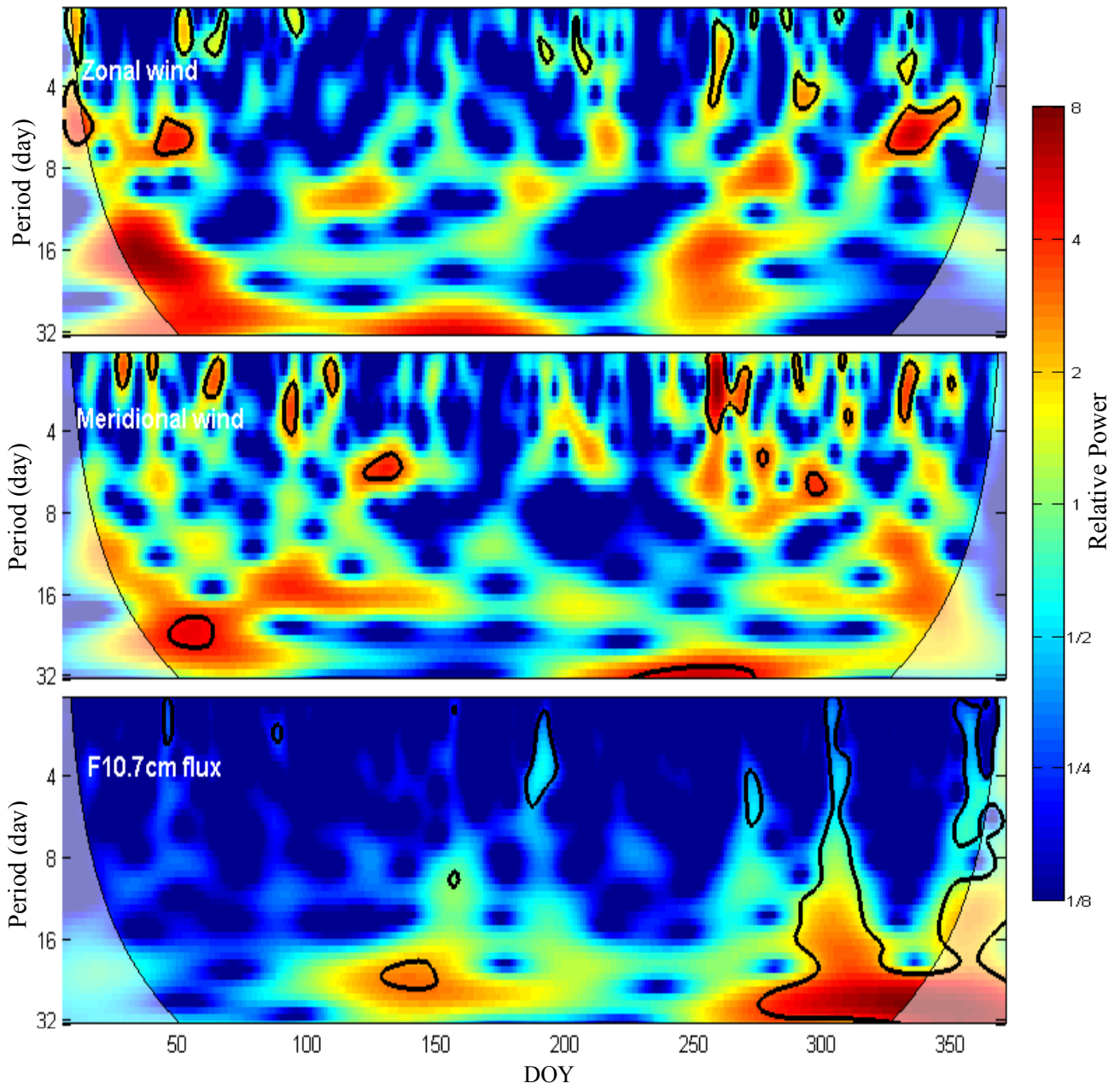


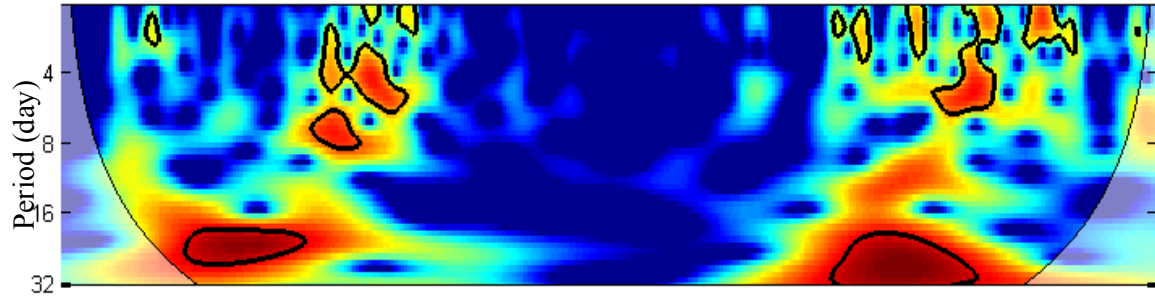
Figure 5.19 - Power spectra analysis distribution of 2009 solar minimum daily average zonal wind, meridional winds(both at 100 km) and solar flux from top to bottom respectively. The vertical axis represent the daily period and the horizontal axis represent the day of the year.

The same wavelet power spectra analyzed for 2009 low solar activity were analysed also for 2001 high solar activity. Similar observations were noted as shown in Figure 5.20 and 5.21. The intensity of the F10.7 is stronger as expected. The 16 days periodicity is observed only in the meridional wind and in TEC for all stations (Figure 5.21), while 8 to 10 days, 1 to 2 and 5-7 days oscillations are observed in the zonal and meridional wind respectively. These periodicities are found to corresponding to some of the periodicities observed in the TEC particularly the 16 days periodicity which is common to all the TEC stations. A wave decomposition analysis by Abdu et al. (2006) which showed dominance of 4 - to 5- day and 7 -day periods in vertical drift using digisonde data and meridional and zonal winds from meteoric radar are also observed in our larger spectra distribution.

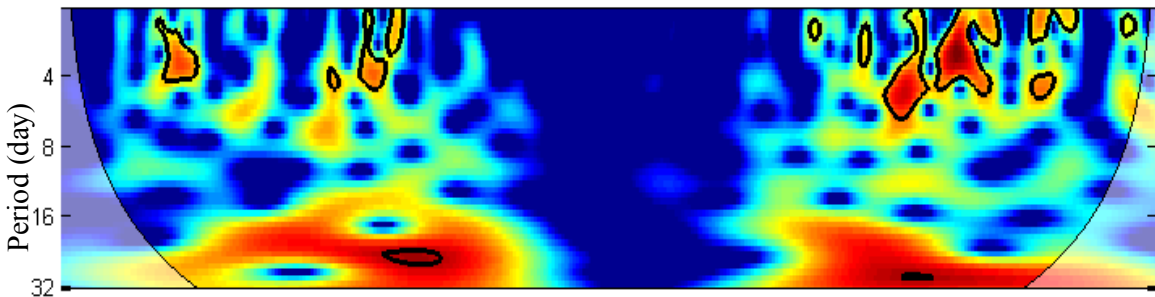
Generally, these results demonstrate the existence of a strong vertical coupling through upward propagating waves leading to day-to-day oscillation in TEC. A possible electrodynamic coupling mechanism connecting these oscillation could be included in future studies.

2001 STATIONS

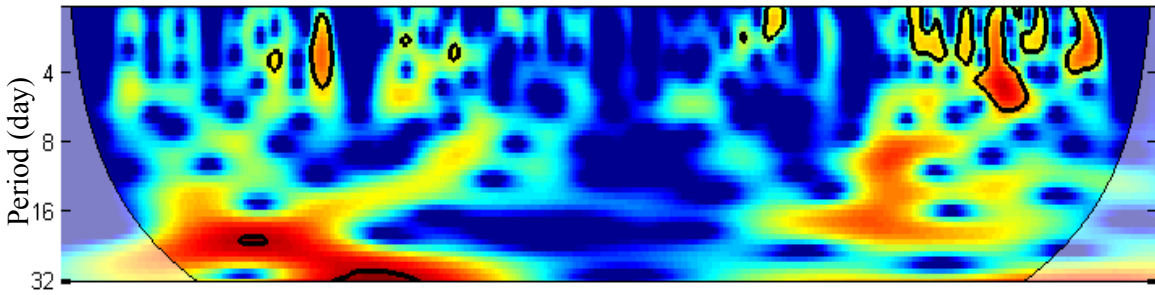
TEC-Cachoeira Paulista



TEC-Porto Alegre



TEC-Arequipa



TEC-São Luis

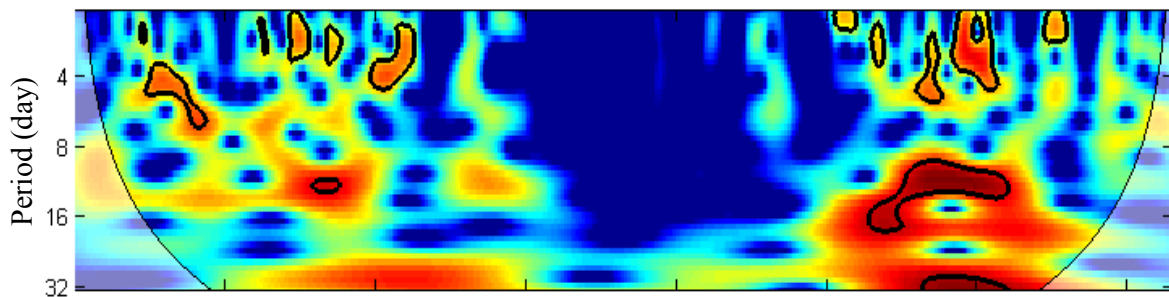


Figure 5.20 - The Power spectra analysis distribution of 2001 solar maximum daily average TEC contour plots of Cachoeira Paulista, Porto Alegre, Arequipa and São Luís from top to bottom respectively not considering the daily and semiannual periodicities. The vertical axis represent the daily period and the horizontal axis represent the day of the year.

2001 PARAMETERS

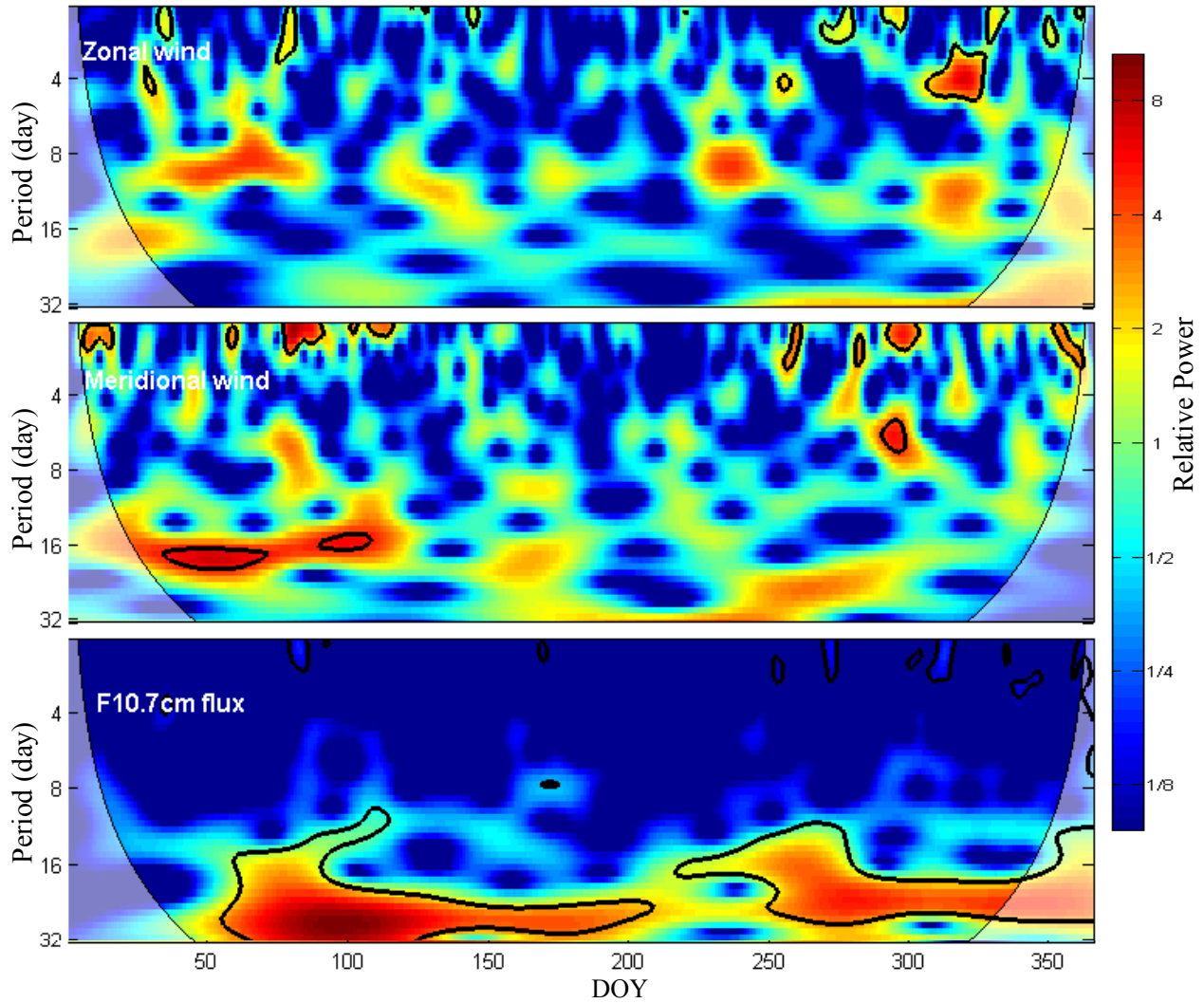


Figure 5.21- Power spectra analysis distribution of 2001 solar maximum daily average zonal wind, meridional winds and solar flux from top to bottom respectively. The vertical axis represent the daily period and the horizontal axis represent the day of the year.

5.4 Study of 2007-2008 and 2008-2009 Sudden Stratospheric Warmings Effects over TEC

Nowadays, studies show series of reports about ionospheric perturbation in connection with the lower atmospheric forcing centered on SSW events. The SSW, as described in section 1, represent the most spectacular meteorological fluctuation in the polar stratosphere. At low-middle latitudes SSW is associated with warming in the lower thermosphere and cooling in the upper thermosphere, with both features exhibiting semidiurnal behavior (Goncharenko and Zhang, 2008 and Chau et al., 2009). Using the Jicamarca Incoherent Scatter radar located under the magnetic equator Chau et al. (2009) reported a strong semidiurnal variation on vertical drifts during the SSW event. Goncharenko et al. (2010b) using TEC-GPS data demonstrated that the vertical drift motion leads to the large-scale redistribution of electron density in the daytime ionosphere. Fejer et al. (2010) using CHAMP satellite and ground-based magnetometer data concluded that semidiurnal variations observed during SSW events are caused by enhanced lunar tides.

In this section, we followed the Goncharenko et al. (2010b) in analyzing GPS-TEC during SSW events, which occurred during the periods of 2007-2008 and 2008-2009 low solar activity. The TEC data were collected along the magnetic longitude of 60°W using the method of IGRF magnetic field trace, method used in Section 5.2.3. Our observation shows larger amplitude of TEC in the northern hemisphere compared to the southern hemisphere during SSW period which could be as a result of the high magnetic declination (the declination varies between -13° and -17°) and high separation between geographic and geomagnetic equators, which affects substantially the meridional and zonal wind effects on TEC along the selected geomagnetic longitude (60°W) at the magnetic dip latitude. More studies necessary to ascertain the actual factor responsible for this asymmetry will be carried out in future studies. Our observations show some similarities with that of Goncharenko et al. (2010b). For example, in our results, SSW perturbation on EIA starting a few days after the peak of the stratospheric temperature, was observed as an enhancement of the EIA in the morning sector and a suppression of the EIA in the afternoon sector. In some cases, there is also evidence of a secondary enhancement in the post sunset hours.

5.4.1 2008-2009 SSW Observations

Figure 5.22 represents the summary of stratospheric, solar and geomagnetic conditions for the summer in south hemisphere of 2008-2009. The red lines from the upper 5 panels represents the historical mean (1979 to 2008) of the corresponding parameters plotted at the same panels. Data were collected from the National Centre for Environmental Prediction (NCEP). The first and second upper panels are the stratospheric temperature at 10hPa (~32 km) and 90-90°N and 90-60°N respectively. There is a sharp increase in both cases by more than 70K relative to the historical mean. From the top the third panel shows the zonal mean wind at 60°N and at ~32 km which reversed from eastward (winter hemisphere) to westward (summer hemisphere) indicating a major warming. The fourth panel indicates the planetary wave number 1 activity at 60°N which is relatively low compared to the planetary wave number 2 shown in the fifth panel from top which exceeds the long-term mean level by a factor of ~3. The lower 2 panels indicate the extremely low solar and geomagnetic activity, showing the F10.7 cm flux and daily ΣKp indices respectively.

2008/2009 SSW Parameters

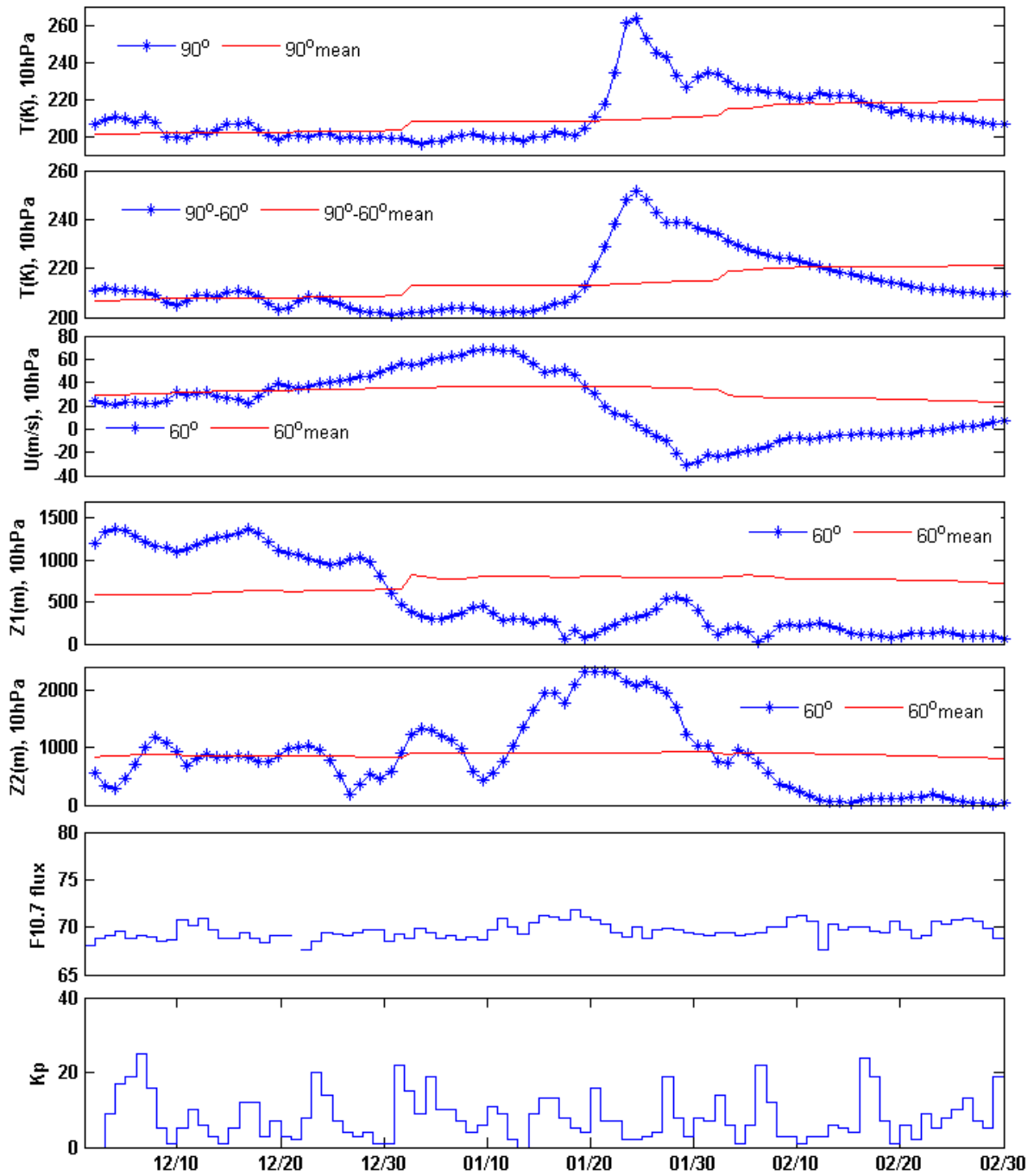


Figure 5.22 - Summary of stratospheric and geomagnetic conditions for the of 2008–2009 SSW events.

Figure 5.23 shows, as represented in Goncharenko et. al., (2010a), the anomalous variation in the Jicamarca vertical ion drift indicating the characteristic of the ionosphere changes during the January 2009 SSW event. The radar upward drift in the morning sector and downward drift in the afternoon sector are responsible for the subsequent electron density redistribution observed in our GPS-TEC during the same period, assuming that the vertical plasma drift behavior at our sector (60°W) is similar or at least close to Jicamarca drift.

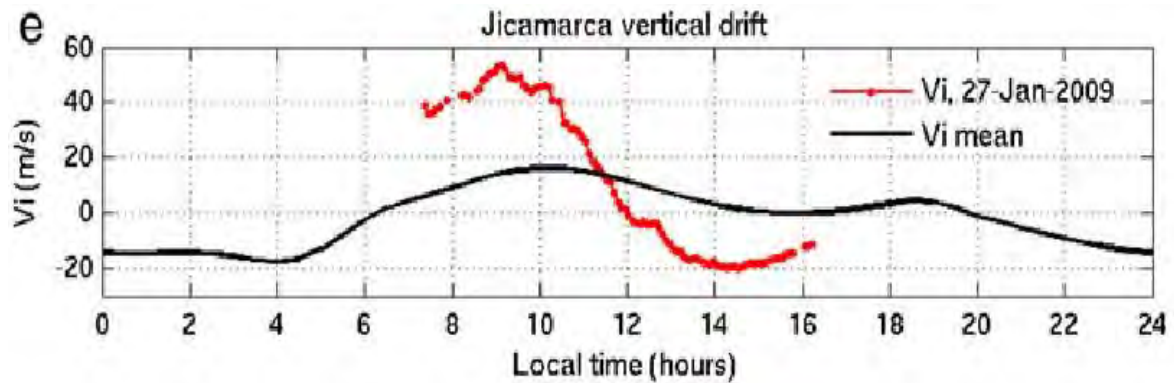


Figure 5.23 - Vertical drift observations by Jicamarca radar (12°S, 75°W) at 200-500 km above the ground.

Source: Goncharenko et. al., (2010a).

To carry out the observation on TEC data, mean of 10 days TEC (from 3 - 12 Jan) representing quiet time (non SSW) was calculated. The 10 days mean of TEC represented in Figure 5.24 (top panel) shows that the EIA was well developed as expected and at the right time with maximum TEC value (20 TECU) during the day due to the EIA and minimum at night (around 1-2 TECU). However, in the subsequent panels of the same figure the TEC of each day is estimated by subtracting the mean TEC of ten days without SSW effects from each day under SSW effects (i.e. $TEC_{(SSW)} - TEC_{(10 \text{ controlled days})}$).

Before the SSW peak, the average TEC difference shows normal daytime variation behavior as showed in the example of January 19, 2009 on the 2nd upper panel. Around the SSW peak on 24th, a clear semidiurnal signature appears during the daytime hours, with TEC enhancement coming earlier in the morning around 8 LT to 12 LT, TEC decreases occurring during afternoon around 12 LT to 18 LT and a secondary TEC increases appearing at 19 to 22 LT. This semidiurnal signature reduces several days after the SSW peak, while moving to later local times. The vertical ion drift observed by Jicamarca incoherent scatter radar (ISR) during this period (Goncharenko et al 2010a, Chau et. al., 2010 and Fejer et al., 2010) indicates that TEC perturbations are caused by the upward (during the morning hours) or downward (during the

afternoon hours) motion of the ionospheric plasma due to enhanced (decreased) zonal electric field during these periods. Upward plasma drift at the magnetic equator (eastward electric field) causes uplift of ionosphere plasma to altitudes of lower recombination rates. The uplifted plasma diffuses along the magnetic field lines forming two crests of EIA as in Figure 5.24 at 8-14LT for 26th to 29th and 31st Jan 2009. Downward plasma drift on the other hand, moves ionospheric plasma to lower altitudes and leads to a decrease in TEC as observed at 15-19LT of all event days (Figure 5.24).

In contrast to the Goncharenko et al. (2010b), we observed large asymmetry in the northern and southern crests of the magnetic equator in both magnitude and location and it seems clear from Figure 5.24 that the afternoon suppression in TEC is more pronounced in the Northern hemisphere.

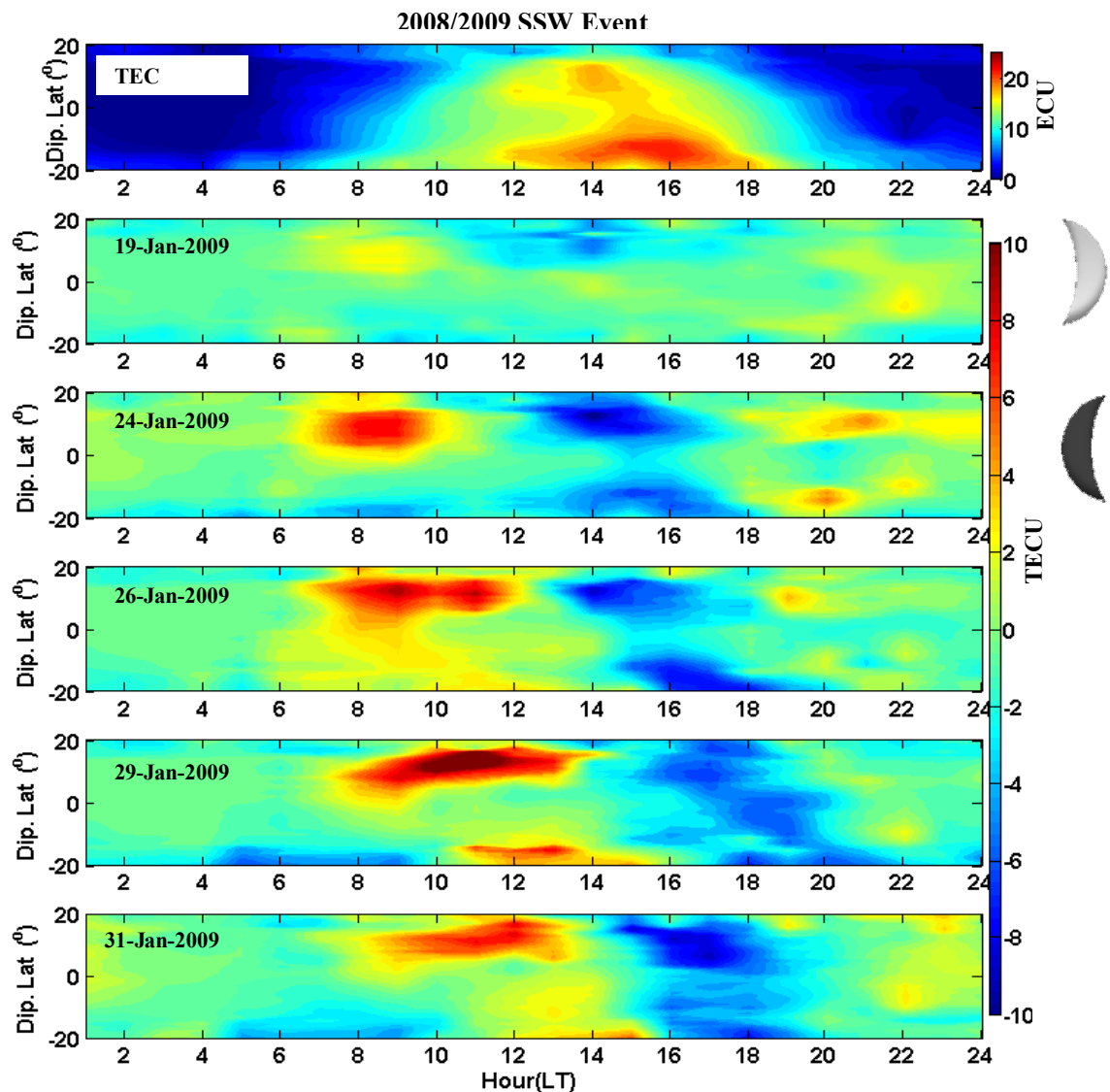


Figure 5.24- Latitudinal TEC variation as a function of local time during the January 2009 SSW.

5.4.2 2007-2008 SSW Observations

The event of Sudden Stratospheric Warming events of December 2007 January - February 2008 was characterized by minor and major warmings. The strong decrease in the zonal wind at 60°N (Figure 5.25) but having no change in the direction for 3 consecutive peaks for stratospheric temperature at 90°N and 10hPa observed on 24 January, 6 February and 16 February respectively, signified minor warming events. On the other hand, the last warming of 24 February fulfilled the condition for a major stratospheric warming when the zonal wind at 60°N turned westward (negative) and the temperature at 90°N increased by ~40K relative to the historical mean within 3 days. In contrast to 2008-2009 SSW event, these 2007-2008 warmings were dominated by the planetary wave number 1 activity which led to the displacement of the polar vortex off the pole and formation of a two-cell pattern of warming and cooling at stratosphere altitude while the activity of the planetary wave number 2 remained relatively low as show in Figure 5.25. This polar vortex condition is similar to the one shown in Figure 1.1 of section 1 of this write-up.

Unlike 2009 SSW which was a completely quiet period, in 2008 SSW there was little enhancement in the solar flux activity (F10.7 cm flux varied between 75-80 units) up till 20 January 2008 and return to very low level after this day. The geomagnetic activity also showed some enhancement during some days. Although there were increases in the daily ΣKp index at some days (e.g. days 5-6 and 14 January and days 2, 10 and 28 February 2008), we only considered the periods that were predominantly quiet.

2007/2008 SSW Parameters

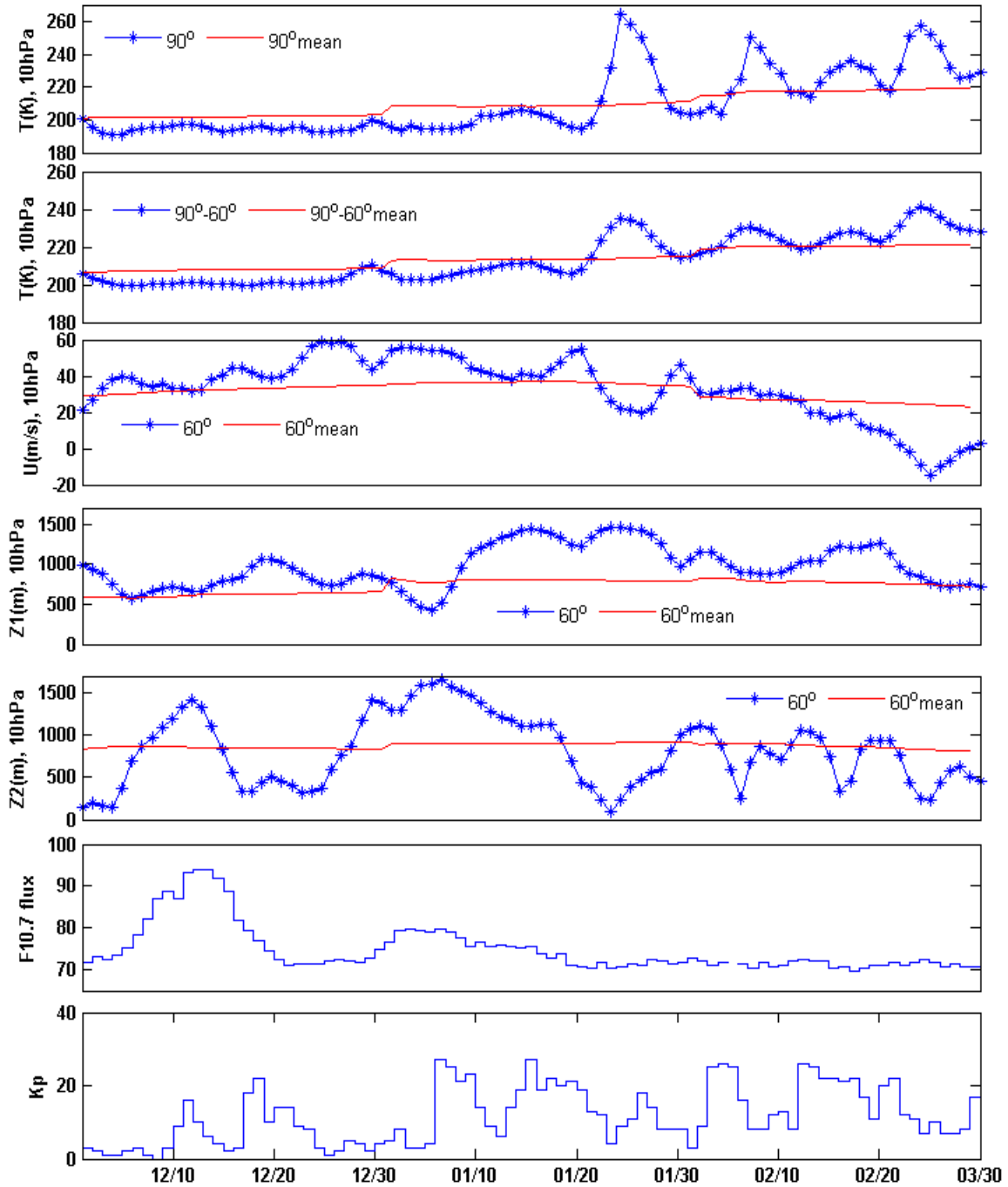


Figure 5.25- Summary of stratospheric and geomagnetic conditions for the of 2007–2008 SSW events.

The periods 1-4 and 7-12 of January 2008 were selected to characterize the previous SSW mean state of the ionosphere during 2008. The days were so selected because they represent the first 10 quiet (daily $\Sigma Kp \leq 24$) days of January 2008, and the solar activity (F10.7cm flux) was relatively higher compared to 2009 SSW.

Figure 5.26 (top panel) represents the local time variation of 10 days mean TEC and differences from the mean for several days around the peak of the stratospheric warming are shown in the remaining panels. The value of TEC for daytime is generally higher than as observed in 2009. This could likely be due to the relative higher solar irradiation. Before the SSW, TEC as observed on 21 January and 24 January show less perturbation particularly on 24 January. If the idea of Fejer et al. (2010) is applied, it is possible to observe that the suppression in TEC during these periods could also be intensified by enhancement of lunar tide variation. Shortly after the January 24 peak in the stratospheric temperature at high latitudes, TEC in the lower latitude ionosphere develops semidiurnal perturbations with a very weak amplitude during night hours. Enhancement of TEC is clearly seen at the equatorial ionization anomaly (EIA) in the morning sector around 8 - 12 LT on 26 January 2008 and decreased few hours later (around 15 - 20LT) as shown in Figure 5.26. The pattern of the enhancement is consistent with the semidiurnal variation in vertical ion drift shown by Chau et al. (2009). The phase shift continued in similar manner on 28 January 2008, showing gradual recover from the afternoon suppression (going back to the normal expected time of the EIA). By 31 January 2008, the phase shift leads to a new perturbation pattern different from the one observed on 26 and 28 January 2008 showing TEC decrease in the morning sector and EIA well developed peak in the afternoon sector. The EIA development observed in the afternoon sector of the 31 January 2008 came a little late (outside the expected time) with a suppression of EIA in Northern hemisphere. The late development of EIA is not yet understood as at the time of this write-up. This would be investigated in future works.

2007/2008 SSW Event

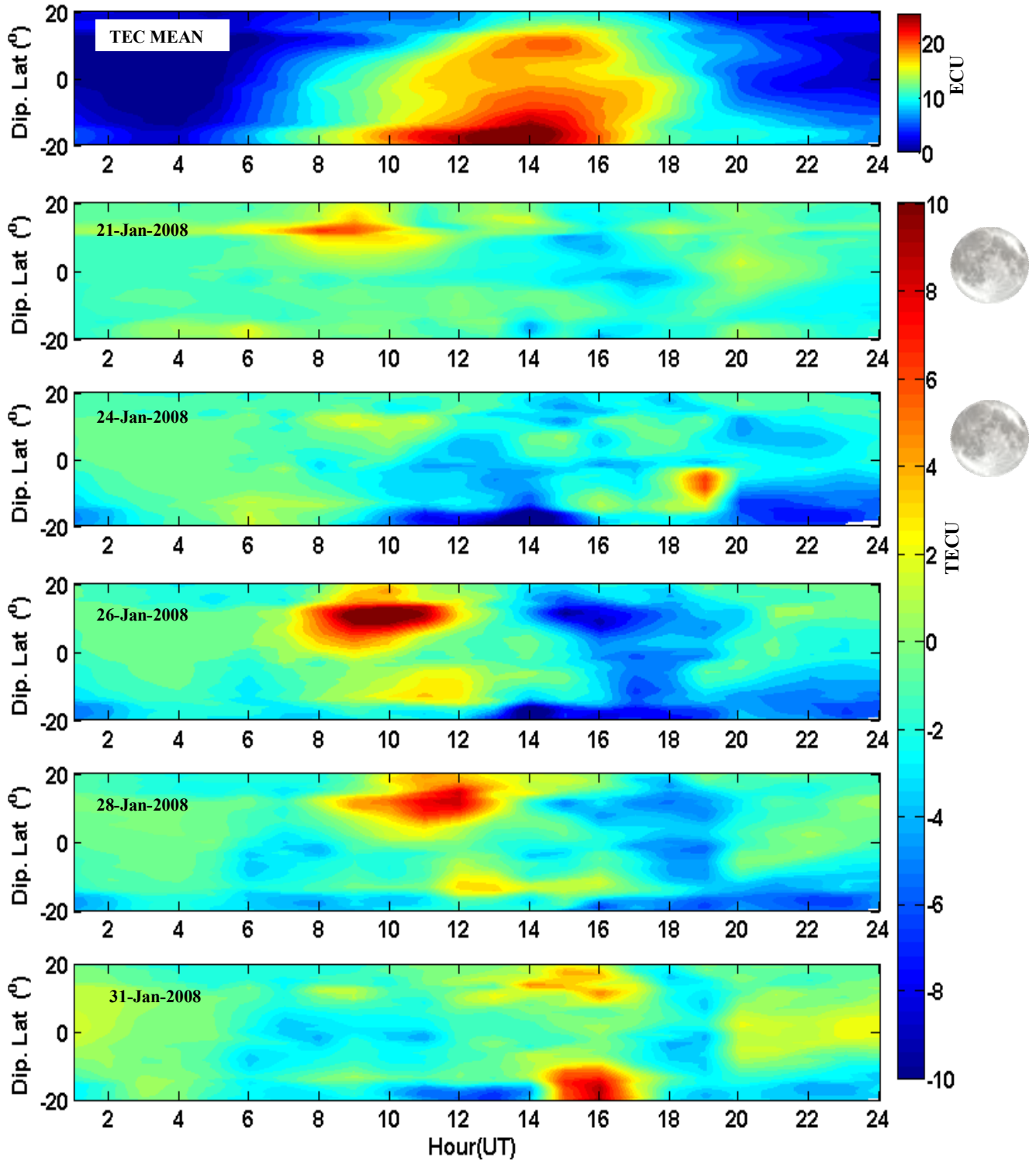


Figure 5.26 - Latitudinal TEC variation as a function of local time during the January 2008 SSW.

The interpretation of the second and third stratospheric warming of winter 2008 becomes difficult due to some geomagnetic activities observed during these days. Figure 5.27 shows highlights of the TEC on the peak days (left panel) and few days later (right panel) for the remaining stratospheric warming events. Day 06 February 2008 shows that TEC demonstrates normal suppression similar to that of January 2009 and January 2008. By 9 February 2008, TEC shows some minor increase at 10-12 LT, a decrease around 16-19 LT and a later increase at 20 - 22 LT indicating a semidiurnal activity.

The third stratospheric warming was the weakest warming of February 2008. The peak temperature occurred on 16 February (Figure 5.27) and corresponding suppression is shown in EIA (Figure 5.27 on 16 February). The suppression indicates negative TEC variations around 10 - 16 LT and few positive TEC variations towards nighttime. This could be in accordance with the increase in the geomagnetic activity to daily $\Sigma Kp = 24$. Moderate variability was observed without any definite pattern during 17-20 February (figure not shown). By 21 February 2008 positive TEC increase was observed stronger at the northern hemisphere than at the southern hemisphere and negative TEC changes was seen around 14-22 LT only in the southern hemisphere. This behavior could be an asymmetry SSW effect on both hemispheres (i.e. the impactation of the SSW effect). Semidurnal pattern was not clearly seen probably because the warming was a weak one.

The last stratospheric warming is the only major warming in the winter of 2008 since the zonal wind did not only slow down but also reversed direction as shown in Figure 5.26. The corresponding TEC on 23 February 2008, at the SSW peak is indicated in Figure 5.27. Although semidiurnal perturbation during daytime in TEC is clearly seen at the peak of SSW, EIA is not as suppressed as the early cases. This is because it is not possible to clearly separate the start and end times of the ionospheric impact of the individual event as one could influence the other. EIA shows larger intensities during the days of 22-25 February and on 26 February 2008. As observed in Figure 5.27, TEC perturbations during this stratospheric warming was maximum, EIA was well developed and a semidiurnal variation can be observed in the perturbation. TEC changes are characterized by positive variations at 11-17 LT and negative at 6 - 10 LT and at 20 - 23 LT.

The increase in the geomagnetic activity was moderate (less than daily ΣKp of 27 in all) and the perturbation in TEC could not be due to variation in solar irradiation as the F10.7 solar flux during the 20-29 February 2008 period was between 70-72 units which implies decrease in

comparison with the F10.7 of the control days period (between 80 - 82). Besides, this two parameters cannot explain the semidiurnal rule nature of the variation and persistence over several days. Therefore the enhancements of TEC (ionospheric variations) during these periods are principally and convincing due to the SSW event.

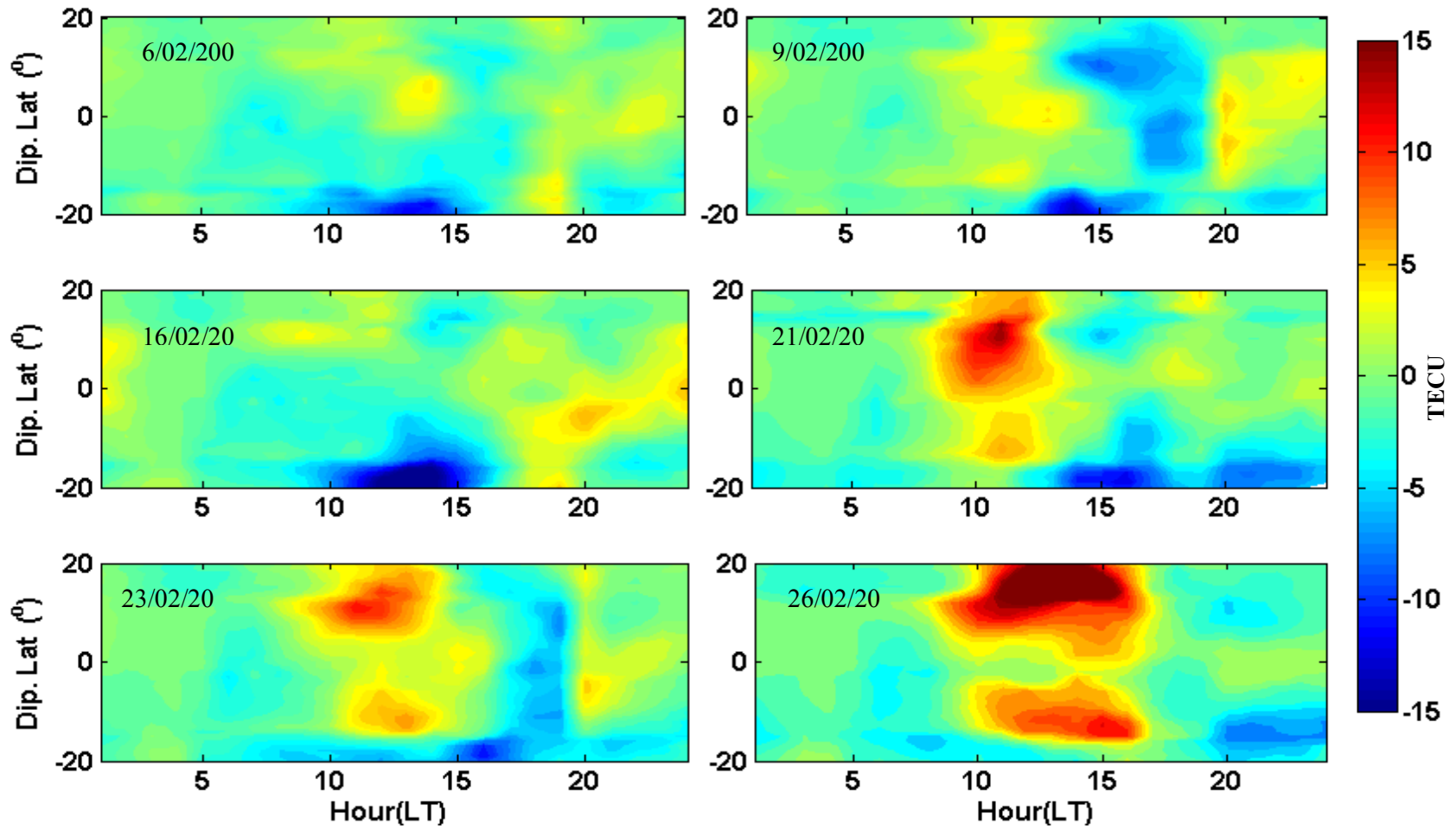


Figure 5.27 - The variation of latitude as a function of local time during February 2008 SSW.

In order to further prove our SSW TEC effects findings, we have made TEC map grids of time resolution of 10 minutes and spatial resolution of $1^\circ \times 1^\circ$ in longitude and latitude. Although our data cover most of the South America sector, interpolation were carried out where necessary.

The maps shown in Figures 5.28 and 5.29 are obtained at 17 UT and for January 2008 and 2009 respectively. This is important to see how the equatorial ionization anomaly is actually affected by the stratospheric warming events. We are showing these only for the controlled and the disturbed SSW days shown in the discussion above.

At Figure 5.28, starting from the first panel of day 10 January 2008, we can see that EIA was well developed indicating the presence of two crests and a trough at the equator. However, after this day, a decrease trend was observed in EIA and latter lead to a clear suppression of TEC particularly on 24 January 2008 and after which EIA starts reappearing again on 28 to 30 January 2008.

In the same vein, Figure 5.29, shows similar phenomena, starting from the first panel of day 10 January 2009, when EIA is also well developed indicating the two crests and a trough at the equator. However, after this day, a decrease trend was observed in EIA and latter, a clear suppression of TEC particularly on 19 and 24 January 2009 and a well recovered EIA started reappearing again on 26 to 28 January 2009.

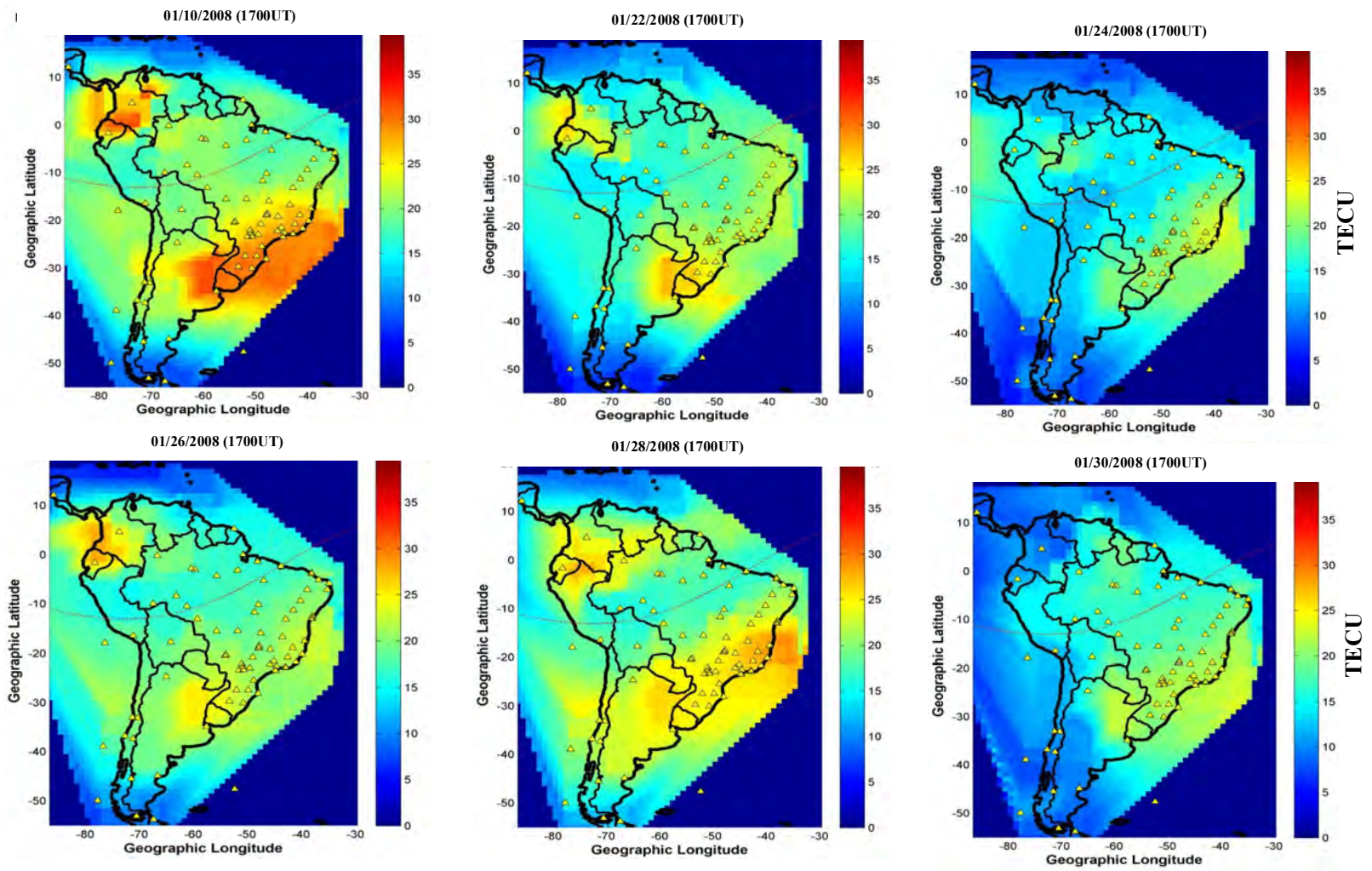


Figure 5.28 - TEC mapping for days 10, 21, 24, 26, 28 and 30 of January 2008.

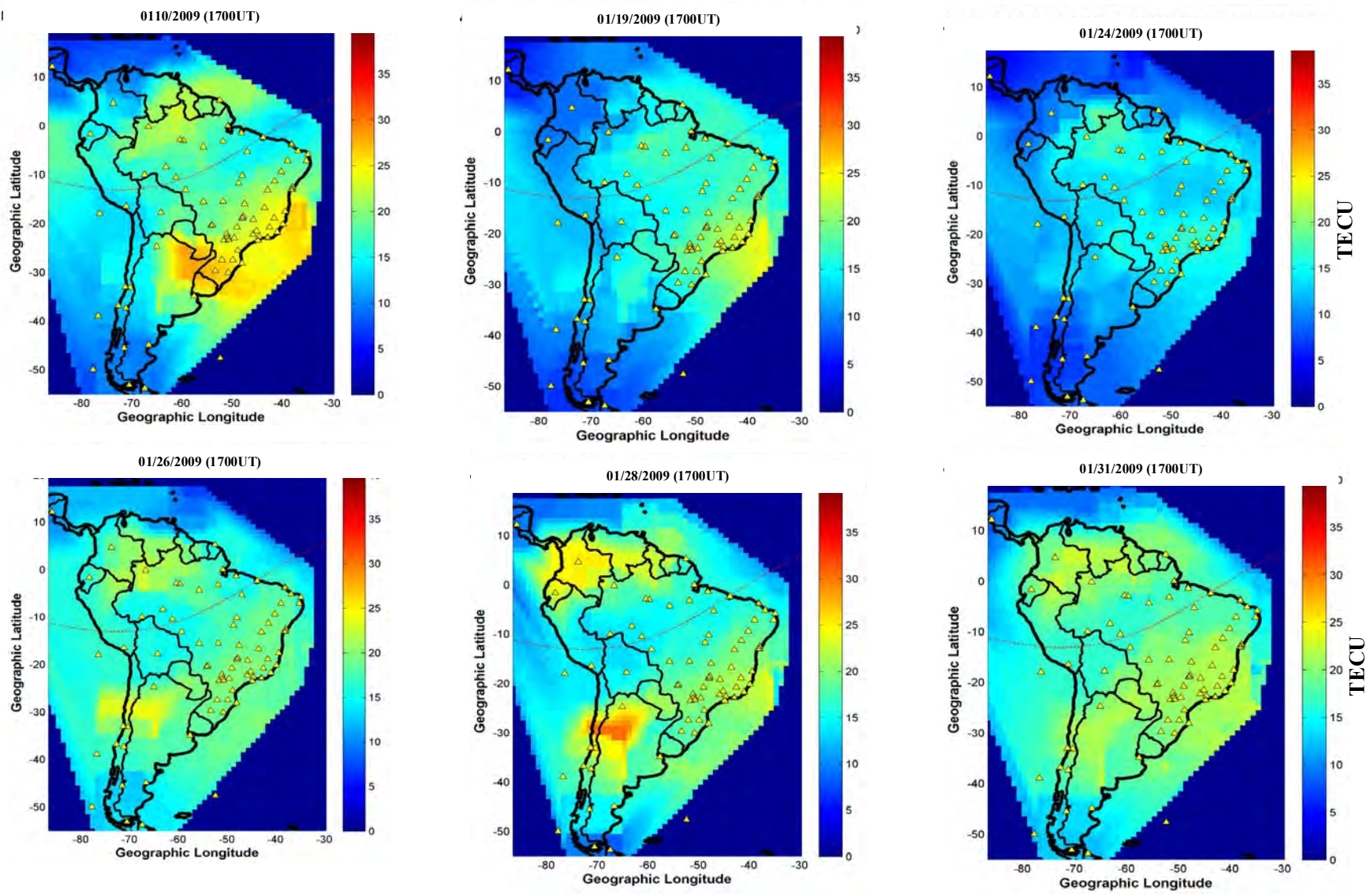


Figure 5.29 - TEC mapping for days 10, 19, 24, 26, 28 and 31 of January 2009 .

6.0 CONCLUSIONS

In this study we have used more than millions of TEC observations from more than 90 globally distributed GPS receivers within the South American sector to describe the TEC variation in the ionosphere in terms of diurnal, day-to-day, seasonal, latitudinal and longitudinal variations during quiet time for low and high solar activities during 2009 and 2001 respectively. Using the power wavelet analysis spectra, periodic TEC variations were analyzed and some physical mechanisms responsible for these variations were suggested. Finally, observations on the SSW events of 2007-2008 and 2008-2009 on GPS-TEC data were also reported.

In order to study the diurnal, day-to-day, seasonal and longitudinal TEC variations as well as to observe the EIA strength and its characteristics, we have focused mainly on some stations located near the equator and low latitude stations. We made a mass hourly plots of each month, and grouped month into seasons for both phases of the solar cycle. The standard deviation (STD) was also used to describe the local and spatial TEC variability at different locations on the South American sector. Our results indicate that the local TEC variability, as shown in the STD, is largest around the locations of low latitude stations with maximum around afternoon and late in the evening. The largest STD values was between 5 and 6 TECU during solar minimum and between 25 and 30 TECU during solar maximum. TEC variability was larger in equinox followed by summer solstice and low in winter solstice for solar maximum, while for solar minimum larger TEC variability was observed during summer solstice followed by equinox and lowest during winter solstice. Generally, our results show that TEC increases from 2009 solar minimum to 2001 solar maximum by 200%. It should be mentioned that during winter solstices for both phases of the solar cycle, TEC diurnal values at the crest of the anomaly region exhibits lower values than TEC at the equatorial regions. This could be because sun radiation during winter solstice is not as intense as during equinox and summer therefore fountain effect is not well developed and plasma is not effectively transported off the magnetic equator. An annual seasonal variation is observed in the solstices and a semiannual variation is observed in the equinoxes.

To study TEC variation with magnetic latitude we considered the magnetic field of 60°W from 20°N to 20°S of dip latitude using the IGRF model. We found TEC asymmetry between March and September equinoctial months as shown in Figure 5.3 for both low and high solar activities. Results showed March exhibits the larger TEC values compared to September in both cases.

SAMI2 model was used by feeding it with different parameters such as photochemistry, transport owing to electric field and transport owing to wind, to point out the liable factors responsible for TEC asymmetry between March and September equinoxes. Our result indicated that the temperature and O/N₂ ratio which is larger in March than September could be the factor responsible for the asymmetry.

It can also conclude that the ionosphere from summer to equinox responds differently (more ionization) during the February to March transition than from winter to equinox during August to September transition (less ionization). Therefore equinox as represented by March exhibits larger TEC values despite the fact that it has lower F10.7 (particularly in solar maximum) compared to September and September shows low TEC despite its higher F10.7.

Our analyses also show hemispheric equinoctial asymmetries and also illustrate the ionospheric latitudinal variation of TEC evolution which indicates smooth transitions from summer to equinox and from winter to equinox. The TEC values exhibits asymmetry during the solstices at low latitudes which was found to be due to photoionization rather than wind effect as could be in opposite case when ionization is larger in winter compared to summer solstices for solar maximum. During the solstices, the daytime TEC variations were found to be larger in summer hemisphere than is the winter hemisphere in contrast to the well-known winter anomaly.

In order to investigate mechanisms which are responsible for TEC periodicities as observed in our data, we applied wavelet spectral analysis to daily means of TEC data over Cachoeira Paulista, Porto Alegre, São Luís and Arequipa stations as well as to the daily means of meridional and zonal winds at the altitude of 100 km along with F10.7 to compare their periodicities.

Apart from the strong 27 days period and 16 day period observed in F10.7 and wind parameter respectively, we also observed a strong 1 to 5 and 7 day periods was common both to all the stations but not so strong at both Cachoeira Paulista and Porto Alegre stations and the two parameters (zonal and meridional winds). A day-to-day variation in TEC was reported to contain a component driven by planetary waves enhanced by tides as they propagate upward. A strong vertical coupling through the upward propagating waves could also lead to day-to-day oscillation in TEC and our study also indicates that often changes in the meridional wind and zonal as well as solar flux wind can lead to corresponding changes in TEC.

Lastly, five SSW events have been investigated in this study and similar features were observed in all five events. The 2008/2009 SSW was uniquely strong with a long lasting event and with low geomagnetic conditions, and these conditions makes it a better event to study. On the other hand the 2007/2008 event was composed of 4 subsequent stratospheric warmings and they were characterized with some few days of geomagnetic storms and have few days of relative high solar flux which make it a more complex event for study. However, we ensured that only the geomagnetic quiet days were used in our study.

From our analysis we observed that a persistent semidiurnal variation with larger intensity during daytime was a common feature for the all events. This semidiurnal feature can be observed particularly during and after few days of the peak of the stratospheric temperature, which gives origin to an enhancement of the EIA during the morning sector, a suppression during the afternoon sector and a another enhancement during nighttime hours. It was also observed that the amplitude of the semidiurnal variation reduces after a numbers of days and the normal condition of the EIA begins to normalize again as shown in all of our SSW result of section 5.4. There is a clear interhemispheric difference in TEC perturbations during SSW events with stronger EIA north crest. One interesting fact is that the repeatable event can be used to predict the day-to-day TEC variability during SSW events.

6.1 Future Works

- The thermospheric neutral wind for both meridional and zonal components could be a better parameter to use for the confirmation of TEC variations. To carry out this research there is a need for thermospheric wind model as well as thermospheric wind data which are not available at the time of this study, therefore further studies are needed.
- our study indicates that significant changes in the meridional wind and zonal wind around 100 km can also lead to basically the same TEC changes. Consequently, the physical causes of observed changes in TEC cannot often be uniquely determined without considering additional wind information. Therefore, further studies are needed.
- If more meteor radars were installed at strategic locations close to GPS stations, their data will improve investigation of possible electrodynamic coupling mechanisms connecting upward propagating wave with the ionospheric TEC variation, particularly during quiet period. This could be also an interesting future research work.
- From our study of the SSW events, some TEC peaks were observed at the northern hemisphere, the reason for this is not fully understood as at the complete of the dissertation. More studies are necessary to ascertain the actual factor responsible for this asymmetry could be carried out in future studies. The EIA development observed in the afternoon sector of 30 January 2008 came a little late (outside the expected time) in Figure 2.26. This late development of EIA is not yet understood at the time of this write-up. This should be investigated in future works.
- Finally, the electric field during day time and during nighttime over the Brazilian sector could not be used due to time constraints, however by using the Anderson's methodology (Anderson et al. 2002) and using digisonde data respectively, the electric field can be calculated in future research works.

REFERENCES

- AARONS, J.; MENDILLO, M.; YANTOSCA, R.; KUDEKI, E. GPS phase fluctuations in the equatorial region during the MISETA 1994 campaign. *Journal of Geophysical Research*, v. 101, p. 26851, 1996.
- ABDU, M. A. Equatorial ionosphere–thermosphere system: electrodynamics and irregularities *Advances in Space Research*, v. 35, p. 771–787, 2005.
- ABDU, M. A.; BATISTA P. P.; BATISTA I. S.; M. BRUM C. G.; CARRASCO A. J. Equatorial evening prereversal electric field and spread F, *Journal of Geophysical Research*, doi:10.1029/1005GL024837, 2006.
- ABDU, M. A. AND BRUM, C.G.M. Electrodynamics of the vertical coupling processes in the atmosphere-ionosphere system of the low latitude region. *Journal of Geomagnetism and Earth Planets Space*, v. 61, p. 385–395, 2009.
- ABDU, M. A.; BRUM, C.G.M.; BATISTA, I.S.; SOBRAL, J.H.A.; DE PAULA, E.R.; SOUZA, J.R. Solar flux effects on equatorial ionization anomaly and total electron content over Brazil: observational results versus IRI representations. *Journal of Advances in Space Research* v. 42 p. 617–625, 2007.
- ANDERSON, D.; ANGHEL, A.; YUMOTO, K.; ISHITSUKA, M.; KUDEKI, E. Estimating daytime vertical $E \times B$ drift velocities in the equatorial F-region using ground-based magnetometer observations. *Journal of Geophysical Research* , doi:10.1029/2001GL014562, 2002.
- ANDERSON, D.N. AND ROBLE. Neutral wind effects on the equatorial F-region ionosphere, *J. Atmos. Sol. Terr. Phys.*, v. 43, p. 835, 1981.
- ANDERSON, D. N., AND KLOBUCHAR J. A., Modeling the total electron content observations above Ascension Island, *J. Journal of Geophysical Research* , v. 88, p. 8020-8024, 1983.
- BAGIYA, M. S.; JOSHI H.P.; IYER K.N.; AGGARWAL M.; RAVINDRAN S.; PATHAN B.M. TEC variations during low solar activity periods (2005-2007) near the equatorial ionospheric anomaly crest region in *India, Ann Geophys (Germany)*, v. 27, p 1047-1057, 2009.
- BALAN, N.; BAILEY G. J. AND JAYACHANDRAN B., Ionospheric evidence for a non-linear relationship between the solar EUV and 10.7-cm fluxes during an intense solar cycle, *Planet. Space Sci.*, v. 41, p. 141-145, 1993.
- BALAN, N.; OTSUKA Y.; FUKAO S.; ABDU M. A.; BAILEY G. J. Annual variations of the ionosphere: A review based on MU radar observations, *Adv. Space Res.*, v. 25, p. 153–162, 2000.
- BATISTA, I.S. AND ABDU, M.A., Ionospheric variability at Brazilian low and equatorial latitudes comparison between observations and IRI model. *Journal of Advances in Space Research* v. 34 p. 1894–1894, 2004.

- BATISTA, I.; M. ABDU, M.A.; BITTENCOURT J., Equatorial F region vertical plasma drifts: Seasonal and longitudinal asymmetries in the American sector, *Journal of Geophysical Research*, doi:10.1029/JA091iA11p12055. 1986.
- BEACH, T.L., KELLEY, M.C., KINTNER, P.M., MILLER, C.A. Total electron content variations due to nonclassical travelling ionospheric disturbances: theory and global positioning system observations. *Journal of Geophysical Research* v. 102, p. 7279, 1997.
- BELWITT, G. An automatic editing algorithm for GPS data, *Journal of Geophysical Research*, v. 17, p. 199-2002, 1990.
- BLEWITT, G. Basics of the GPS technique: observation equations. In: Johnson. B. (ed.). *Geodetic applications of GPS*. Sweden: Nordic Geodetic Commission, 1997. p. 10–54. ISSN 0280-5731.
- BHUYAN P K, Diurnal, seasonal and solar cycle variation of TEC, NmF2 and slab thickness at Luning, *India J. Radio Space Phys*, v. 21, p. 170 - 178, 1992.
- BILITZA, D. *Report from 33rd COSPAR Scientific Assembly, Warsaw, Poland, 16-23 July 2000*. IRI News Lett., 7: p. 1-4. , 2000.
- BROWN, G. M., AND WILLIAMS D. C., Pressure variations in the stratosphere and ionosphere, *J. Atmos. Terr. Phys.*, v. 33, p. 1321–1328, 1971.
- CHARNEY, J.G. AND DRAZIN P.G. Propagation of planetary-scale disturbances from the lower into upper atmosphere. *Journal of Geophysical Research* v. 66, p. 83-110, 1961.
- CHAU, J.L.; FEJER, B.G.; GONCHARENKO, L.P., Quiet variability of equatorial $E \times B$ drifts during a stratospheric warming event, *Journal of Geophysical Research* , doi:10.1029/2008GL036785, 2009.
- CHAU, J. L.; APONTE N. A.; CABASSA E.; SULZER M. P.; GONCHARENKO L. P.; GONZALEZ S. A., Quiet time ionospheric variability over Arecibo during sudden stratospheric warming events, *Journal of Geophysical Research* , doi:10.1029/2010JA015378, 2010.
- CODRESCU, M. V.; PALO S. E.; ZHANG X.; FULLER-ROWELL T. J. AND POPPE C. TEC climatology derived from TOPEX/POSEIDON measurements, *J. Atmos. Sol. Terr. Phys.*, 61, 281 – 298, doi:10.1016/S1364- 6826(98)00132-1, 1999.
- CODRESCU, M. V.; BEIERLE K. L.; FULLER-ROWELL T. J.; PALO S. E. AND ZHANG X. More total electron content climatology from TOPEX/Poseidon measurements, *Radio Sci.*, doi:10.1029/1999RS002407, 2001.
- DABAS R S, LAKSHMI D R.; REDDY B M, Solar activity dependence of ionospheric electron content and slab thickness using different solar indices, *Pure App Geophys (France)*, v. 140 p. 721-728, 1993.
- DASGUPTA, A., PAUL, A.; DAS, A. Ionospheric Total Electron Content (TEC) studies with GPS in the equatorial region, *Indian Journal Radio Space Physics*, v. 36 p. 278-292, 2007

DE PAULA, E. R.; DE REZENDE, L. F. C.; KANTOR, I. J.; CAMPOS, A. A. N.; SMORIGO, P. F. Ionospheric irregularities studies using GPS. *Simpósio Brasileiro de Geofísica Espacial E Aeronomia*, 2006, São José dos Campos. **Livro de Resumos...** São José dos Campos: SBGF, 2006. p. 29.

CAMARGO, P.O.; Quality of TEC estimated with mod_ion using GPS and GLONASS data. *Journal of Hindawi Publishing Corporation* doi:10.1155/2009/794578, 2009.

DE SIQUEIRA, P. M.; DE PAULA, E. R.; MUELLA, M. T. A. H.; REZENDE, L. F. C.; ABDU, M. A.; GONZALEZ, W. D. Storm-time total electron content and its response to penetration electric fields over South America. *Ann. Geophys*, doi: 10.5194/angeo-29-1765-2011, 2011.

FEJER, B.G.; DE PAULA E.R.; GONZALEZ, S.A.; WOODMAN, R.F. Average vertical and zonal F region plasma drifts over Jicamarca, *Journal of Geophysical Research*, doi:10.1029/91JA01171. 1991.

FEJER, B.G.; OLSON M. E.; CHAU J. L.; STOLLE C.; LUHR H.; P.GONCHARENKO L.; YUMOTO K., AND NAGATSUMA T., Lunar-dependent equatorial ionospheric electrodynamic effects during sudden stratospheric warmings *Journal of Geophysical Research*, doi:10.1029/2010JA015273, 2010.

FEJER, B.G.; TRACY, M.E.; OLSON; CHAU J.L., Enhanced lunar semidiurnal equatorial vertical plasma drift during sudden stratospheric warmings, *Journal of Geophysical Research*, doi:10.1029/2011GL049788, 2011.

FEJER, B. G. AND SCHERLIESS L., Time dependent response of equatorial ionospheric electric fields to magnetospheric disturbances, *Journal of Geophysical Research*, v. 22, p. 851-854, 1995.

FEJER, B.G.; SCHERLIESS L.; DEPAULA E.R., Effects of the vertical plasma drift velocity on the generation and evolution of equatorial spread F, *Journal of Geophysical Research*, v. 104, p. 19,859–19,870, 1999.

FEDRIZZI, M.; DE PAULA, E. R.; KANTOR I. J., Ionospheric effects of the August 26, 1998 magnetic storm over South America, In: *International Beacon Satellite Symposium* Proceeding, Boston, 2001.

FORBES, J.M.; PALO S.E.; ZHANG X. Variability of the ionosphere, *J.Atmos. Sol. Terr. Phys.*, v. 62, p. 685 - 693, 2000.

FREDERIC G.; SNIDER, R.P.G. *GPS: theory, practice and applications*. 2012. Available at: <http://www.pdhcenter.com> . Access: 30 Apr. 203. PDH Course L116, October, 2012

FULLER-ROWELL, T.; WANG H.; AKMAEV R.; WU F., FANG T.-W.; IREDELL M.; RICHMOND A. Forecasting the dynamic and electrodynamic response to the January 2009 sudden stratospheric warming, *Journal of Geophysical Research*, doi:10.1029/2011GL047732, 2011.

GONCHARENKO, L. AND ZHANG S.R. Ionospheric signatures of sudden stratospheric warming: Ion temperature at middle latitude, *Journal of Geophysical Research*, doi:10.1029/2008GL035684, 2008.

GONCHARENKO, L. P.; CHAU J.; LIU H.-L.; COSTER A. J., Unexpected connections between the stratosphere and ionosphere, *Journal of Geophysical Research*, doi:10.1029/2010GL043125, 2010a.

GONCHARENKO, L. P.; COSTER, A. J.; CHAU, J.L.; AND VALLADARES, C.E. Impact of sudden stratospheric warmings on equatorial ionization anomaly, *Journal of Geophysical Research*, doi:10.1029/2010JA015400, 2010b.

GURTNER W.; BOUCHER C.; BRUYNINX C.; VAN DER MAREL H. The use of the IGS/EUREF Permanent Network for EUREF Densification Campaigns, EUREF Publication No. 6, *Veröffentlichungen der Bayerischen Kommission für die Internationale Erdmessung, Bayerischen Akademie der Wissenschaften*, Munich, p. 50-51, 1997.

HARGREAVES, J.K. *The solar-terrestrial environment*, New York: Cambridge Univ. Press, 1992. Atmospheric and Space Science Series

HEELIS, R.A.; P.C. KENDALL, R.J.; MOFFELT, D.W.; WINDLE and H. RISHBETH. Electrical coupling of the E and F-regions and its effects on F-region drifts and winds, *Planet. Space Sci.*, v. 22, p. 743-756, 1974.

HO, C.M., MANNUCI, A.J.; LINDQWISTER, U.J.; PI, X.; TSURUTANI, B.T. Global ionosphere perturbations monitored by the worldwide GPS network. *Journal of Geophysical Research* v. 23, p. 3219, 1996.

HOFMANN-WELLENHOF, B.; LICHTENEGGER, H.; COLLINS, J. *GPS - theory and practice*. Wien: Springer-Verlag, 3 ed. 355 p. 1994.

HUNSUCKER, R. D., AND HARGREAVES, J. K. The high latitude Ionosphere and its effect on Radio propagation. *Cambridge University Press*. 1995.

HUBA, J. D.; JOYCE G.; FEDDER J. A., SAMI2 is another model of the ionosphere (SAMI2): A new low-latitude ionosphere model, *Journal of Geophysical Research*, 105(A10), v. 23, p. 035–23,053, 2000.

JEE, G.; SCHUNK R. W.; SCHERLIESS L., Analysis of TEC data from the TOPEX/Poseidon mission, *Journal of Geophysical Research*, doi:10.1029/2003JA010058, 2004.

JEE, G., SCHUNK R. W.; SCHERLIESS L. On the sensitivity of total electron content (TEC) to upper atmospheric/ionospheric parameters, *J. Atmos. Sol. Terr. Phys.*, v. 67, p. 1040-1052, 2005.

KANE R.P., Day-to-day variability of quiet-time ionospheric foF2. *India Journal of Radio & Space Physics*. v. 32, p. 344 - 348, 2003.

KELLEY, M.C.; KOTSIKOPOULOS, D.; BEACH, T.; HYSELL D.; MUSMAN S. Simultaneous global positioning system and radar observations of equatorial spread F at Kwajalein. *Journal of Geophysical Research* v. 101, p. 2333, 1996.

KELLEY, M. C. *The Earth's ionosphere: plasma physics and electrodynamics*. 1. ed. San Diego: Academic Press. 1989. v. 43. International Geophysics Series.

KELLEY, M. C. *The Earth's ionosphere: plasma physics and electrodynamics*. 2. ed. v.96, London: Elsevier, 2009. International Geophysics Series.

LIU J. Y.; LIN C. H.; CHEN Y. I., LIN Y. C.; FANG T. W.; CHEN C. H.; CHEN Y. C.; HWANG J.J. Solar flare signatures of the ionospheric GPS total electron content, *J Geophys Res (USA)*, doi: 10.1029/2005JA011306, 2006.

LIU, H.-L.; WANG W.; RICHMOND A. D.; AND ROBLE R. G. Ionospheric variability due to planetary waves and tides for solar minimum conditions, *Journal of Geophysical Research*, doi:10.1029/2009JA015188, 2010.

LIU, H., M.; YAMAMOTO; TULASI R. S.; TSUGAWA T.; OTSUKA Y.; STOLLE C., DOORNBOS E.; YUMOTO K.; NAGATSUMA T., Equatorial electrodynamics and neutral background in the Asian sector during the 2009 stratospheric sudden warming, *Journal of Geophysical Research*, doi:10.1029/2011JA016607, 2011.

MOHANNAKUMAR, K. *Stratosphere troposphere interaction: an introduction*. Cochin, India: Springer, 2008.

MATSUNO, T., A dynamical model of the stratospheric sudden warming, *J. Atmos. Sci.*, v. 28, p. 1479–1494, 1971.

MENDILLO, M.; H. RISHBETH, R. G.; ROBLE, W. J. Modeling F2-layer seasonal trends and day-to-day variability driven by coupling with the lower atmosphere, *J. Atmos. Sol. Terr. Phys.*, v. 64, p. 1911 – 1931, 2002.

MUELLA, M. T. A. H.; KHERANI, E. A.; DE PAULA, E. R.; CERRUTI, A. P.; KINTNER, P. M., KANTOR, I. J.; MITCHELL, C. N.; BATISTA, I. S.; ABDU, M. A. Scintillation-producing Fresnel-scale irregularities associated with the regions of steepest TEC gradients adjacent to the equatorial ionization anomaly. *Journal of Geophysical Research* , vol. 115, A03301, doi:10.1029/2009JA014788, 2010.

OTSUKA, Y.; OGAWA, T.; SAITO, A.; TSUGAWA, T.; FUKAO, S.; MIYAZAKI; S. A new technique for mapping of total electron content using GPS network in Japan. *Journal of Earth Planets Space*, v. p. 54, 63–70, 2002.

PANCHEVA, D., MUKHTAROV P.; ANDONOV B., Non-migrating tide activity related to the sudden stratospheric warming in the Arctic winter of 2003/2004, *Ann. Geophys.*, v. 27, p. 975–987, 2009.

PARK J., LÜHR H., MARKUSKUNZE, FEJER B.G.; WOOKMIN K., Effect of sudden stratospheric warming on lunar tidal modulation of the equatorial electrojet. *Journal of Geophysical Research*, doi:10.1029/2011JA017351, 2012.

RAMA RAO, P. V. S., GOPI KRISHNA S., NIRANJAN K.; PRASAD D. S. V. V. D., Temporal and spatial variations in TEC using simultaneous measurements from the Indian GPS network of

- receivers during the solar activity period of 2004-2005, *Ann. Geophys.*, v. 24, p. 3279-3292, 2006.
- RASTOGI, R. G. AND KLOBUCHAR, J. A. Ionospheric electron content within the equatorial F2 layer anomaly belt. *Journal of Geophysical Research*, v. 95, n. A11, p. 19045-19052, 1990.
- REN, Z., WAN, W., LIU, L., CHEN, Y., LE, H. Equinoctial asymmetry of ionospheric vertical plasma drifts and its effect on F-region plasma density *Journal of Geophysical Research*, doi: 10.1029/2010JA016081, 2011.
- RICHMOND, A.D. The ionospheric wind dynamo: effects of its coupling with different atmospheric regions. In: JOHNSON, R.M.; KILLEEN, T.L. (ed.). *The upper mesosphere and lower thermosphere*. Washington: American Geophysical Union, 1994
- RISHBETH, H., AND MENDILLO M. Patterns of F2-layer variability, *J. Atmos. Sol. Terr. Phys.*, v. 63, p. 1661–1680, 2001.
- RISHBETH, H., The F region dynamo. *Planet Space Sci.*, v. 19, p. 263, 1971.
- RISHBETH, H. AND M. MENDILLO, Patterns of F2-layer variability, *J. Atmos. Sol. Terr. Phys.*, v. 63, p. 1661 – 1680, 2001.
- RISHBETH, H.; MULLER -WODARG, I. C. F.; ZOU, L.; FULLER-ROWELL T. J.; MILLWARD G. H.; MOFFETT R. J.; IDENDEN D. W.; AYLWARD A. D. Annual and semiannual variations in the ionospheric F2-layer: II. Physical discussion, *Ann. Geophys.*, v. 18, p. 945-956, 2000.
- RISHBETH, H., F region links with the lower atmosphere?, *J. Atmos Sol. Terr. Phys.*, doi:10.1016/j.jastp.2005.03.017, 2006.
- RISHBETH, H., AND GARRIOTT, O. K., Introduction to Ionospheric Physics, *Academic, San Diego, Calif.*, 1969
- SCHERHAG, R., *Die explosionsartigen Stratosphärenwärmungen des Spätwinters 1952*, Ber. Dtsch. Wetterdienstes US Zone, v. 6, p. 51–63.
- SCHERHAG, R., Stratospheric temperature changes and the associated changes in pressure distribution, *J. Meteorol.*, v. 17, p. 572–585, 1960.
- SCHERLISS L. AND FEJER B. G., Radar and satellite global equatorial F region vertical drift model. *Journal of Geophysical Research*, v. 104, NO. A4, p. 6829-6842, 1999.
- SCHERLISS L., THOMPSON D. C.; SCHUNK, R. W., Longitudinal variability of low-latitude total electron content: Tidal influences. *Journal of Geophysical Research*, doi:10.1029/2007JA012480, 2008
- TSURUTANI, B. T.; VERKHOGLYADOVA, O. P.; MANNUCCI, A. J.; SAITO, A.; ARAKI, T.; YUMOTO, K.; TSUDA, T.; ABDU, M. A.; SOBRAL, J. H. A.; GONZALEZ, W. D.; MCCREADIE, H.; LAKHINA, G. S.; VASYLIŪNAS, V. M. Prompt penetration electric fields (PPEFs) and their ionospheric effects during the great magnetic storm of 30–31 October 2003. *Journal of Geophysical Research*, doi:10.1029/2007JA012879, 2008.

WU, CHIN.-CHUN.; FRY, C.D.; LIU, J.-Y.; LIOU, K.; TSENG, C.-L., Annual TEC variation in the equatorial anomaly region during the solar minimum: September 1996–August 1997. *Journal of Atmospheric and Terrestrial Physics*, v. 66, p. 199–207, 2004.